AN INVESTIGATION OF FINITE-DIFFERENCE SEISMIC MODELLING APPLIED TO MASSIVE SULPHIDE EXPLORATION

CHRISTINA DEMERLING

An Investigation of Finite-Difference Seismic Modelling Applied to Massive Sulphide Exploration

by

Christina Demerling

A thesis submitted to the School of Graduate Studies in partial fulfillment of the requirements for the degree of Master of Science.

Department of Earth Sciences,
Faculty of Science
Memorial University of Newfoundland
St. John's, Newfoundland
September, 2004

Abstract

Seismic exploration is an excellent method for massive sulphide exploration because of its sensitivity to density and velocity changes. The density contrast between sulphides and host rocks is significant enough that contacts between these rock types are visible in seismic data.

New 2D acoustic finite difference modelling was completed for this study, simulating a combination of one surface seismic and two VSP arrays over a hypothetical massive sulphide deposit. The results from a scattering massive sulphide body in a scattering host rock have shown that added value is obtained from simultaneous recording of surface and VSP data and concurrent processing of the resulting data. For best results, pre-migration processing of the VSP data should include wavefield separation to remove downgoing energy followed by concurrent pre-stack depth migration. This study shows simultaneously recorded data from a surface and two vertical seismic profile (VSP) arrays decrease the effects of an attenuating surface low velocity layer and the irregular geometry of mineralisation.

Examination of the imaging properties of the model space indicate that for optimal imaging results, the VSP arrays should be placed on either side of the expected target extending at least to target depth, with the surface array crossing the target and connecting the two VSPs.

Acknowledgements

There are many people without whom this thesis would not have happened, and I have appreciated their wisdom, knowledge, patience, and encouragement very much. First, I would like to thank my supervisors, Chuck Hurich and Jim Wright, for allowing me the freedom to explore this newer area of seismology and for having superhuman patience while I finished my thesis write-up. I would like to thank Larry Matthews for providing me with personal insight on how seismology applied to massive sulphide exploration was working in "the real world", and for encouragement. I would like to thank the National Science and Engineering Research Council of Canada (NSERC) for their financial support, and for the opportunity to work within my field of research.

On a more personal note, I would like to thank my husband Mike for his seemingly unending patience, encouragement, and editorial skills—I'm not sure I would have finished without him. Thanks also to my Mom and Dad who kept on my case about finishing. Thanks also to my very good friend Susan for being a great sounding board when I needed to talk about my thesis with someone.

Table of Contents

Table of Figures

Chapter 1. Introduction

In recent decades, the number of new economic ore deposits discovered has declined because the more obvious deposits (those that are near-surface and/or near infrastructure) have been found and exploited. It is now necessary to look deeper in the earth and farther away from existing infrastructure to satisfy the growing demand for most metals. In addition to searching for new deposits, there is also a need to determine that there are no more mineable reserves in mining camps nearing depletion.

Exploration and mining companies in the past have used various geophysical methods, such as magnetics, gravity, electromagnetics (EM), and seismics, to achieve this goal. The advantages and disadvantages of each method are discussed later in this thesis. Seismic methods may hold the most promise since they are sensitive to variations in density and velocity and can be used to investigate deeper in the earth with higher resolution than is possible with most other methods.

One possible method of adequately detecting and/or imaging massive sulphide deposits is to use simultaneous surface and borehole seismic recording. In this configuration, the recording aperture has been widened to effectively "catch" more reflected and forward-scattered energy from subsurface anomalies than surface arrays would alone. The same coverage could be achieved with surface arrays if they extended very far in the downdip direction of a planar deposit (which is difficult to plan for if geometry of targets is unknown) (Spencer *et al.*, 1993), or were arranged in a 3D surface seismic configuration (which is very expensive and still may not provide sufficient offset) (Eaton *et al.*, 1997).

The purpose of this thesis is to use numerical modelling to simulate the imaging capability and relative added value of recording surface and vertical seismic profile (VSP)

data simultaneously over a massive sulphide deposit and then processing the data concurrently (see Chapter 3). This investigation builds upon the work of McMechan and Hu (1996) and Kirtland Grech and Lawton (2001) by examining whether the increased recording aperture created by recording seismic data simultaneously in VSPs and on surface in crystalline terrains can lead to successful direct imaging of massive sulphide deposits. The design for a combined borehole and surface seismic array can be easily modified to maximise data quality for a particular geological setting. The increased aperture should improve resulting migrated images because the VSPs should have a higher signal-to-noise (S:N) ratio and will record energy reflected from dipping faces of a target object that would not be recorded within the maximum offset of a surface seismic array.

This thesis gives background information on what geophysical methods are currently used for exploration, in particular the challenges of applying exploration seismology to massive sulphide exploration. A brief review of the previous work with VSPs and surface seismic data and past field applications of seismic to mineral exploration is followed by a discussion of the physical properties of massive sulphides. The thesis continues with details about how numerical modelling was used to simulate simultaneous surface and borehole seismic recording, including the different parameters and why they were used. The observations and results of this numerical modelling are discussed, and recommendations are made for future work.

Chapter 2. Background Information

Before discussing methods used to create the simulations and the resulting data from them, some background information is necessary to explain why more massive sulphide discoveries are needed, why current geophysical exploration methods are not ideal for the task, and why exploration seismology may be a better solution than other methods. This chapter will cover these topics, review challenges to seismic applications in crystalline terrains, and will include a short summary of previous work integrating VSPs with surface seismic surveys and past applications of seismology to mineral exploration.

2.1 Why a New Massive Sulphide Exploration Programme is Necessary

Mineral exploration is driven by a continuous need for discovering more ore reserves to meet manufacturing needs throughout the world. It is evident that most of the "easy-to-find" deposits up to 200-300 m in depth have been developed and existing mining camps are becoming depleted. There is a need to determine whether any other economic deposits are present near existing infrastructure in mining camps (up to 1 km in depth) such as Horne (Canada), Kidd (Canada), and Brunswick (Canada) ("sterilising" an exploration property) (Gingerich *et al.*, 2000). Exploration can be done a number of ways, one of which is drilling, but drilling a property is very expensive and if it is based on a poor dataset it may waste money without gaining significant understanding of the prospect. Alternatively, geophysical methods provide data on physical properties of the subsurface (due to geological structures and/or mineralisation) and have been used successfully in the past to identify and delineate ore deposits. Seismic methods specifically can bridge the exploration gap between 300 and 1000 m in depth and can

detect mineralisation directly. Mineral exploration and mining companies would benefit from following the lead of oil and gas exploration companies to use more complex exploration methods (using high-resolution, multi-channel digital data, and integrating geological and geophysical data) to find new targets or to "sterilise" properties that have been under exploration for a long period of time.

2.2 Geophysical Methods Used for Mineral Exploration

There are three main geophysical methods used for massive sulphide mineral exploration: magnetics, gravity, and electromagnetics (EM). A fourth method, seismics, is proposed here as an alternative that may be more sensitive at greater depths to the physical properties of massive sulphide minerals.

Magnetic exploration methods measure local changes in the Earth's magnetic field due to contrasts of magnetic susceptibilities of media. Most magnetic anomalies are associated with magnetic minerals (mainly magnetite and pyrrhotite); therefore, direct exploration for mineralisation is limited to ores associated with magnetic minerals. Magnetic surveys can detect bodies of both regional and local scale and are less expensive than gravity surveys. (Telford *et al.*, Chapter 3, 1995).

Gravity exploration methods are sensitive to changes in the Earth's gravity field due to contrasts of density between rock types. Gravity surveys are more expensive than magnetic surveys but less expensive than seismic surveys. Gravity surveys are also slow and tend to be sensitive only to large, regional structures. Therefore gravity methods are not as suitable for small anomalies such as massive sulphide deposits (Telford, Chapter 2, 1995).

Electromagnetic (EM) exploration methods are most commonly used for mineral exploration and are sensitive to local changes in electromagnetic fields due to electrical conductors at shallow depths. EM methods are very sensitive to overburden conditions, and when variable or highly-conductive overburden exists (such as over glaciated terrain) the depth penetration of an EM survey is severely impaired (Telford *et al.*, Chapter 7, 1995). Unfortunately, current EM exploration methods are severely limited for exploring deeper than 500 m within crystalline terrains in Canada because most of these terrains have been glaciated and have highly conductive overburden.

Seismic methods are sensitive to changes in acoustic rock properties such as density and seismic wave velocity, which combined (as acoustic impedance—see Section 2.3) determine how much energy will be reflected at an interface between two different materials. Petroleum exploration uses seismic methods primarily because they offer data of high accuracy, high resolution, and deep penetration. Seismic surveys can be scaled to examine large regional features and small local ones, and while it is primarily an indirect exploration method (it detects geological structures and lithologic contacts) (Telford *et al.*, 1995), recent surveys in mineral exploration indicate it can also directly detect thick zones of mineralisation (Gingerich *et al.*, 2000). Although seismic exploration is more expensive than the other conventional mineral exploration methods (EM and magnetics), its depth of penetration is far superior to those methods. As a cost comparison between seismic surveying and drilling, Salisbury *et al.* (1996) recognised that at current prices, a vertical seismic profiling survey could be conducted for the same cost as a conventional logging survey, a 2D surface multichannel survey costs the same as drilling a 2 km borehole, and a 3D survey, at approximately \$50,000/km^2 (Adam *et al.*,

1997; Gingerich *et al.*, 2000), costs less than a multihole drilling programme. Also, the application of seismics in all stages of exploration and mine development (including reconnaissance exploration, delineation, and mine design) would be highly beneficial because ground conditions and mineralisation zones would be well-mapped and better understood (Salisbury *et al.*, 1996).

2.3 Physical Properties of Massive Sulphides

The seismic reflection exploration method depends upon the reflection of energy from an interface and detection by an array of geophones. Every interface between two rock types has a reflection coefficient, R (ratio of reflected to incident energy) that determines how much energy is reflected from and how much is transmitted through the interface. For a plane wave normally incident on a plane boundary, R is defined as:

$$R = \frac{Z_2 - Z_1}{Z_2 + Z_1},$$

where Z_1 and Z_2 are the acoustic impedances of the upper and lower media. Z (for P-waves) is defined as:

$$Z = v_p \rho,$$

where v_p=compressional (P-)wave velocity, and ρ=density of the medium. For most basement rock settings, the minimum reflection coefficient required to give a reasonable reflection is 0.06 (Salisbury *et al.*, 1996). Therefore, if rock properties of mineralisation and host rock are known, it should be possible to predict whether the mineralisation would be a strong enough reflector for detection. Salisbury *et al.* (1996) made laboratory measurements at high confining pressures of v_p and ρ of massive sulphide ores and host

rock from a wide variety of mining camps in Canada and determined that the ores lie in a distinct v_p and ρ field that is separate from that occupied by common silicate rocks and that the properties of combined silicate rocks and ore mineralisation are governed by simple mixing rules of the two, see Figure 2.3-1. Silicate rocks have a predictable V_p-ρ

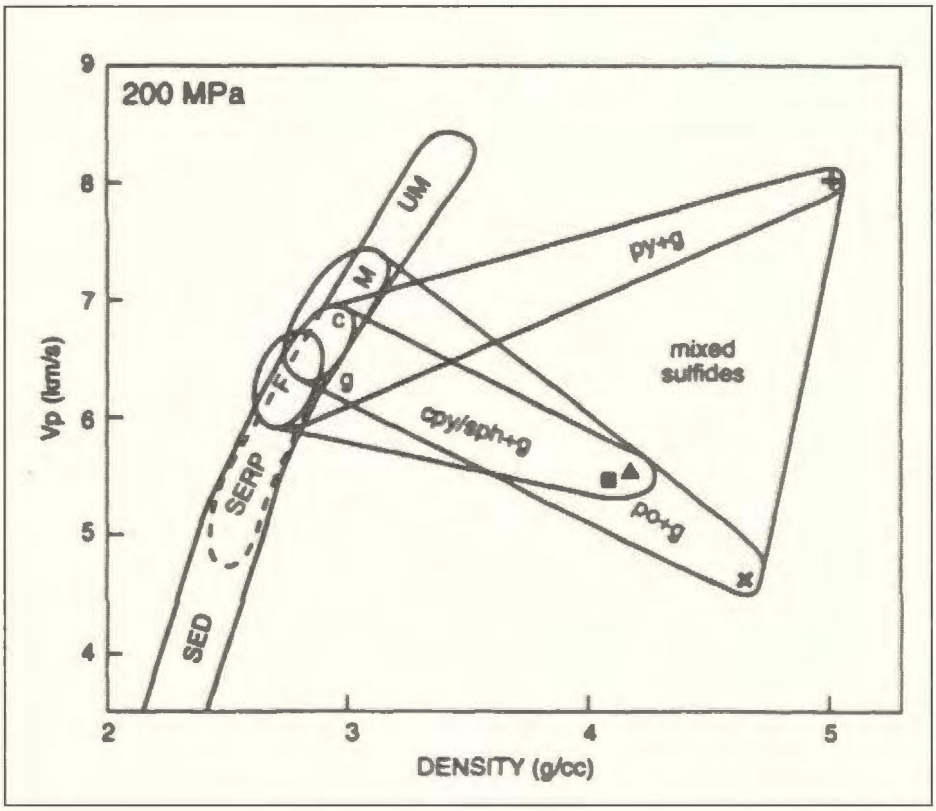

Figure 2.3-1: Velocity (Vp)-density fields for sulphide minerals and silicate host rocks. g=gangue, cpy=chalcopyrite (pure ore=▲), po=pyrrhotite (pure ore=×), py=pyrite (+), sph=sphalerite (pure ore=■), UM=ultramafic, M=mafic, SED=sediments (including carbonates), SERP=serpentinite, F=felsic. After Salisbury *et al.*, 1996.

relationship (V_p increases as ρ increases) but massive sulphide minerals don't exhibit the same behaviour because of bonding and mean atomic weight differences. The compressional wave velocities of sulphide ores vary widely: 3.7 km/s (galena); 4.7 km/s (pyrrhotite); 5.6 km/s (sphalerite and chalcopyrite); and 8.0 km/s (pyrite); while densities are systematically high (for the previously-mentioned minerals, they are: 7.6 g/cm^3, 4.6

g/cm^3, 4.1-4.2 g/cm^3, and 5.0 g/cm^3) (Salisbury *et al.*, 1996). The high density values ensure that acoustic impedances of even intermediate-grade ores are significantly larger than most mafic and felsic host rocks, making large massive sulphide bodies theoretically very strong seismic reflectors in common geologic settings (Salisbury *et al.*, 1996). However, it should be noted that the quality of a seismic reflector depends mostly upon its size and geometry and also mineralogy, grade, geologic setting, and type of contact between country rock and ore rock (transitional or abrupt) (Salisbury *et al.*, 1996). In situ rock velocities, densities, and impedances can be measured effectively by borehole logging techniques and can be very useful for relating seismic observations to lithology, as was used to identify fracture and fault zones at the Bell Allard deposit in Matagami, P.Q. and lithology identification at the Corner Bay Cu-deposit in Chibougamau, P.Q. (Pflug *et al.*, 1997).

2.4 Methodology and Challenges to Seismic Exploration in Crystalline Terrains

Although the application of the seismic method over crystalline rocks is fundamentally sound in theory, there is a lack of applied field testing of the method, processing and interpreting the resulting data. The petroleum industry has been working for decades to understand seismics to successfully refine the method to find oil and gas reservoirs. While some of this knowledge can be transferred to mineral exploration in crystalline rock, much of the knowledge base must be developed by building up a repertoire of seismic surveys in crystalline terrain.

There are a few geological challenges for seismic exploration in crystalline terrains. In Canada, most of these areas have been glaciated and as a result they are locally covered by layers of unconsolidated material or weathered bedrock. This variable-depth

near-surface zone has high attenuation and high velocity contrasts at its boundaries, which tend to trap scattered and mode-converted energy (Holliger and Robertsson, 1998). The trapped energy interacts repeatedly with the free surface and its topography, creating multiples and scattering energy that could possibly obscure real data. This scattering is amplified by moderate topographic or velocity variations (Holliger and Robertsson, 1998). Even anomalies with strong reflection coefficients ($R>0.1$, see Section 2.3) in the shallowest 5 km of crust may not be imaged because of interference from near-surface conditions (Holliger and Robertsson, 1998). The steep dips (sometimes near-vertical) of mineralized zones would be very difficult to illuminate and record data from, especially if only surface arrays are used. Irregular geometries of deposits with few large, flat surfaces means that energy is more likely to be diffracted and/or scattered than return to sensors as specular reflections.

There are also some seismological challenges to this work. Experimental field work has shown that crystalline terrains tend to have high noise levels (from source-generated noise in the low frequency band) that can obscure real data and is sometimes difficult to remove during processing (Milkereit and Eaton, 1998). Milkereit and Eaton (1998) found that reflection seismic amplitudes of shallow crustal structures (e.g., the contact between the mafic norite and felsic granophyre of the Sudbury Igneous Complex) at high frequencies (>150 Hz) were larger than at typical seismic frequencies (<50 Hz). Therefore, high-frequency sources with wider bandwiths should provide better signal than low-frequency ones, although high frequency signals undergo more scattering and attenuation than lower frequency signals. The seismic sources need to be repeatable (for VSP work), and have a high-energy impulse so that the returned signal is strong enough

to be detected, even after reflecting (or diffracting) from an uneven surface. Milkereit and Eaton (1998) note that simple 2D seismic surveys are generally not appropriate for mineral exploration since they are designed for targets with a long strike length compared with the depth of investigation, and are easily contaminated by reflections from structures out of the plane of investigation. Figure 2.4-1 illustrates the differences in geological structure and seismic exploration methodology between a duplex structure in a foreland basin and a mineral deposit.

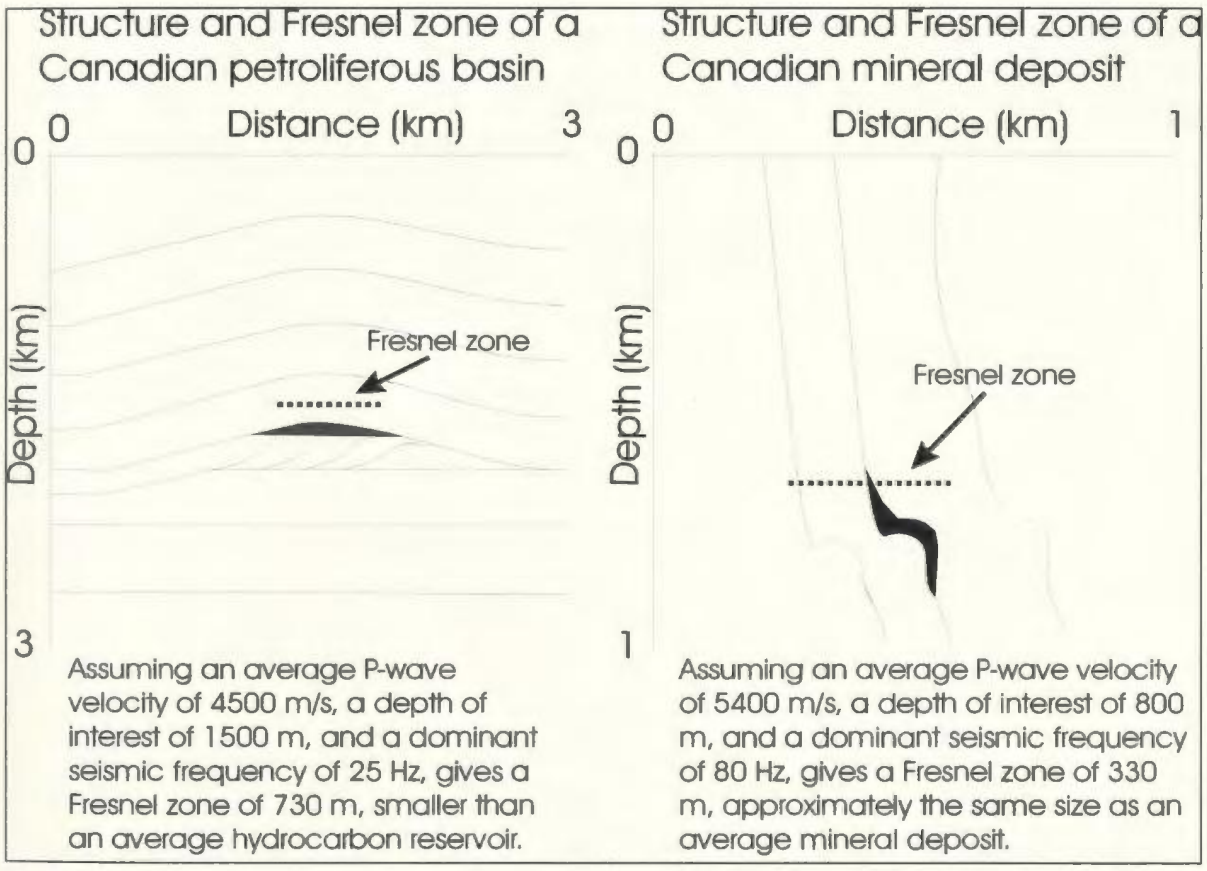

Figure 2.4-1: Comparison of geological structure and Fresnel zone (horizontal resolution of seismic data—see Chapter 3) of a petroliferous basin and a mineral deposit.

The cost of conducting seismic surveys is an obstacle in itself. Crystalline terrains are usually quite far away from petroleum districts (where most seismic crews operate) and

therefore scheduling equipment transfer and set up/strike down is expensive. Typically, holes drilled for mineral exploration have a much smaller diameter than petroleum wells and there is not an abundance of slim-hole tools to use for the VSP work. The processing is challenging due to scattering of signals, multiples and lack of experience with mineral exploration in the processing industry. To conduct a seismic survey combining surface and downhole methods discussed as here may require re-drilling of two existing boreholes (if they are in friable rock), which may be costly and challenging due to geological conditions.

Interpretations of seismic data are non-unique and "discovering" a false positive (at high cost) is always a possibility. This risk alone may be a strong deterrent to mineral exploration companies. Like all geophysical methods, this application of seismics may work better in some situations than others (depending on mineralisation and structure of the rock) and during its development time there may be surveys conducted in situations that would be of no benefit. All geophysical methods have limitations and costs, but the exploration industry must continue to stretch its boundaries and create new opportunities for itself, or risk stagnating and becoming obsolete.

2.5 Previous Work with VSPs and Integration of VSP and Surface Seismic Data

Vertical seismic profiling (VSP) is a specific type of borehole seismic recording where geophones are lowered down a monitoring well and seismic sources are located on the surface at different offsets from the monitoring well (walk-away VSP). This type of survey avoids the near-surface low-velocity zone, eliminating the need for careful statics corrections during processing. Furthermore, a VSP survey will record energy reflected and diffracted from steeply-dipping faces that would not ordinarily return to

the surface (Eaton *et al.*, 1997) (Figure 2.5-1). VSP data commonly have better resolution than surface seismic data because of the smaller Fresnel zone (horizontal resolution of seismic data—see Chapter 3) and larger bandwidth, and the seismic energy travels through the distorting overburden only once (Payne *et al.*, 1994). Unfortunately, VSP data from a single borehole have relatively poor lateral extent, especially in cases where structures dip away from the borehole (Payne *et al.*, 1994). Wu and Toksöz (1987) investigated diffraction tomography applied to seismic exploration and predicted that surface reflection profiles would have best spectral coverage toward the geophone line; VSPs would generally have better spectral coverage than the surface profile; and a combination of surface reflection profiles and VSPs would provide the best spectral coverage.

A possible solution to this VSP problem would be to include two boreholes, one on either side of the ore body to record data from dipping faces, and a surface array between the two boreholes to record data from horizontal and sub-horizontal faces. This thesis examines such an integrated seismic array geometry for the following: 1) the ability to detect massive sulphide deposits from the added value of recording and migrating simultaneous surface and VSP datasets; and 2) the imaging capability of a combined surface and VSP dataset over a zone of mineralisation with complex geometry in crystalline terrain.

This research is based on concepts developed by McMechan and Hu (1986) who examined simultaneous VSP and surface recording to obtain a better image quality from synthetic seismograms of a petroleum structural trap (Figure 2.5-2).

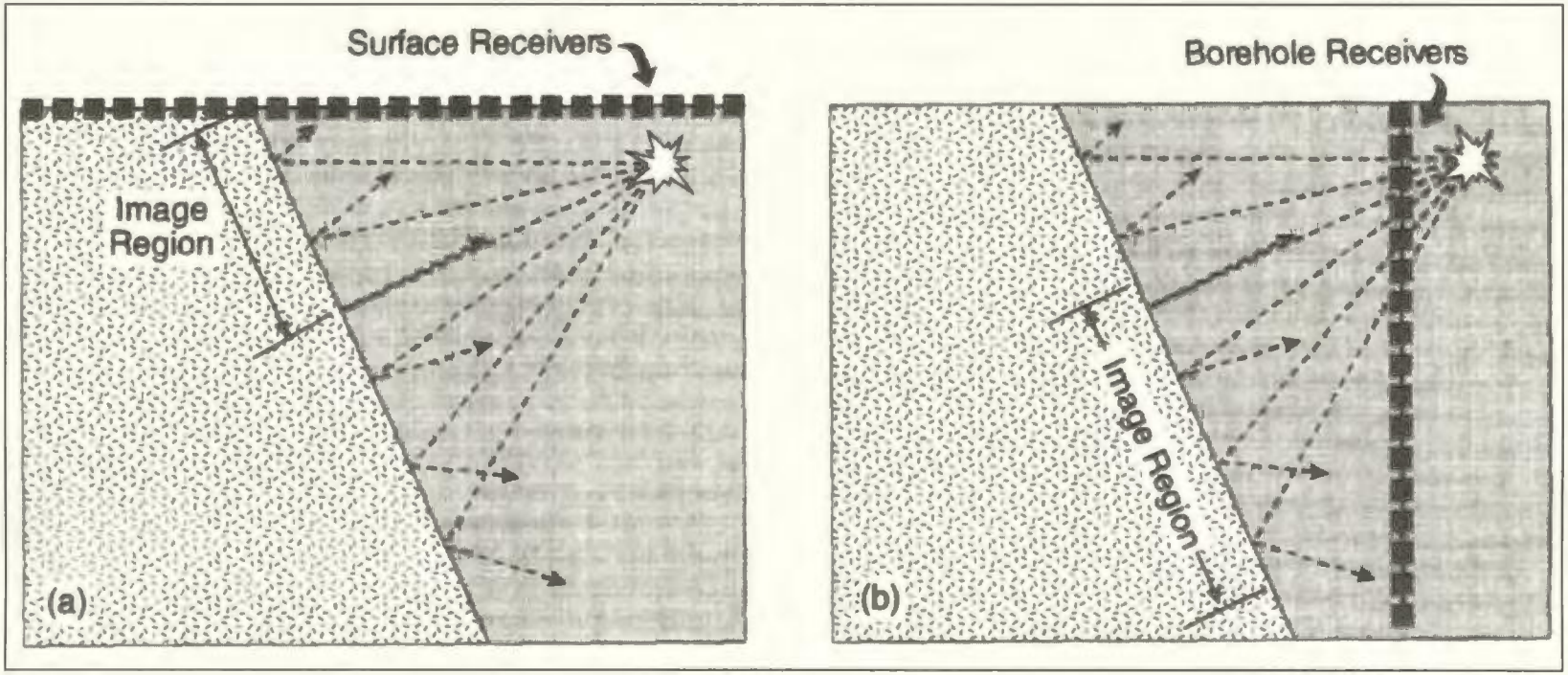

Figure 2.5-1: a) Energy from a horizontal body being directed to a surface seismic array; b) energy reflected from a steeply-dipping structure into a VSP. After Eaton *et al.*, 1996.

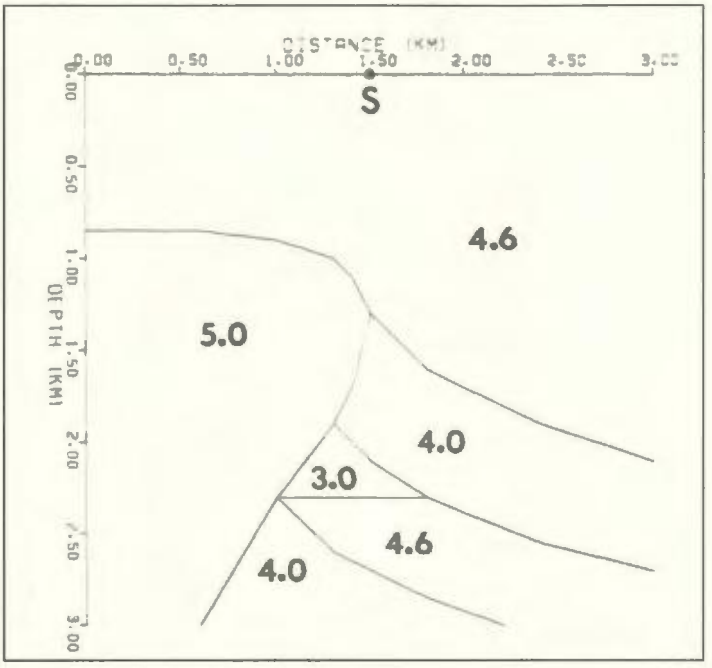

Figure 2.5-2: Numerical model space used by McMechan and Hu, 1986. Values in the body of the diagram indicate acoustic velocities (in km/s) of the different rock types.

The model space they used recorded surface seismic data across the entire top of the model space (3 km long), and along two VSPs located at the left and right edges of the model space. The single seismic source was located at the centre top of the model space and the target (a structural trap—looks like a triangle with velocity 3.0 km/s) was located at a depth of 2-2.5 km. The resulting synthetic seismograms (Figure 2.5-3) were processed minimally (first break muting and data tapering to decrease migration artefacts) before they were pre-stack migrated in four data subsets.

The first subset included data only recorded from the surface array (see Figure 2.5-4a), the second subset had data only from the left VSP array (see Figure 2.5-4b), the third had data only from the right VSP array (see Figure 2.5-4c), and the fourth migrated all data (surface and two VSPs) simultaneously (see Figure 2.5-4e). The resulting data from

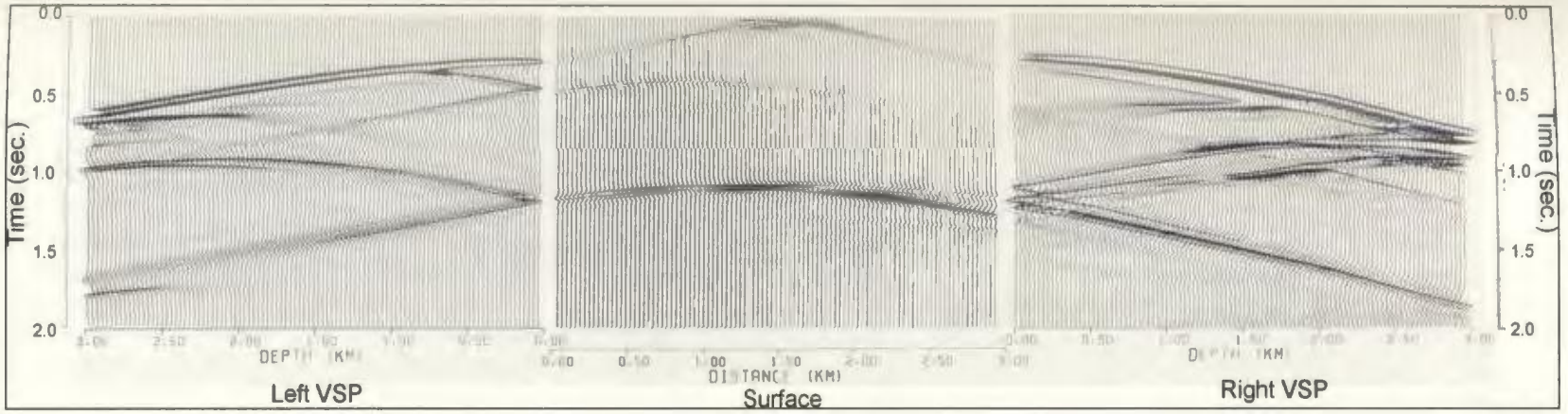

Figure 2.3-3: Raw synthetic seismograms from the work of McMechan and Hu, 1986.

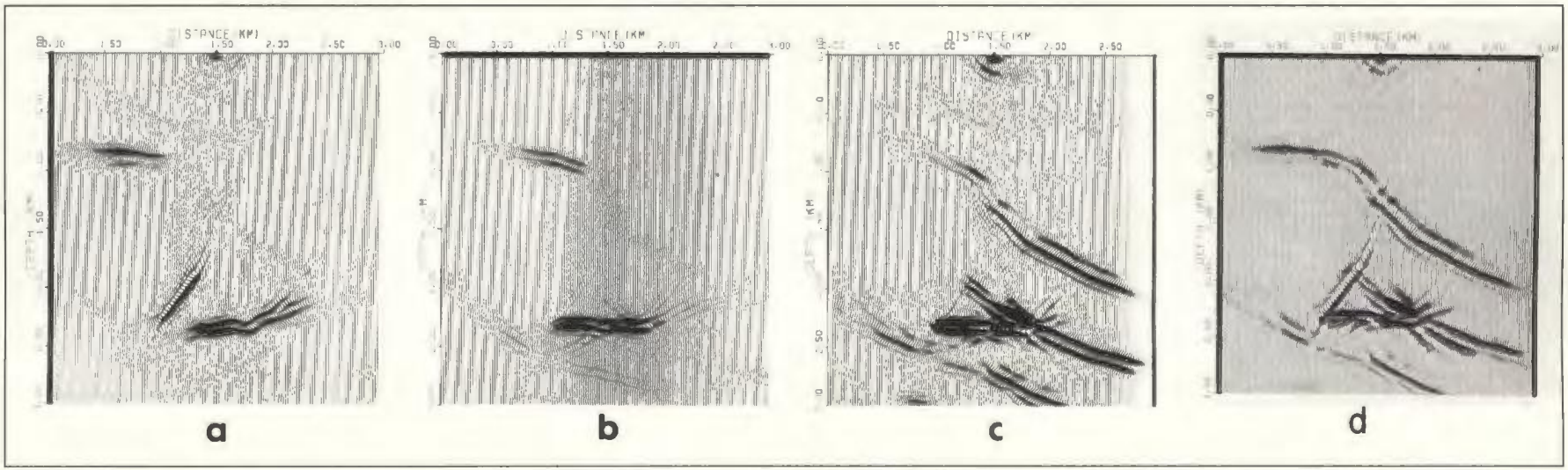

Figure 2.5-4: Compare with Figure 2.5-2. a) migrated image using only data recorded at surface; b) migrated image using only data recorded from the left VSP; c) migrated image using only data from the right VSP; d) migrated image using all synthetic data together. Note the significant increase in image quality when data is integrated together. After McMechan and Hu, 1986.

the first three subsets imaged only discrete parts of the model that were either close to the survey line or imaged parts of the model that were optimally oriented to reflect energy back to that particular seismic line. The fourth dataset, which used all the data simultaneously, successfully imaged the entire structural trap. McMechan and Hu (1986) found that migrated image resolution depended greatly on the recording aperture (the degree to which the survey geometry was capable of recording data reflecting and diffracting from as many sides of the target object as possible) and positioning of seismic sources.

Kirtland Grech and Lawton (2001) created synthetic VSP and surface seismic data computed over a 2D model (based on structures found in the Rocky Mountain Foothills in southern Alberta, Canada). Each model response was convolved with a zero-phase wavelet with peak frequencies of 35 Hz (for surface data) and 45 Hz (for VSP data) to simulate the frequency content of typical field data. The two datasets were integrated in a pre-stack depth migration algorithm. The resulting image was superior to that obtained from migrating the datasets separately, having enhanced resolution at the target depth (from the higher bandwidth VSP data) and contained better structural detail. Kirtland Grech and Lawton (2001) do not specify whether the improved migration image was due to the higher frequency content in the VSP data or the increased recording aperture by including the VSP data.

2.6 Past Applications of Seismics to Mineral Exploration

For approximately the past 20 years, seismic surveys have been used in the mineral exploration industry in Canada, southern Africa, and Australia to increase ore reserves and map fault structures. Seismic surveys have been used in Canada for two different

approaches to massive sulphide exploration. In the Sudbury, ON (Eaton *et al.*, 1996; Milkereit *et al.*, 1996; Eaton *et al.*, 1997; Milkereit *et al.*, 2000) and Matagami, ON (Li and Calvert, 1997; Adam *et al.*, 1997) mining camps; the Thompson nickel belt, MB (White *et al.*, 2000); and the Buchans Mine, NF (Spencer *et al.*, 1993) it has been used to detect and map fault systems that are related to the ore mineralisation, while surveys at Halfmile Lake, NB (Salisbury *et al.*, 2000; Gingerich *et al.*, 2000; Bellefleur *et al.*, 2002) and borehole logging in Manitouwadge, ON (Roberts *et al.*, 1997) focussed on direct detection of massive sulphide mineralisation. The majority of work carried out in Sudbury, Matagami and at Halfmile Lake was completed by a coalition of geoscientists at the GSC (Geological Survey of Canada), Inco, Falconbridge, and Noranda Inc. In southern Africa, surveys over the Witwatersrand have been used to delineate structures associated with gold and platinum mineralisation, and others have been used to map fault systems critical for mine planning (Stevenson and Durrheim, 1997). Large-scale Australian surveys have been used to map regional fault structures that may have been pathways for mineralizing fluids (Drummond *et al.*, 2000); while surveys in Sweden have successfully imaged diabase intrusions and fracture zones (Julin, 1997). A more detailed overview of the development and application of seismics for mineral exploration can be found in Appendix A.

It is evident that current geophysical exploration methods are inadequate for massive sulphide targets greater than 500 m in depth and that seismic methods offer an alternative that can directly detect mineralisation. Past work with surface seismic surveys have been successful in detecting mineralisation zones but were strongly affected by near-surface low-

velocity zones common in most areas in Canada. Alternatively, a combination of VSP and surface seismics should provide better subsurface coverage because the combination would have a wider aperture (able to record reflections and diffractions from many sides of an target object) and would avoid the near-surface low-velocity zone; simulations to test this survey geometry were run and the methodology is discussed in the next chapter.

Chapter 3. Simulation Methodology

This chapter discusses the method used to test the seismic survey geometry described above. The discussion begins with a description of the generic model space; continues with an explanation of the choices of physical properties (velocity and density, target object geometry); wavelet peak frequencies; and expected resolution are also discussed.

Finite difference numerical modelling (acoustic solution only) was chosen to test whether simultaneous migration of VSP and horizontal seismic data adds sufficient image quality to be of interest to exploration companies. These model data were created using modules from Seismic Unix and a pre-stack depth migration algorithm developed at Memorial University of Newfoundland (A. Kocurko) (see Appendix B). The migration algorithm was used purely as a tool to obtain images for evaluation purposes.

The model space was a rectangle 2000 m long (x-direction) by 1500 m deep (z-direction). Nodes, representing locations for geophones, were spaced 5 m apart along the surface and down each VSP location (see Figure 3-1a,b,c). The horizontal array extended the entire length (in x-direction) of the model space and was located at the top of the rectangle. Although the entire length of the horizontal array would be used in an actual field test, only data recorded from the centre 1000 m of the array (500 m to 1500 m) were processed for this study (see Chapter 4). This was done for two reasons: 1) the array length was chosen to match a presumed maximum depth of interest for massive sulphide exploration (because of high development costs for mines greater than 1000 m deep) and to straddle the depths between more shallow exploration methods (e.g., electromagnetic) and crustal seismic studies; and 2) to simulate a more realistic case where far-offset surface seismic data were

less likely to be useful due to noise and signal degradation. The two VSP arrays extended the full depth of the model space, but because most boreholes in mineral exploration do not extend past 1000 m in depth, only data recorded from the shallowest 1000 m of the array was processed (see Chapter 4). One VSP was located at 80 m, the other at 1720 m. Shotpoints were located across the surface at 200 m intervals from 100 m to 1900 m. Payne *et al.* (1994) indicate that the number of sources (i.e., the ability to adequately illuminate the target) has the greatest impact on data quality of walk-away VSPs. In this investigation, the sparse source spacing may be below the illumination limit but it may be compensated for by the large effective walk away offsets for VSPs that have the effect of increasing the resulting image quality and lateral coverage.

The horizontal resolution of seismic data is defined by the Fresnel zone,

$$d_F = \sqrt{2z\lambda}$$

where z=depth and λ=dominant wavelength (Salisbury *et al.*, 1996). Under ideal conditions, migration should be able to collapse the Fresnel zone to the size of the dominant wavelength (Salisbury *et al.*, 1996), but migration is only partially effective since the signal amplitudes quickly degrade below noise levels. Therefore, the Fresnel zone is a better estimate of horizontal resolution.

To simulate the response from a massive sulphide deposit (sphalerite in this case), target object properties were chosen as follows: ρ_{body}=4.03 g/cm^3 and Vp_{body}=5250 m/s (Salisbury *et al.*, 1996). The background material, chosen to represent crystalline host rocks, had properties as follows: ρ_{bkgrd}=2.7 g/cm^3 and Vp_{bkgrd}=5800 m/s (Holliger, 1996). The numerical model used a Ricker wavelet with a maximum frequency of 150 Hz, and peak

frequency of 85 Hz. The peak frequency was chosen to provide reasonably good horizontal resolution of seismic data (Fresnel zone of 310 m) for a small target just larger than the Fresnel zone.

Three model shapes were used in this investigation: 1) a thin bar (30 m (x) by 10 m (z) (see Figure 3-1a); 2) an octagon (horizontal and vertical faces were 120 m long, dipping sides were 170 m long, the entire body was 360 m (x) and 360 m (z)) (see Figure 3-1b); and 3) a polygon with small box-shaped protuberances on each face (identical to the octagon but with protruding boxes to make horizontal and vertical faces 40 m long and dipping faces 57m long, creating body dimensions 440 m (x) and 440 m (z), centred at (1140, 880) (see Figure 3-1c). Chapter 4 describes the model space in more detail and presents observations made from the results of the simulations.

One of the most important facets of this investigation is the asymmetry of the primary model (the octagon). For most of the simulations, the octagon was centred at (1140, 880) to examine the difference between data recorded by VSPs at two different offsets. It was also of interest to qualitatively evaluate the resulting detection image of the target object from different offsets to determine whether simultaneous downhole and surface recording would be a useful option for exploration purposes. The results of the finite difference modelling program are sensitive to the grid spacing parameter (R). The grid spacing parameter provides the user with a spacing that is less than 10% of the shortest wavelength used and is obtained by the following equation,

$$R = \frac{B_{min}}{HF_{max}}$$

where H=grid nodal distance, B_{min}=lowest velocity, F_{max}=upper half power frequency (the peak frequency was used in this investigation), and R>=10 (for stability). In this case, H=5, B_{min}=5250 m/s, and F_{max}=150 Hz, resulting in R=7.0, which is less than stable. Fortunately, the R-value is close to 10 and should not result in any significant problems in the data.

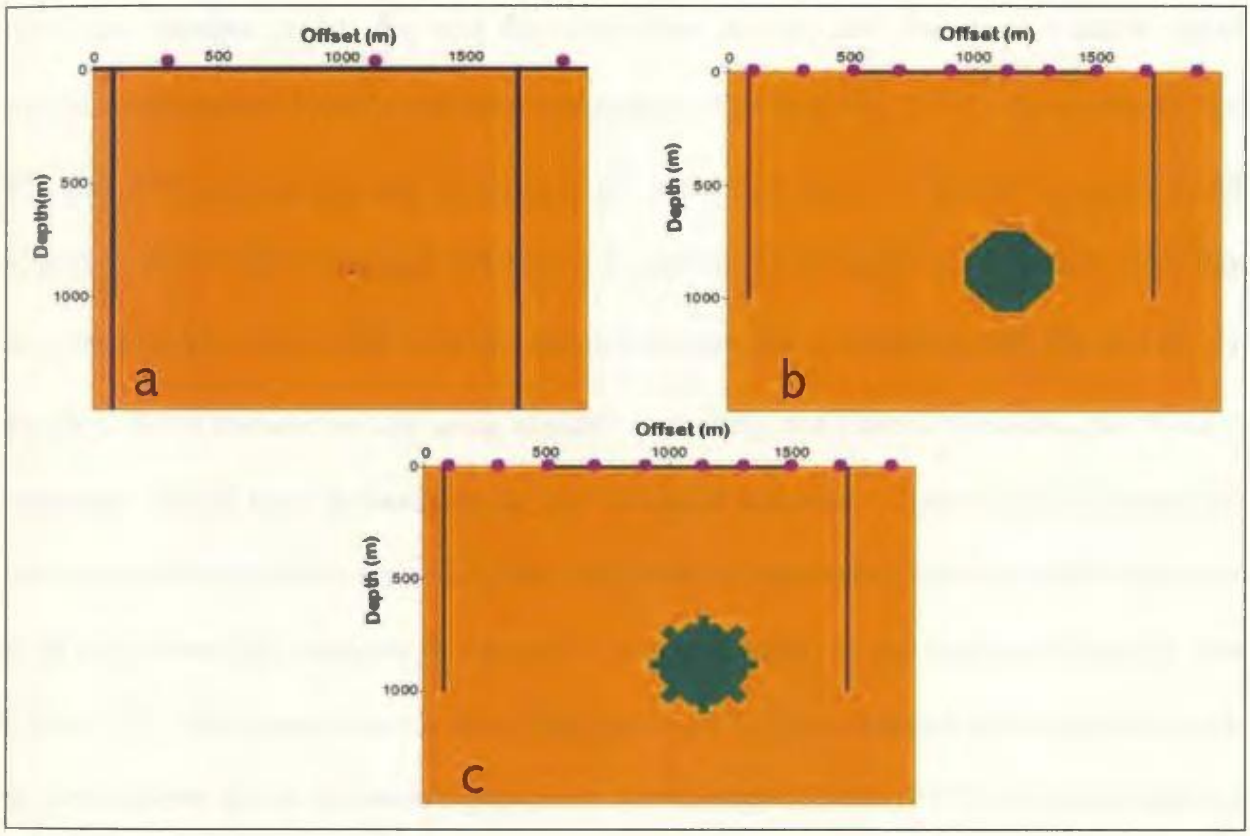

Figure 3-1: Shows the three model spaces used in this research: a) thin bar; b) standard octagon; c) polygon with box-shaped protuberances ("sputnik"). Black lines indicate location of recording arrays, violet circles indicate source locations.

The numerical model used in this investigation is expected to reflect a strong energy field because of the high acoustic impedance contrasts. The reflected energy field is scattered, which occurs when the radius of curvature of an interface is less than a few wavelengths of an incident wave (the incident wave has a much larger wavelength than the roughness of the

surface of the target object), causing the interface to act effectively as multiple point sources (Sheriff and Geldart, 1995). The roughness of the According to Eaton (1999), scattering is a function of two independent variables: composition (Rayleigh scattering) and shape of the inclusion. Rayleigh scattering, where the inclusion acts as a point source, in turn depends upon the changes in $\delta\rho$, $\delta\mu$, and $\delta\lambda$, which are density, and the elastic moduli: shear modulus and Lamé's lambda constant, respectively (Wu and Aki, 1985). According to Wu and Aki (1985), if $\delta\rho$, $\delta\mu$, and $\delta\lambda$ all have the same sign (they are all either positive or all negative), the P-wave scattering will have a maximum in the backward direction. For this investigation, the target body is harder and denser than the surrounding rock ($\delta\rho$ and $\delta\lambda$ are positive, $\delta\mu=0$ because we are using acoustic scattering, not elastic); therefore, the P-wave scattering should have a maximum in the backward direction. Eaton's (1999) numerical modelling of composition scattering from inclusions of sphalerite determined that sphalerite is an impedance-type scatterer that scatters maximum energy in the backward direction (see Figure 3-2). The shape factor is the effect produced by the combined scattering from each of the elements of the inclusion's geometry. For example, Eaton (1999) found that dipping lenticular anomalies tended to have a maximum of scattered energy in the down-dip direction, making them good targets in terms of geometry, while spherical anomalies tended to focus energy in the forward direction, making it a poor geometric target.

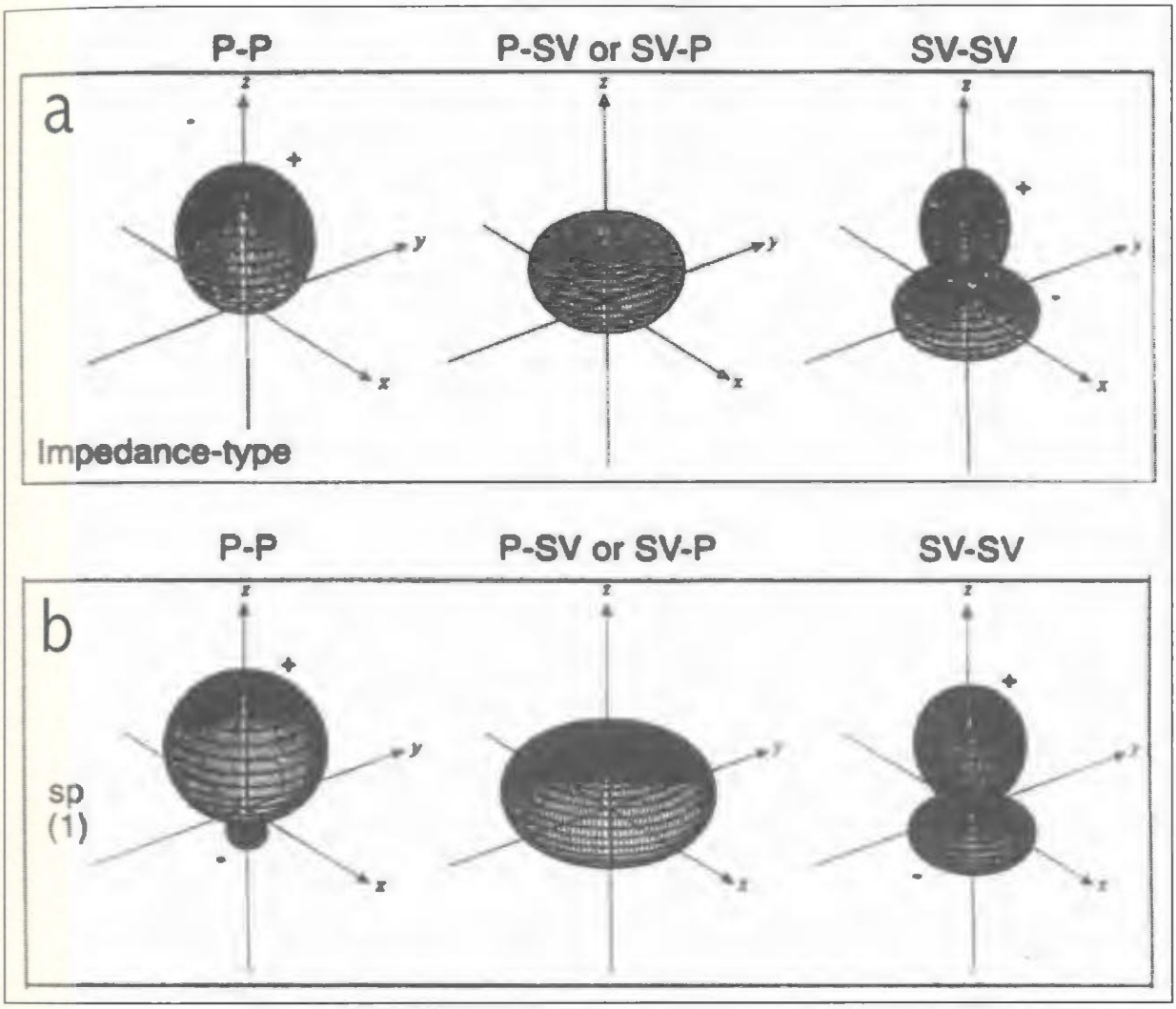

Figure 3-2: a) shows the scattering pattern produced by an impedance-type scatterer; b) shows the scattering pattern produced by an target object made of sphalerite. After Eaton, 1999.

According to Salisbury *et al.* (1996) and Kallweit and Wood (1982), the practical limit of vertical resolvability in seismic data corresponds to Rayleigh's peak-to-trough time separation:

$$t_{min}=1/4\lambda$$

where λ is the dominant wavelength (λ=68 m for this investigation, so t_{min}=17 m). Rayleigh's criterion seems to depend mainly on the highest frequency present, for a band-limited, zero-phase wavelet with a flat amplitude spectrum extending 2 octaves or more in band ratio (Kallweit and Wood, 1982). Figure 3-3 illustrates the effect of frequency bandwidth and centre frequency on wavelet shape, and therefore on resolvability of seismic data. By doubling the bandwidth (compare Figures 3-3a and b), the corresponding time series central lobe becomes narrower with little energy leaking to the sidelobes, which is very good. By increasing the centre frequency without widening the bandwidth (compare Figures 3-3c and d), the corresponding time series central lobe becomes narrower, but much energy is lost to the sidelobes, which is bad for deconvolution of the signal. So for crystalline terrains where targets are smaller than in the petroleum industry (and therefore a higher resolvability is desired), higher predominant frequencies in a broad frequency band should be used to achieve as much resolution as possible.

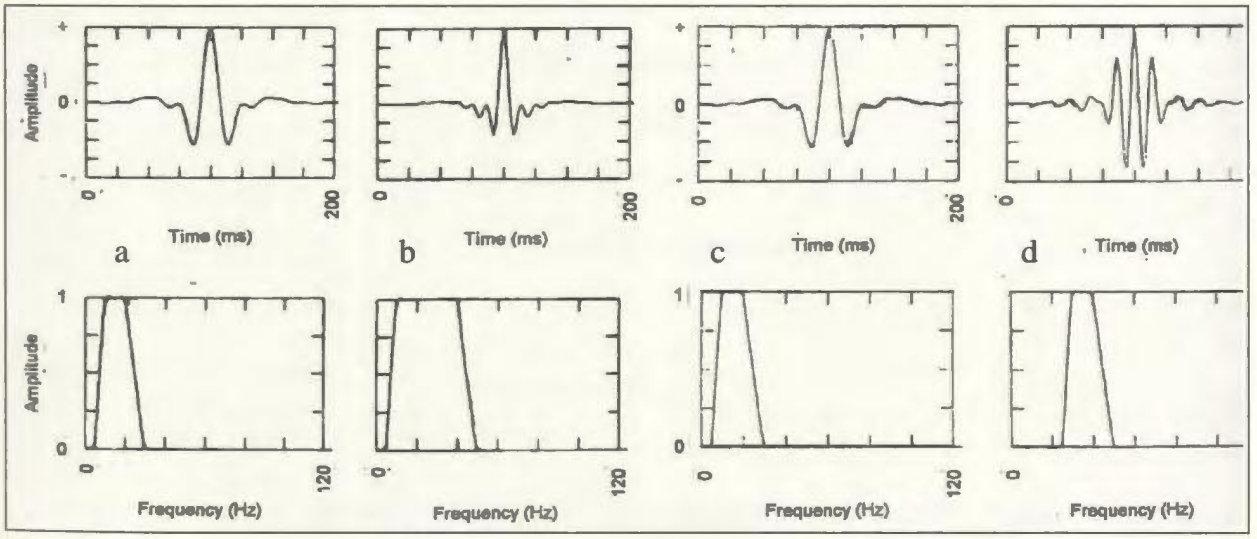

Figure 3-3: Shows the effect of frequency bandwidth and centre frequency on wavelet shape, thereby affecting resolvability. a) ~1 octave (narrow) bandwith; b) ~2 octave (wide) bandwith; c) ~1 octave bandwidth, low centre frequency; and d) ~1 octave bandwidth, higher centre frequency (after Sheriff and Geldart, 1995).

Unfortunately, since the mineralisation geometry for sulphide deposits is complicated, the detection will be strongly affected by scattering and the reflection amplitude will be controlled by the relative sizes of the scatterer and the Fresnel zone. Based upon this, not only should massive sulphides be directly detectable by seismic methods, but, depending on geometry, estimates of mineralisation thickness should also be possible for reflectors greater than the tuning thickness. In fact, L. Matthews (e-mail communication, 2003) completed a simplified thickness estimate for the Noranda Halfmile Lake deposit in 1998. A 3-D seismic survey in 1998 identified an anomaly (see Appendix A) with a two-way-time (TWT) of 16 ms that was subsequently drilled and found to be 49.03 m of pyrite-rich massive sulphide. If a velocity of 6000 m/s is assumed for massive sulphide material, a TWT of 16 ms gives a thickness of approximately 48 m. But the TWT thickness of the anomaly was approximately the same everywhere, which indicated to Matthews that the anomaly was at or below the tuning thickness so he used amplitude to estimate the thickness over the rest of the anomaly, based on the thickness that was encountered in the discovery hole. Matthews was quick to observe that the thickness estimate was possible only because the geometry of the Halfmile Lake deposit was simple—a different approach would have to be used for more complex geometries.

Chapter 4. Observations and Discussion

While the main purpose of this chapter is to present observations of the various simulations that were run, it first discusses testing of the model space for numeric stability. The discussion continues with results from simulations run on an octagon-shaped target object, including the following: from asymmetric and symmetric placement of the target object; from pre-stack and post-stack migration; effect of wavefield separation on the resulting migrated image; the effect of homogeneous and randomly-scattering media (target object and background media); and the imaging qualities of the model space. The chapter continues with results from simulations of a more complex target geometry ("sputnik").

Seismic Unix (SU), a collection of program modules designed to process seismic data, was used in this study to create velocity and density matrices for the model space, collect synthetic seismograms, and perform simple processing and visualization tasks (e.g., muting of first breaks, band-pass filtering, creation of figures for this report, creating amplitude spectra of the data). For one of the models, SU was also used to stack data and perform post-stack migration (see Section 4.1.2). The up- and down-going wavefields were separated by the Vista™ processing package (see Section 4.1.4) and the aplanatic pre-stack depth migration algorithm, used throughout this study (see Appendix B) was created by Kocurko (Department of Earth Sciences, Memorial University of Newfoundland, St. John's, NF).

To test for the appropriateness of the numeric model space and model parameters, and to ensure the inverse solution was reclaimable (i.e., the migration algorithm worked), a simple impulse response model was created. The test model was a 30 m wide by 10 m deep

rectangle centred at 1135 (x-direction), 885 (z-direction). The peak frequency was 85 Hz with a dominant wavelength (λ_{dom}) of 68 m. This is much larger than the dimensions of the target object and therefore should have adequately simulated an impulse response. The rectangle was placed asymmetrically to examine observations from boreholes with different offsets (see Figure 4-1).

Three sets of borehole measurements were collected: the first used the shallowest 200 receivers (1000 m) and the second used the shallowest 500 receivers (2500 m) (the model space was deepened accordingly for the second test). The third experiment had the rectangle centred horizontally (at x=1000 m, z=885 m) as a test to ensure that the differences between the right and left sides of the migrated image were as a result of different offsets from the receivers and not created by the migration algorithm. Each of the three models used three shots located at 300 m, 1140 m, and 1900 m. The VSPs were located at x=80 m and x=1720 m.

In shot gathers, the first (off-centred) model showed clearly-identifiable diffractions on borehole records corresponding to the top of the target object, as well as reflections from the bottom and side of the model space nearest to the VSP (see Figure 4-2a,b). The data were processed by muting the first arrivals and band-pass filtering (20/25-120/125 Hz) (see Figure 4-3a,b). Then they were input to the pre-stack depth migration algorithm. The resulting images (see Figures 4-4a,b,c) show that the diffractions were successfully collapsed to points at the correct location of the top and bottom of the rectangle in the model space. Using only the surface data (Figure 4-4a) achieved the best result (no remaining diffraction tails), but this is believed to be specific to this model geometry, which favours returning energy to the surface instead of directing it to boreholes. The VSP arrays are limited in

aperture and do not collect useful reflection data from horizontal or sub-horizontal lenticular bodies. The image obtained from using data from all 3 recording locations (Figure 4-4c) has some remaining diffraction tails, which appear to be stronger on the right hand side of the model (where the rectangle is closest to a borehole). The interpretation of this result is that the closer borehole (on the right side) is better able to record diffractions because it is at a smaller offset where more sensors may have recorded the waves than the left-hand borehole where waves may not have been recorded by a sufficient number of sensors or may have been removed during processing.

For the second model, the asymmetric impulse rectangle target object remained the same, but the depth extent of the model space was increased to 1500m and the entire 1500m array of VSP data was used during processing using the same methodology as the first model. The resulting image was similar to the first with one significant difference—there were far more (and higher amplitude) diffraction tails (see Figure 4-5). This is attributed to the muting of the direct wave below ~1125 m in borehole data (this depth is specific to this model and would be different for other models depending on the depth and geometry of the target object) where the reflections from the anomalous body start to merge with the direct wave. The muting removes most of the usable high energy, leaving little for the pre-stack depth migration algorithm to work with. Alternatively, if an target object has a larger depth dimension than the impulse response rectangle (see Section 4.1), then the data from the lower part of the boreholes will continue to add value to the lower half of the migrated image until the point is reached where the upper diffractions merge with the direct wave.

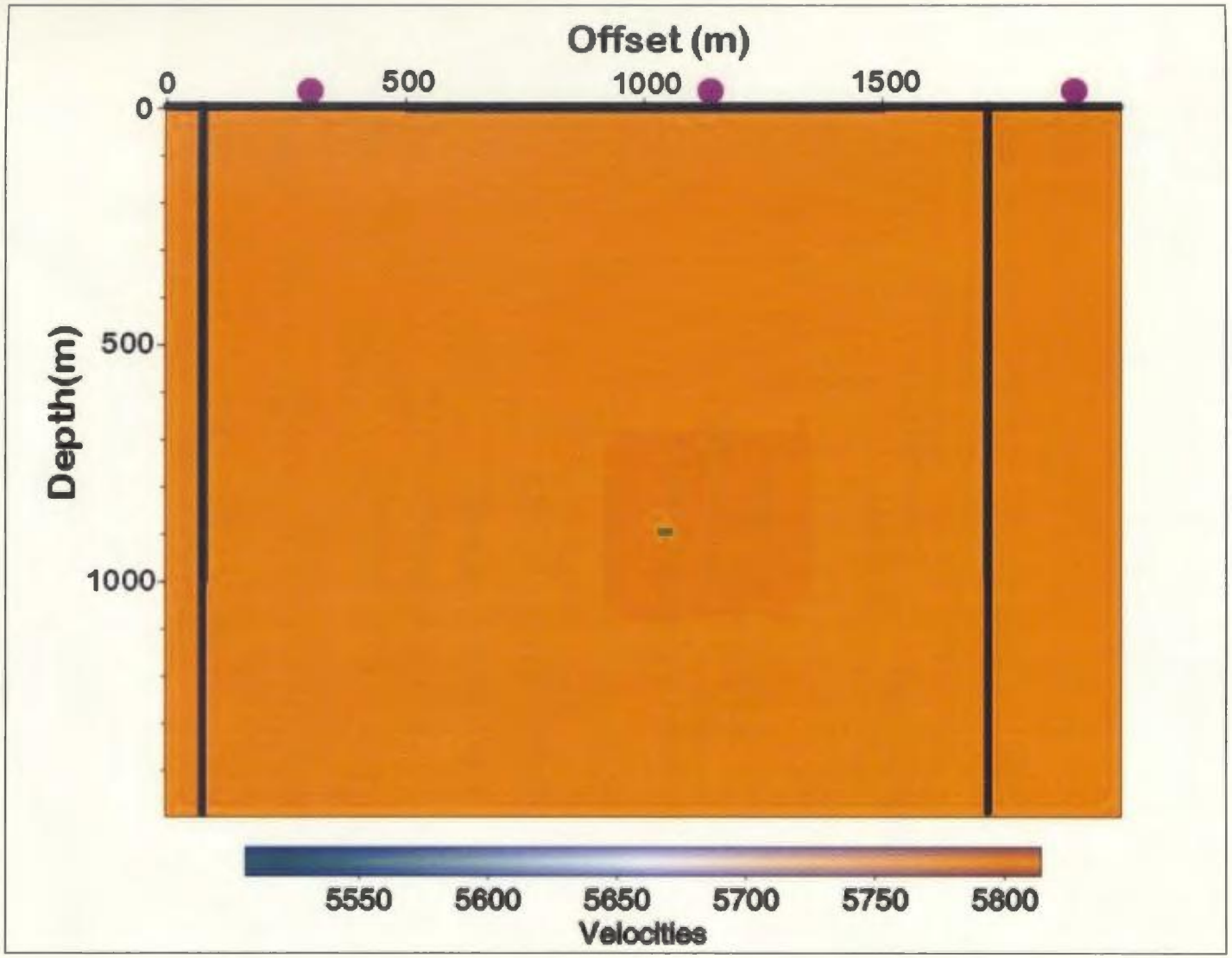

Figure 4-1: Model space for the impulse response test. Violet circles are shot locations, black lines indicate locations of horizontal, left and right VSPs.

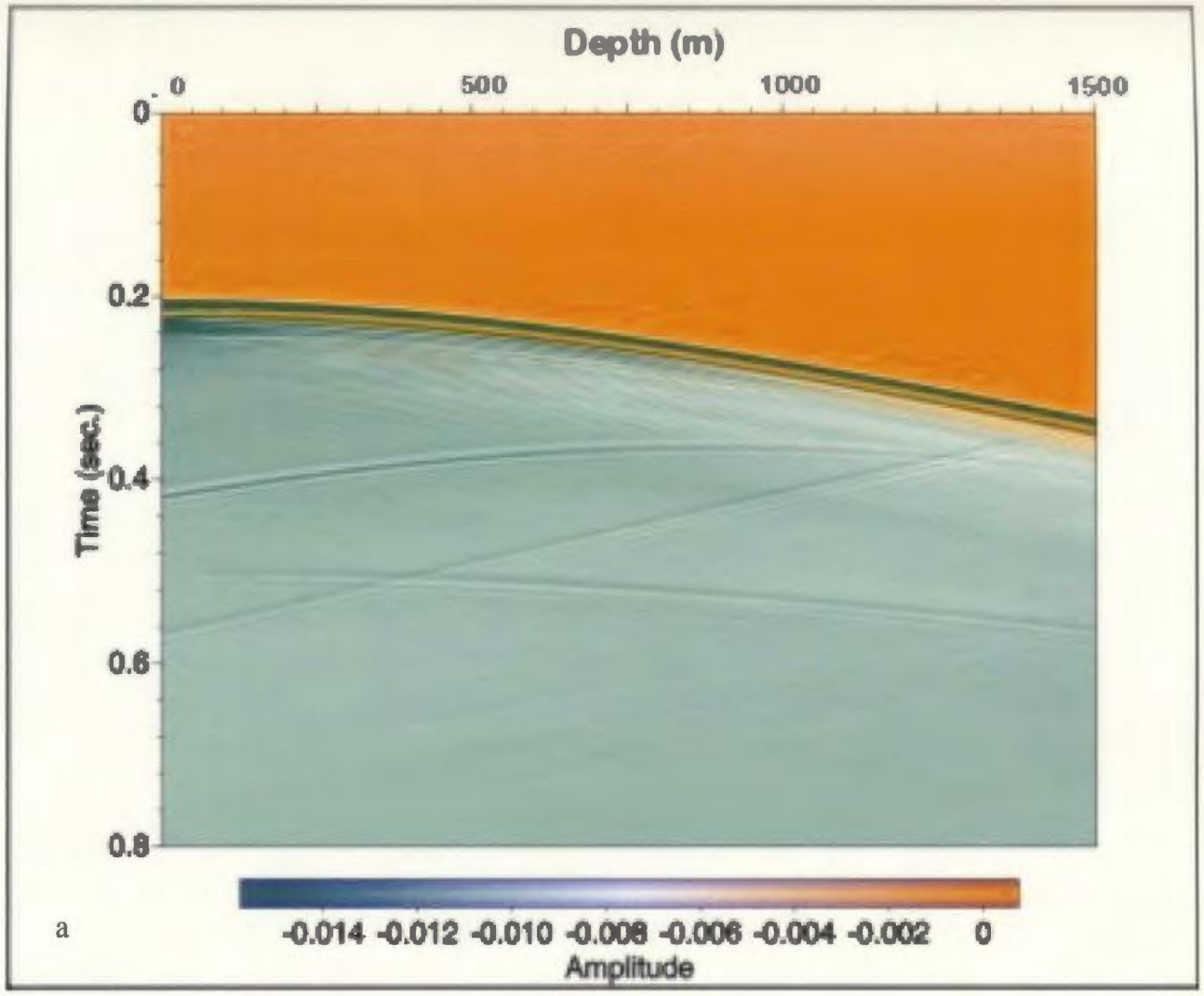

Figure 4-2: a) Raw shot gather of left VSP showing the direct wave arrival as well as reflections from the anomalous body.

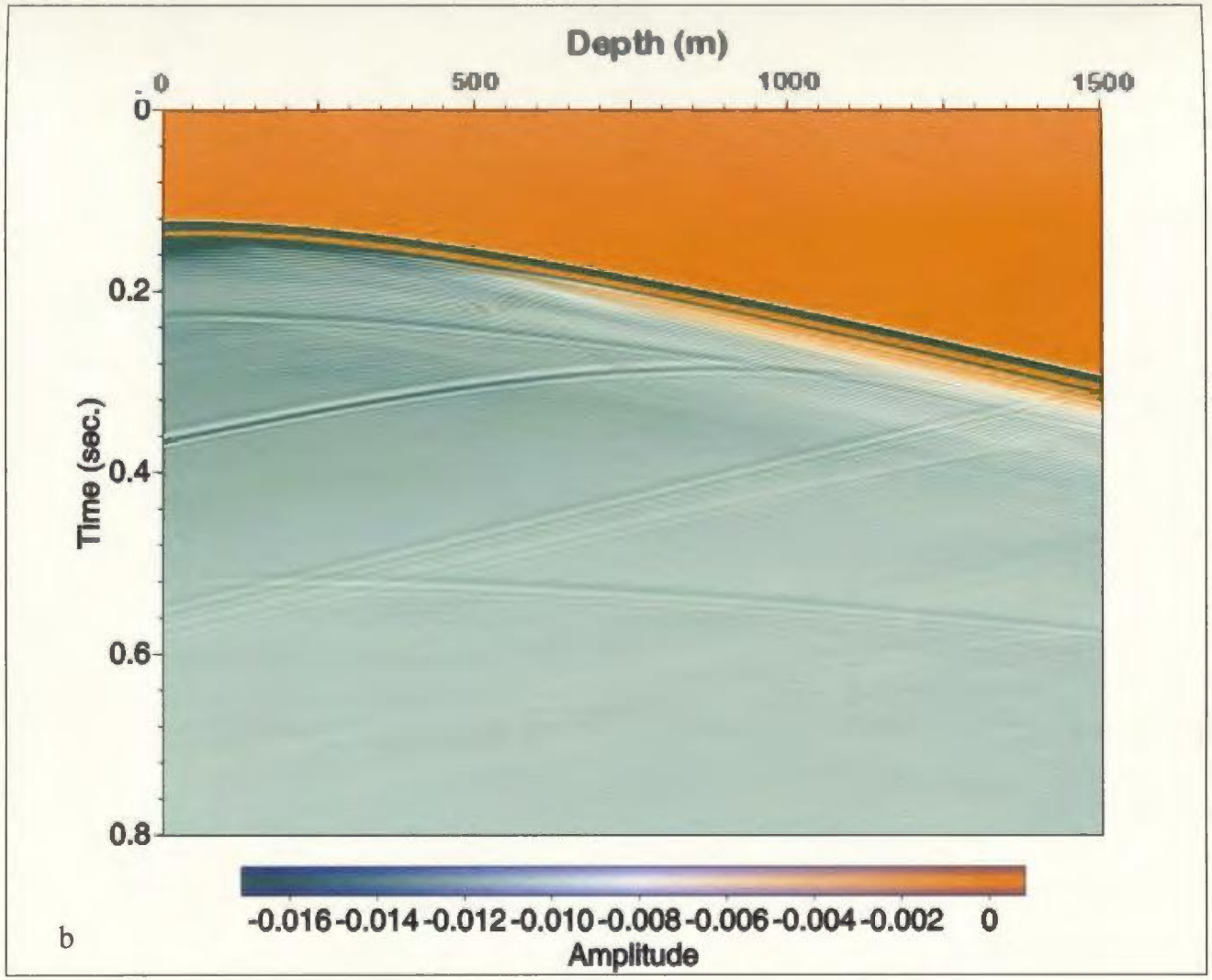

Figure 4-2: b) Raw shot gather of right VSP showing the direct wave arrival as well as reflections from the anomalous body.

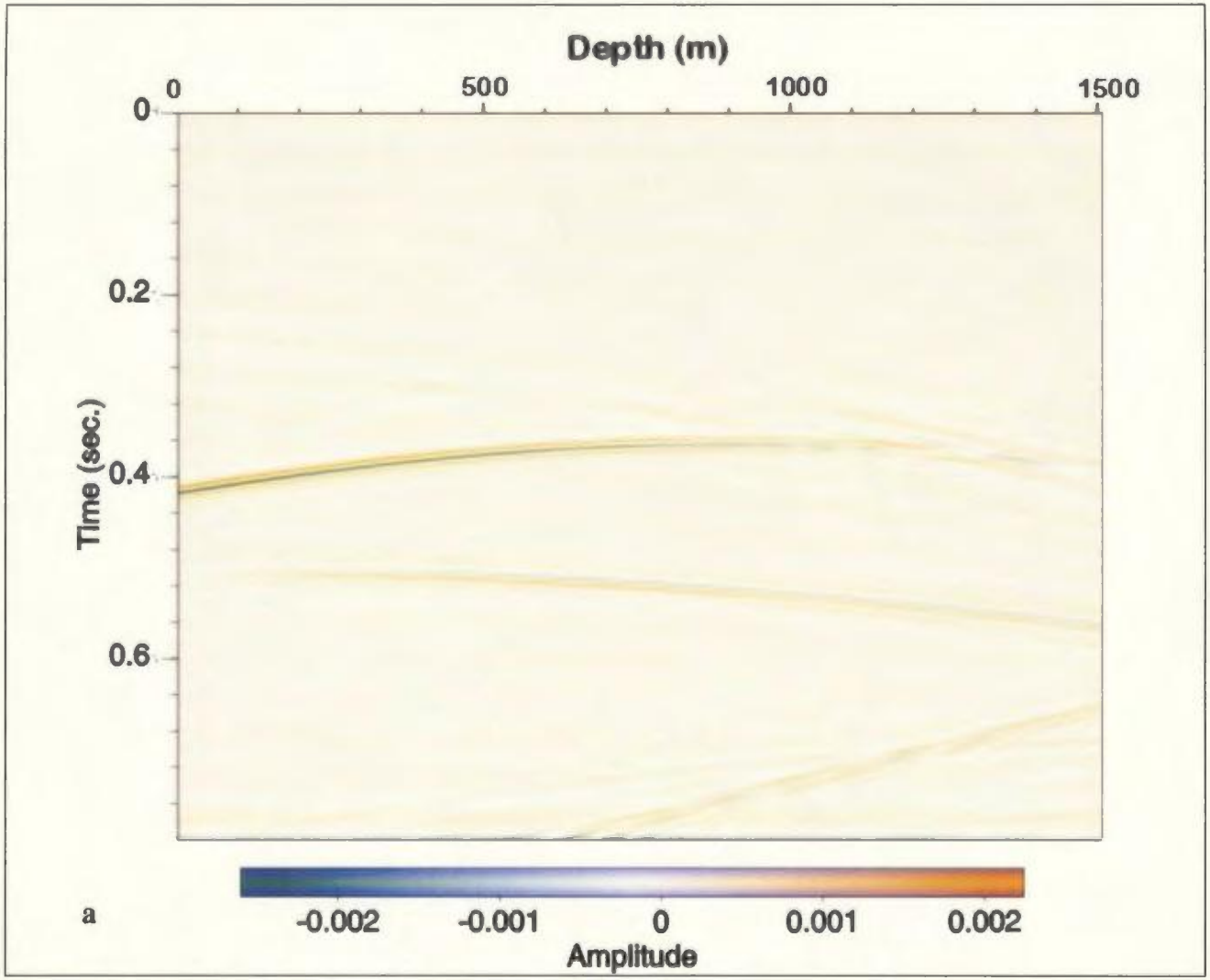

Figure 4-3: a) Shot gather of left VSP after filtering and muting of the direct wave—note how the reflection disappears beyond 230 traces (1150 m) where it has been removed by the muting (compare with Figure 4-2a).

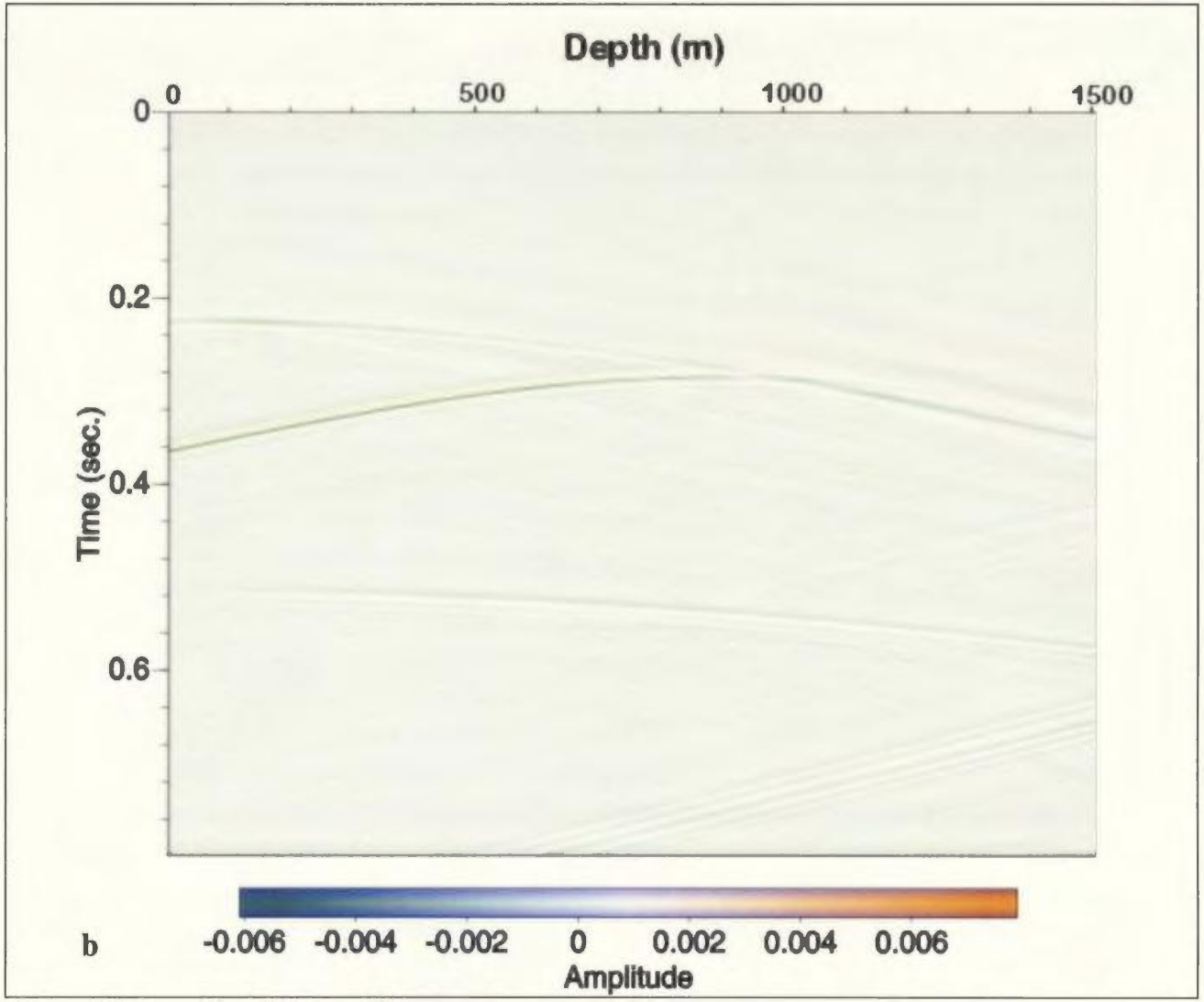

Figure 4-3: b) Shot gather of right VSP after filtering and muting of the direct wave--note also how much of the direct wave has been removed beyond 200 traces (1000 m) (compare with Figure 4-2b).

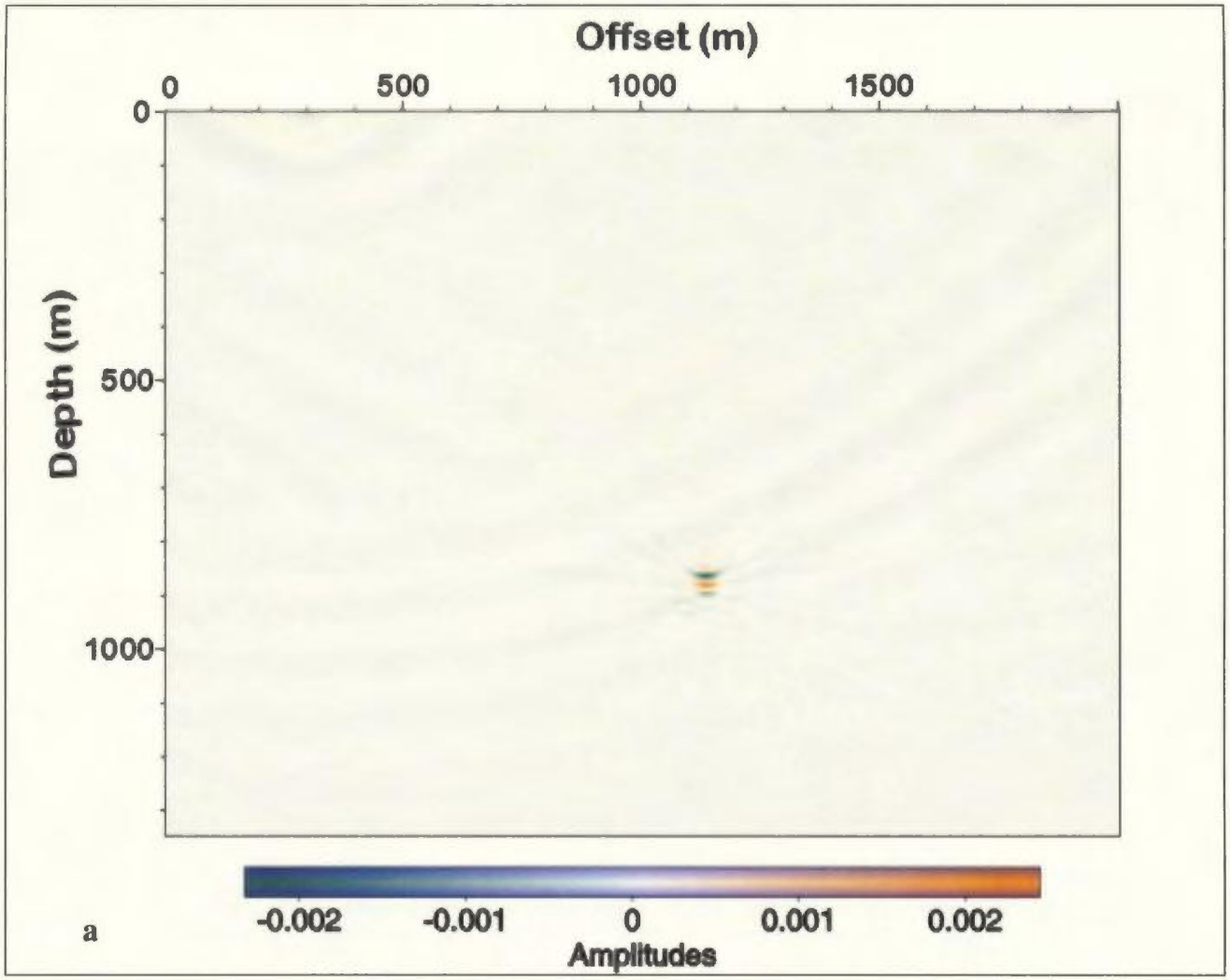

Figure 4-4: a) Migrated image using data from the surface array only.

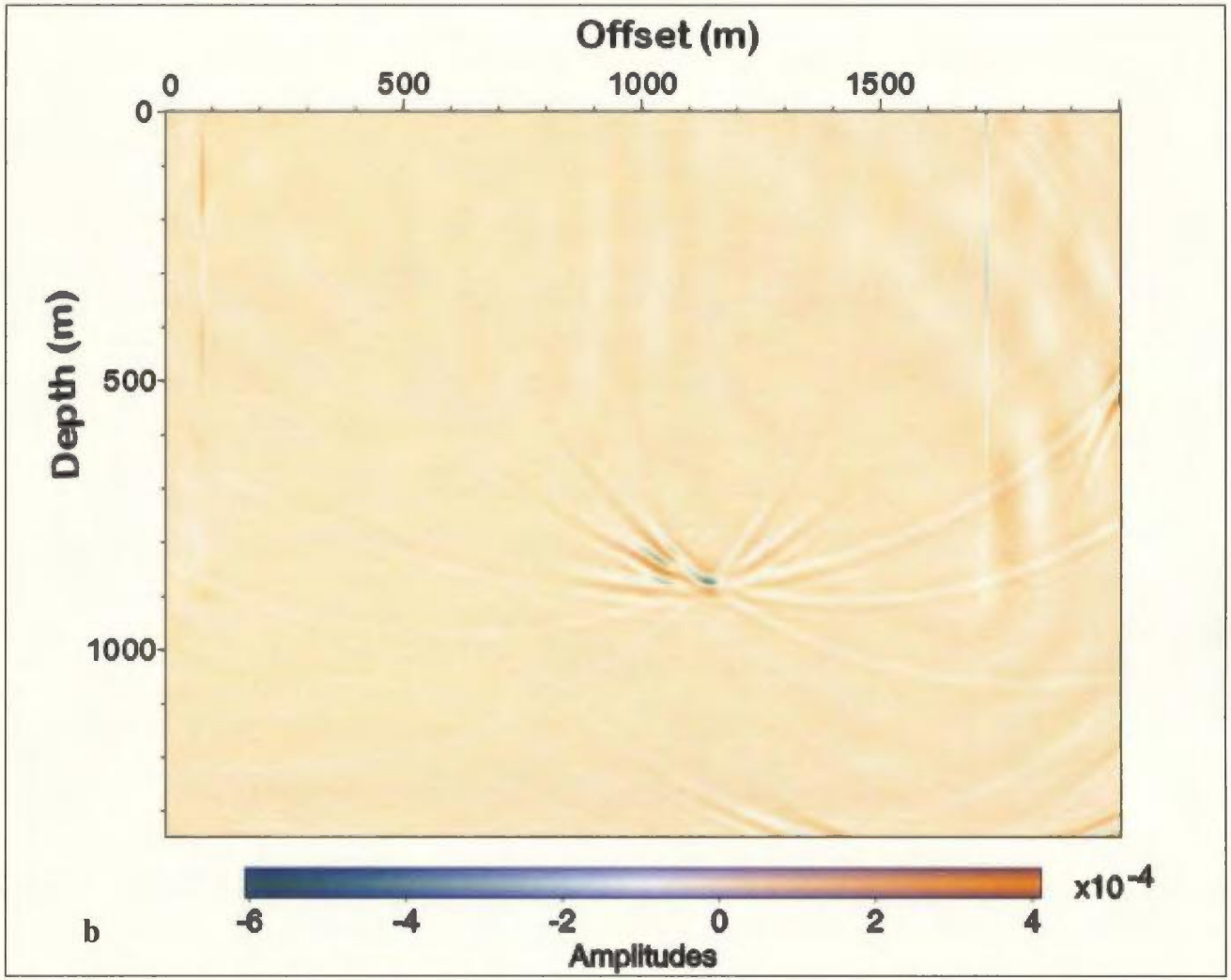

Figure 4-4: b) Migrated image using only data from VSPs.

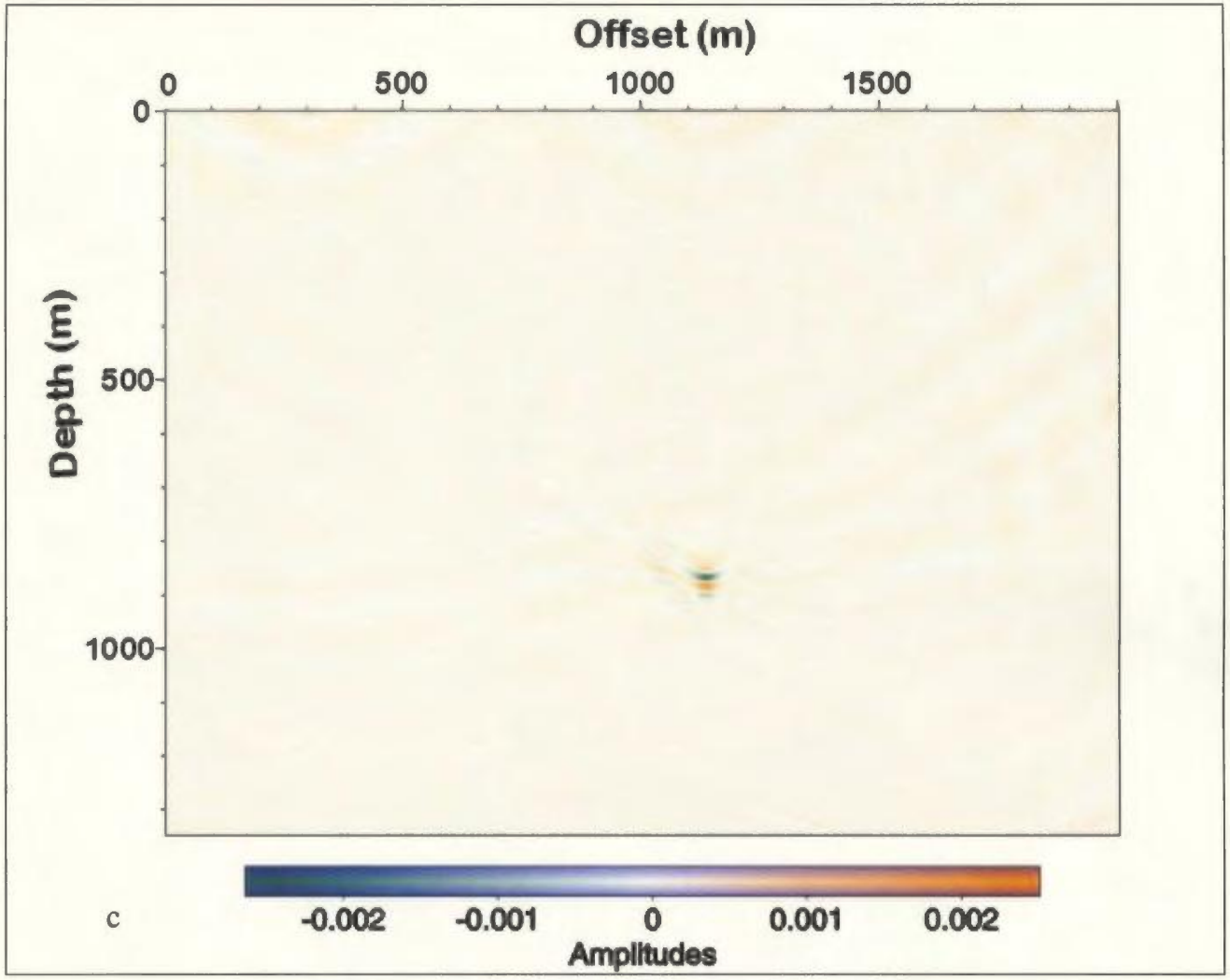

Figure 4-4: c) Migrated image using data from surface and VSP arrays. Note there is no noticeable improvement by including VSP data in the migration, probably due to the elongate nature of the impulse bar model.

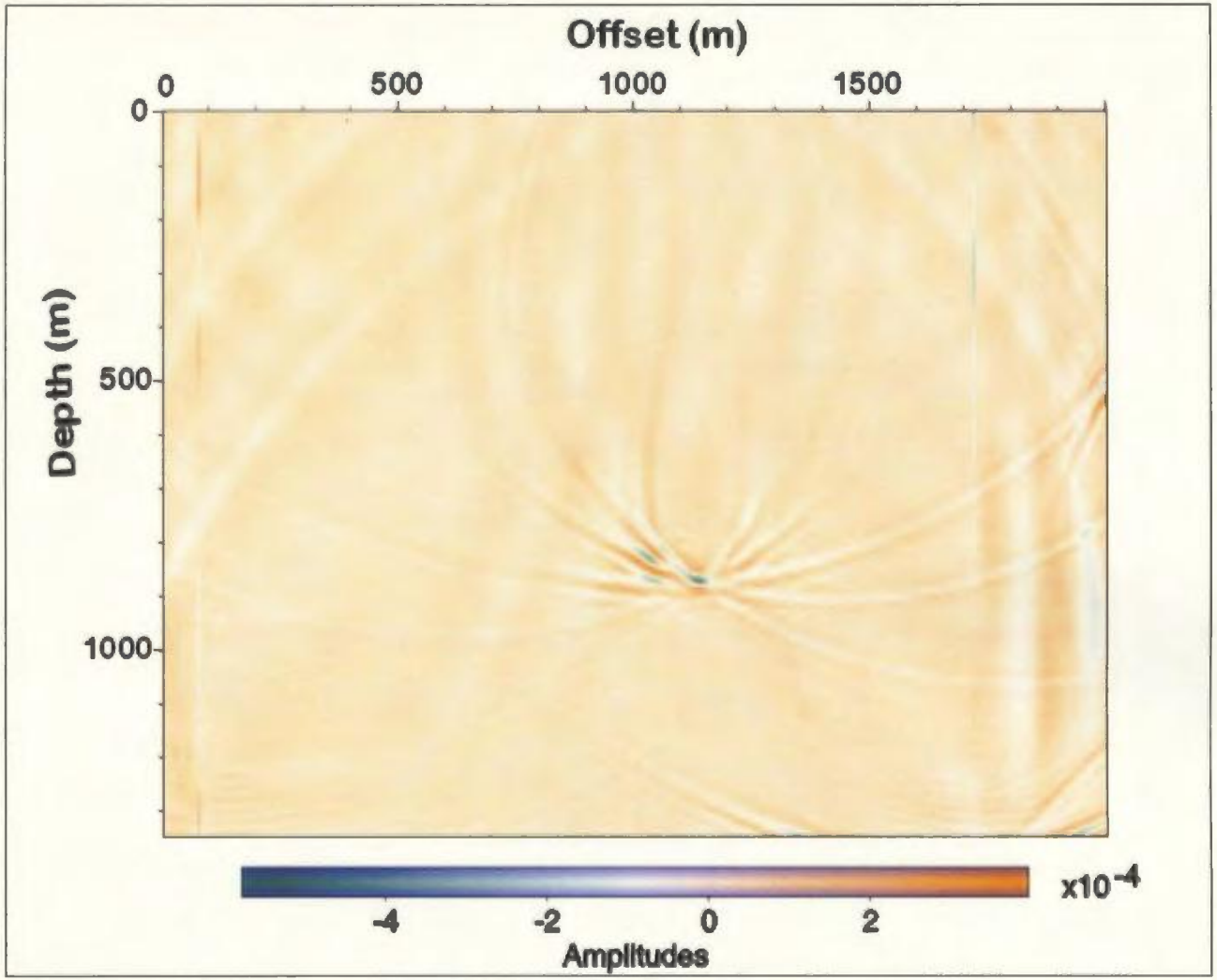

Figure 4-5: Migrated image obtained from surface and VSP data, when the VSPs had been extended in depth to 1500 m. Note the processing artefacts that are not present in Figure 4-4c.

The pre-stack migrated images of the third model (rectangle placed symmetrically in the x-direction in the model space) showed no difference in diffraction tails on the right and left sides of the target object—they are symmetric about the vertical axis of the rectangle (see Figure 4-6). This establishes that the difference in diffraction tails is a result of wave energy attenuation from target object-borehole offset, and not an artefact of the migration algorithm (the evaluation tool).

To ensure the quality of the synthetic seismograms, two models were run to check that the input signal did not degrade significantly as it travelled through the model space. Any such degradation would change the signature of the returned energy. The first test was a rectangle, designed to test the impulse response (30 m wide by 10 m deep rectangle centred at 1135 (x-direction)) at 880 m depth, and the second was an rectangle at 1100 m depth. In raw shot gather (see Figure 4-7a,b) in wiggle trace format, the shallow interface shows a clean Gaussian response to the interface. The deeper interface shows slightly smaller amplitude in the main pulse and some minor ringing after the initial response, but the signal was not altered significantly to be of concern in this study.

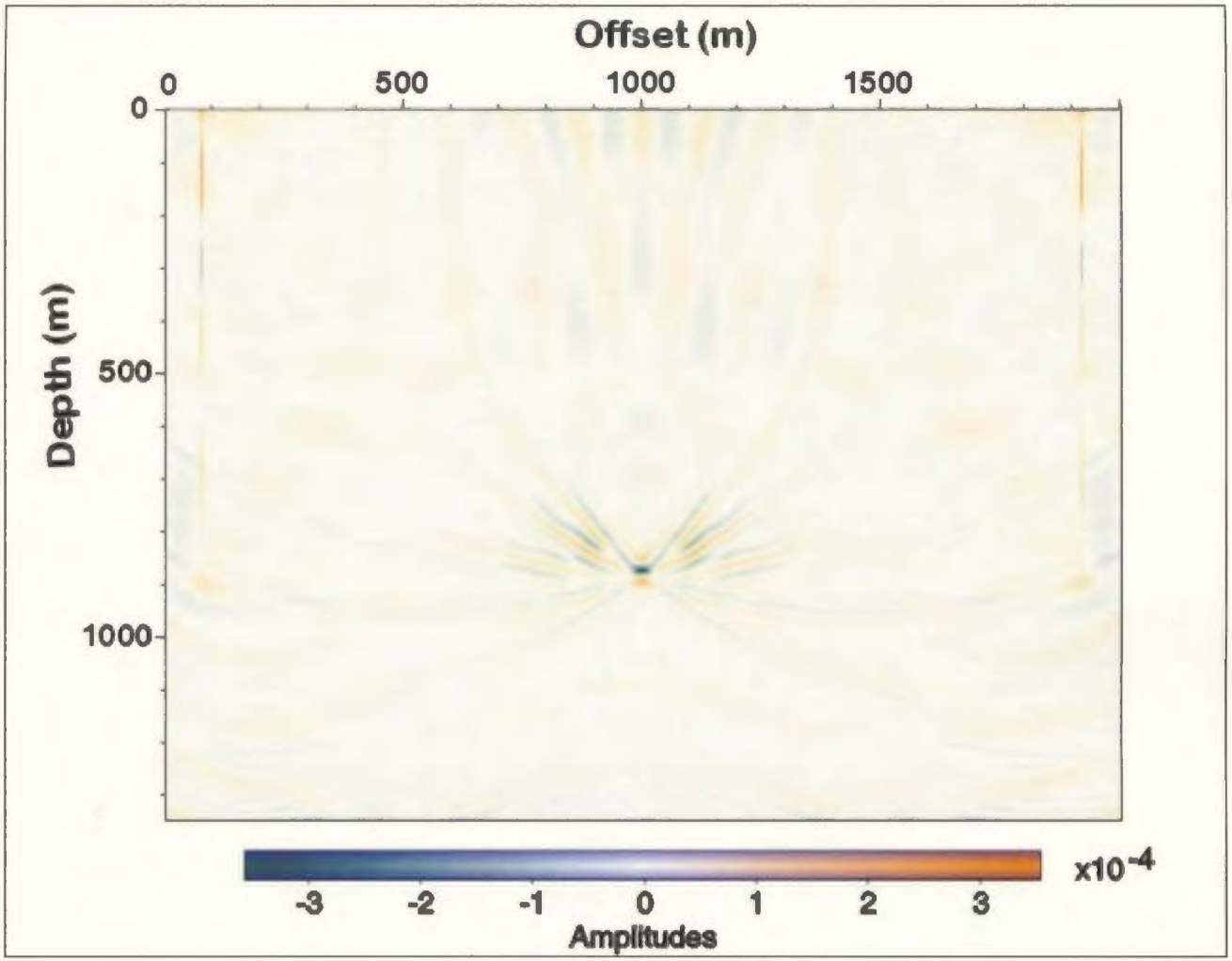

Figure 4-6: Migration image of the impulse bar placed symmetrically between the VSP arrays. Note the migration artefacts on right and left sides of the migrated bar are identical.

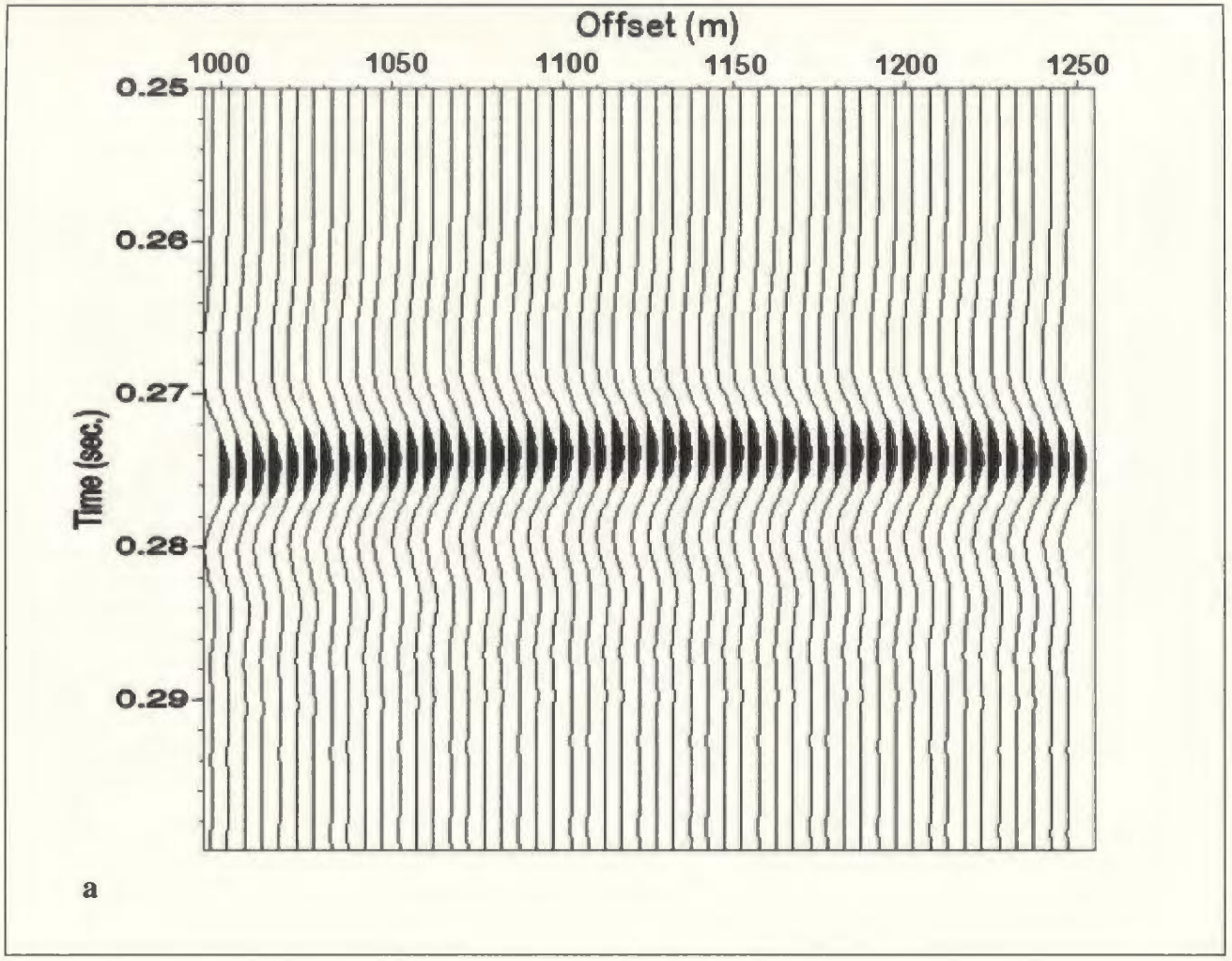

Figure 4-7: Close-up image of the reflection from the impulse bar. a) shows the reflection response from a shallow bar.

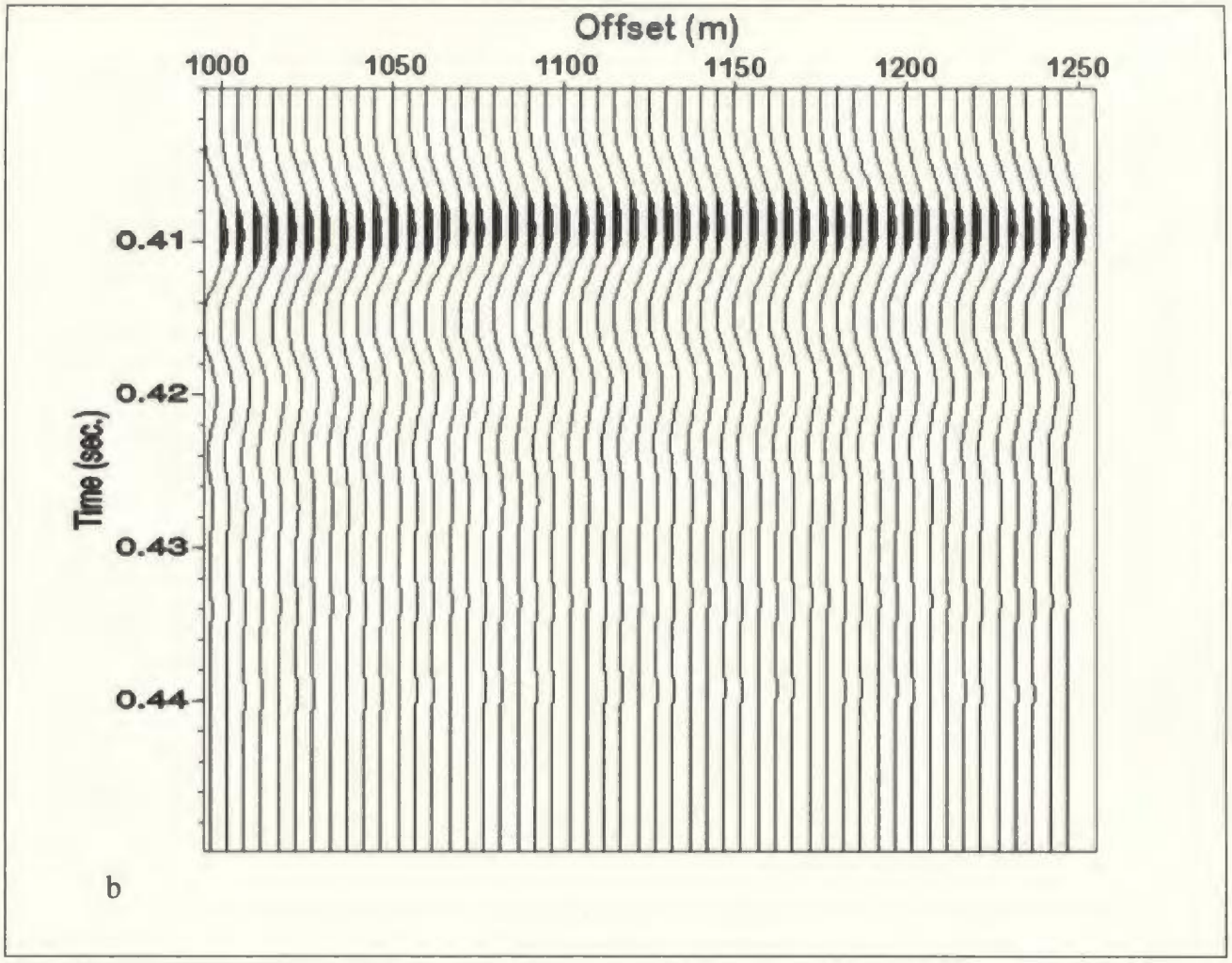

Figure 4-7: Close-up image of the reflection from the impulse bar. b) shows the reflection response from a deep bar. There is no significant change in signal character in b), indicating the synthetic modelling program is stable.

4.1 Octagon

The purpose of this experiment was to explore the seismic response for the octagon as an analogue for the shape of a massive sulphide deposit. Figure 4.1-1 shows the primary model space used in this study. An octagon was used to explore the ability to image a multi-sided object with variable dips. The target object in the standard configuration had a $V_{p\ body}$=5250 m/s and ρ_{body}=4.03 g/cm^3 (the properties of sphalerite, from Salisbury *et al.*, 1996), while the background material had a $V_{p\ bkgrd}$=5800 m/s and ρ_{bkgrd}=2.7 g/cm^3, other configurations will be described below. For each of the models, two vertical arrays of sensors were used, one located at 80 m, the other at 1720 m, and a horizontal array of sensors across the top of the model space. The sensors were spaced at 5 m intervals.

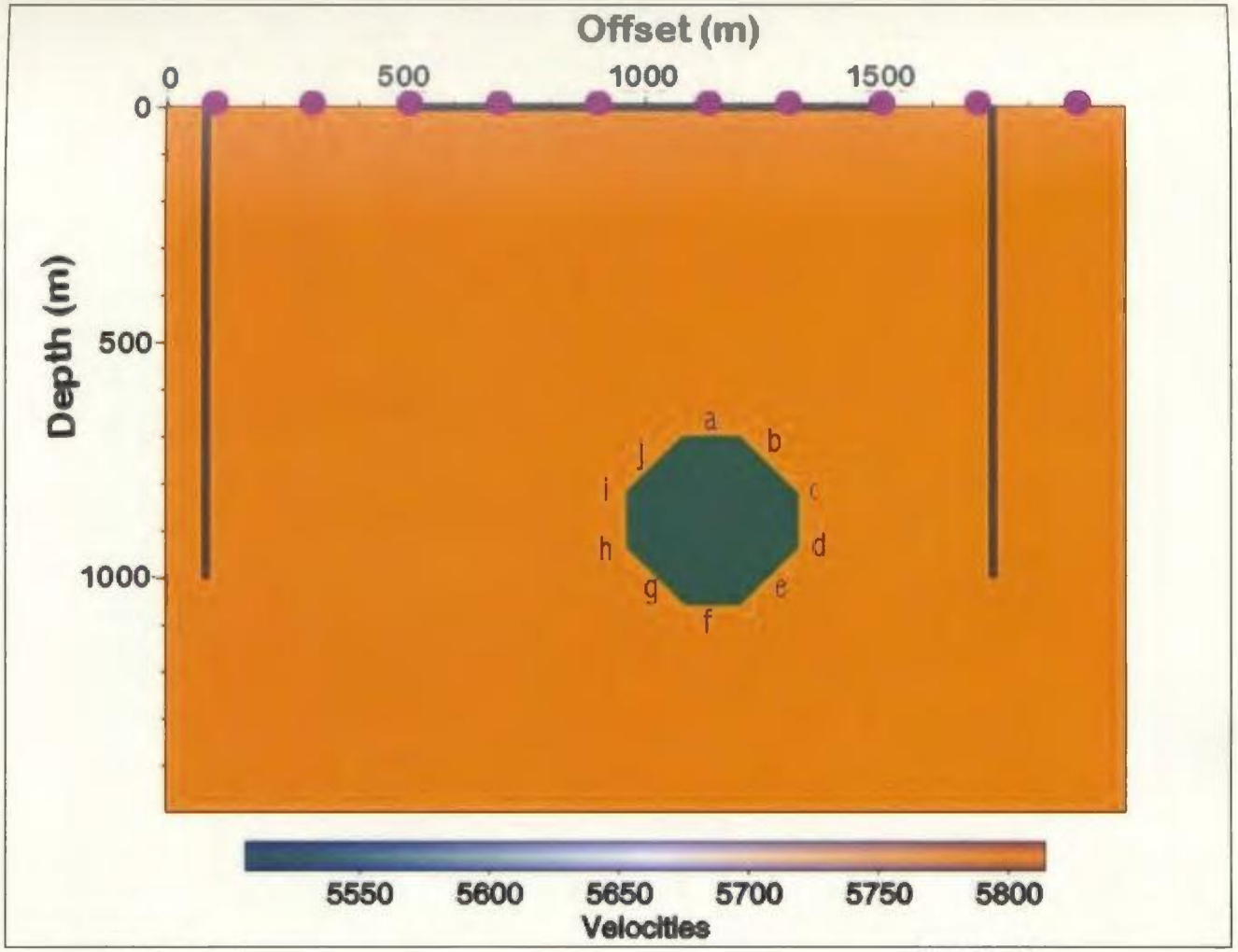

Figure 4.1-1: Model space of the standard octagon. Violet circles indicate shot point locations and black lines indicate locations of the horizontal and VSP arrays. Letters a-j indicate parts of the octagon geometry that have created recognizable reflections in synthetic seismograms (see also Figures 4.1.1-1a, 4.1.1-3b, and 4.1.1-4). Note that c, d, h, and i refer to corners, while all other letters refer to faces of the octagon.

4.1.1 Standard Asymmetric Octagon using Pre-Stack Migration

Figure 4.1-1 shows the standard asymmetric octagon, with faces 125 m long, top face centred at 1140 m horizontally (x) and 720 m vertically (z). This configuration was chosen to examine the response recorded by the borehole sensors at two different offsets (~400 m and ~800 m) as well as horizontal long and shorter offset recordings. Figure 4.1.1-1a,b show a normal-incidence shot gather (shot located at 1140 m) in raw (a) and processed (b) forms as recorded by the horizontal sensor array. Figure 4.1.1-1a clearly shows the direct wave, and very faint reflections from the sides of the model space, which are numerical artefacts as a result of imperfectly-absorbing boundary conditions. In Figure 4.1.1-1a, we have labelled the visible reflections that have been interpreted as follows: a is the top of the octagon; f is the bottom (note the polarity of the signal is reversed compared to a); c is the top corner of the right vertical face; d is the bottom corner of the right vertical face; h is the bottom corner of the left vertical face; and i is the top corner of the left vertical face. In this case, the highest amplitudes occur directly below the shotpoint as a result of the horizontal specular reflectors (top and bottom faces of the octagon).

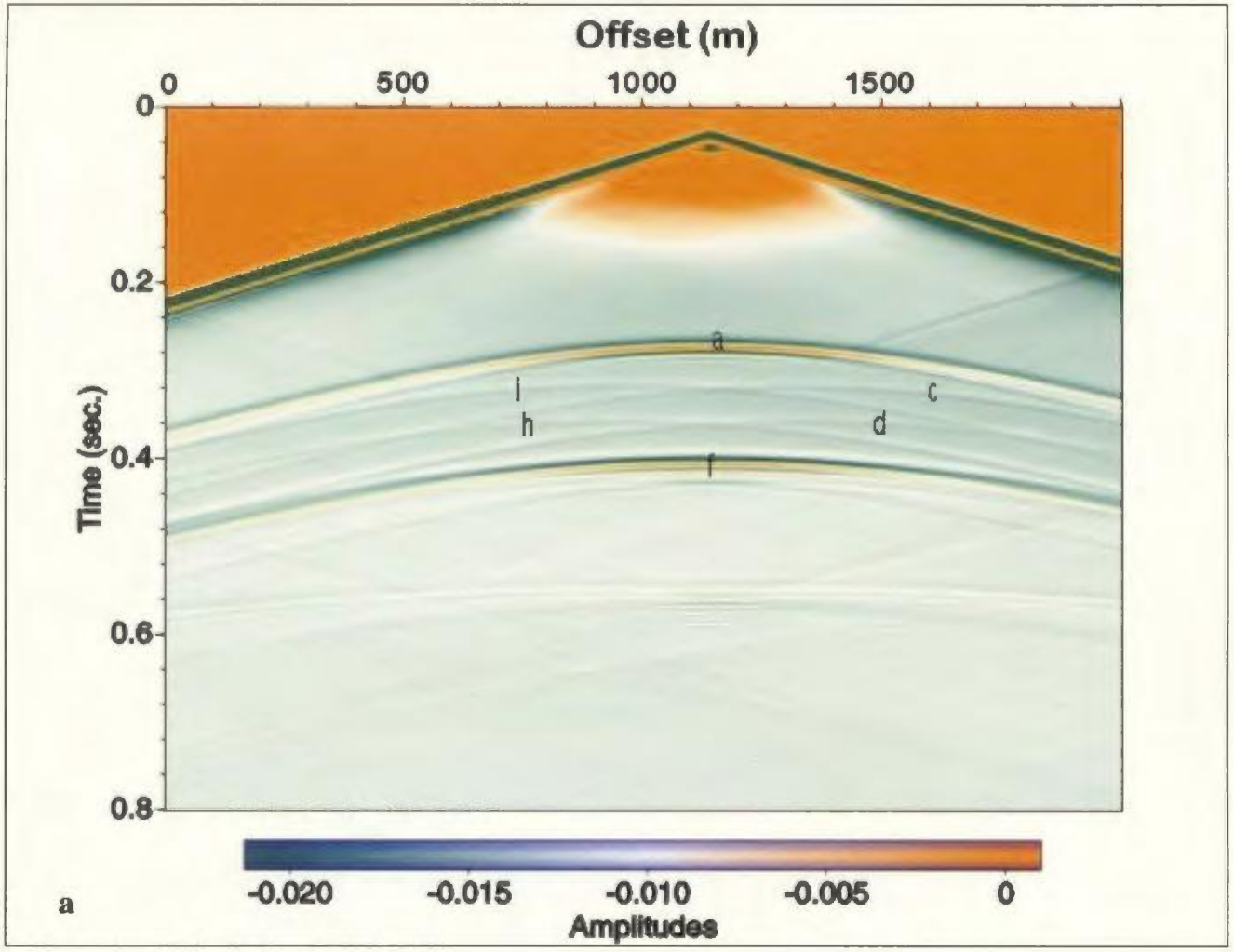

Figure 4.1.1-1: a) Raw shot gather from horizontal seismic array, shot at 1140 m. The direct wave and reflections from the top, bottom and corners of vertical sides of the octagon are clearly visible and labelled (compare with Figure 4.1-1).

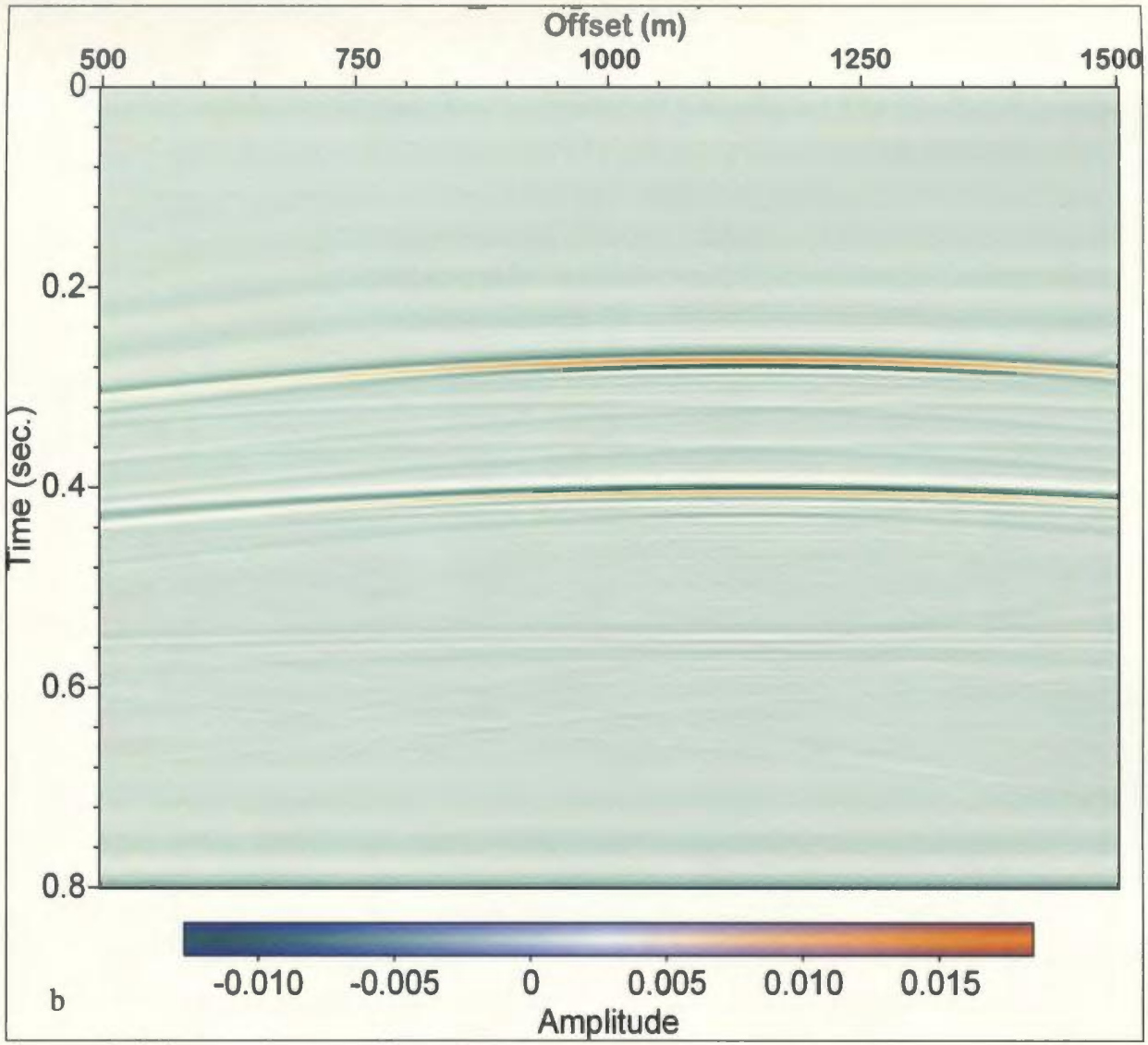

Figure 4.1.1-1: b) Processed shot gather (same as Figure 4.1.1-1a) from horizontal seismic array, shot at 1140 m.

Figure 4.1.1-2a,b shows the horizontal seismic profile recorded from shotpoints at 300 m and 1900 m, respectfully, and these indicate that as the shot-target object offset increases, two high-amplitude zones develop: one at near normal incidence to the shotpoint, and the other on the diffraction tail on the opposite side (horizontally) of the body from the shotpoint. This is supported by observations from the right VSP shot records (see Figure 4.1.1-3a,b,c) that show clearly that as the offset of the shot increases, the zone of high amplitude shifts from the shallow traces to deeper ones, with a secondary high amplitude zone at the deeper end of the diffraction for near offset shots, and at the shallower end for far offset shots. Figure 4.1.1-4 is a shot record from the left VSP (almost twice the distance from the anomalous body as the right VSP) showing it does not record the diffractions and reflections with as high an amplitude, but it does have some advantages in that the recorded events are better separated and therefore may be easier to identify as distinct events. Notice that all VSP records of the octagon shown thus far have included the full depth of the model space (1500 m). It is unlikely (and unrealistic) that many boreholes in mining exploration would extend this deep and therefore this study used only the top 200 traces (1000 m) of each VSP record for migration purposes (with one exception discussed below). Additionally, migrations are usually performed with apertures limited to include energy only from expected directions, which acts to reduce migration artifacts (Payne *et al.*, 1994). As a general rule in surface seismic exploration for hydrocarbons, the surface spread length is approximately equal to the depth of interest and only the centre 1000 m (200 traces) of the surface seismic data were included in the pre-stack migration.

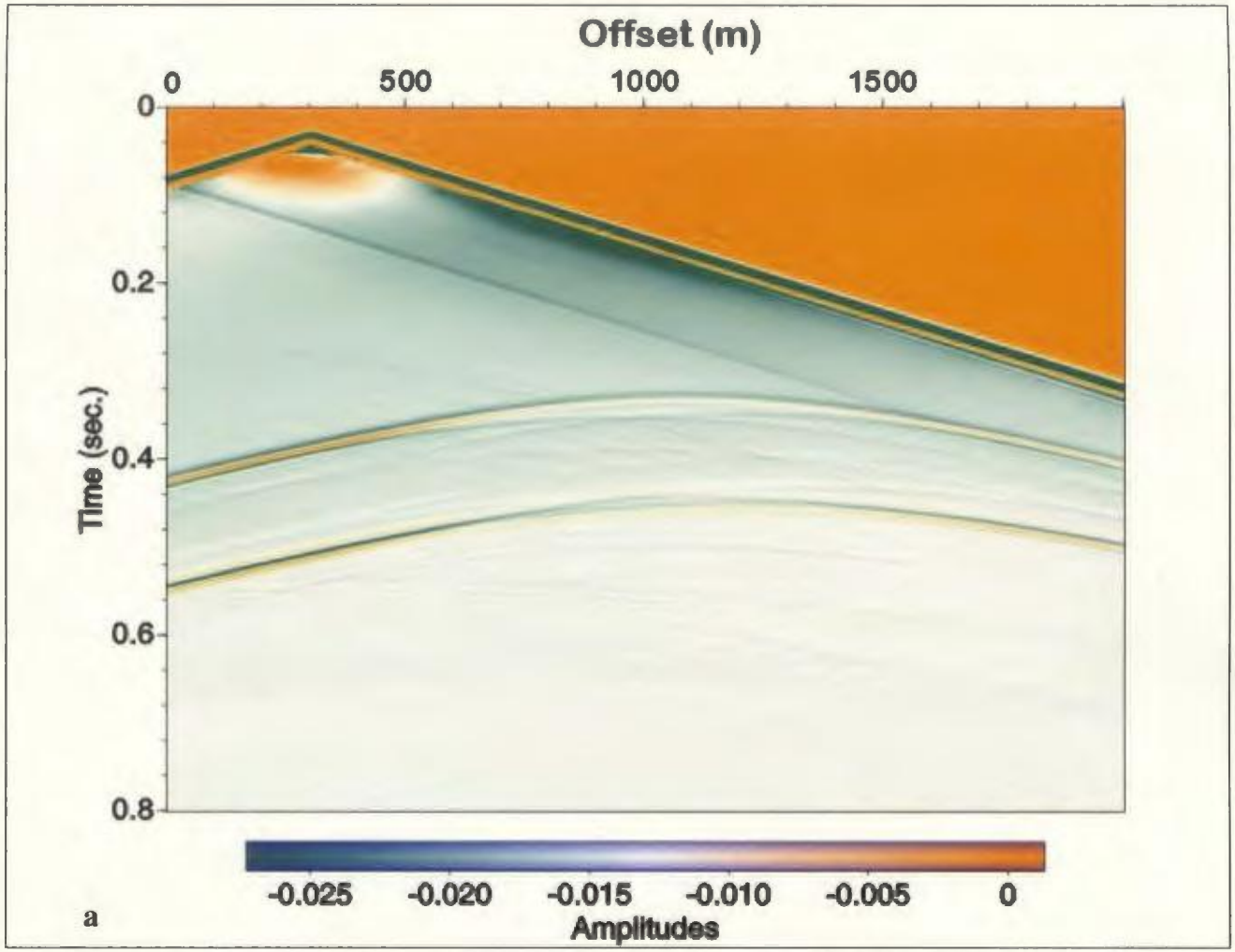

Figure 4.1.1-2: a) Raw shot gather from the horizontal seismic array, with shotpoint at 300 m. Note the change in location of the high-amplitude zones compared with Figure 4.1.1-1a—as the offset increases, high-amplitude zones develop at the ends of the reflection tail, instead of at the centre.

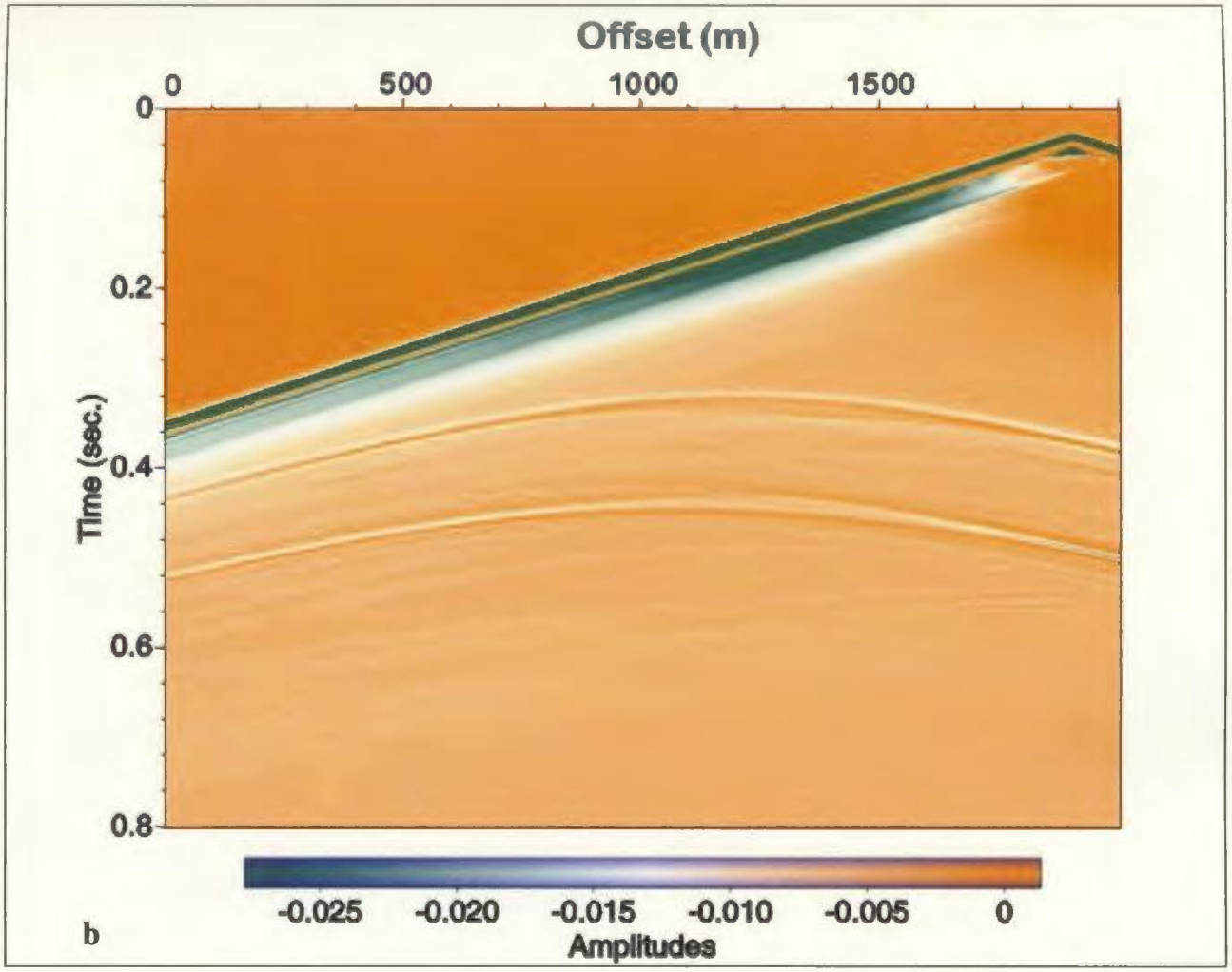

Figure 4.1.1-2: b) Raw shot gather from the horizontal seismic array, with the shotpoint at 1900 m. Note the change in location of the high-amplitude zones compared with Figure 4.1.1-1a—as the offset increases, high-amplitude zones develop at the ends of the reflection tail, instead of at the centre.

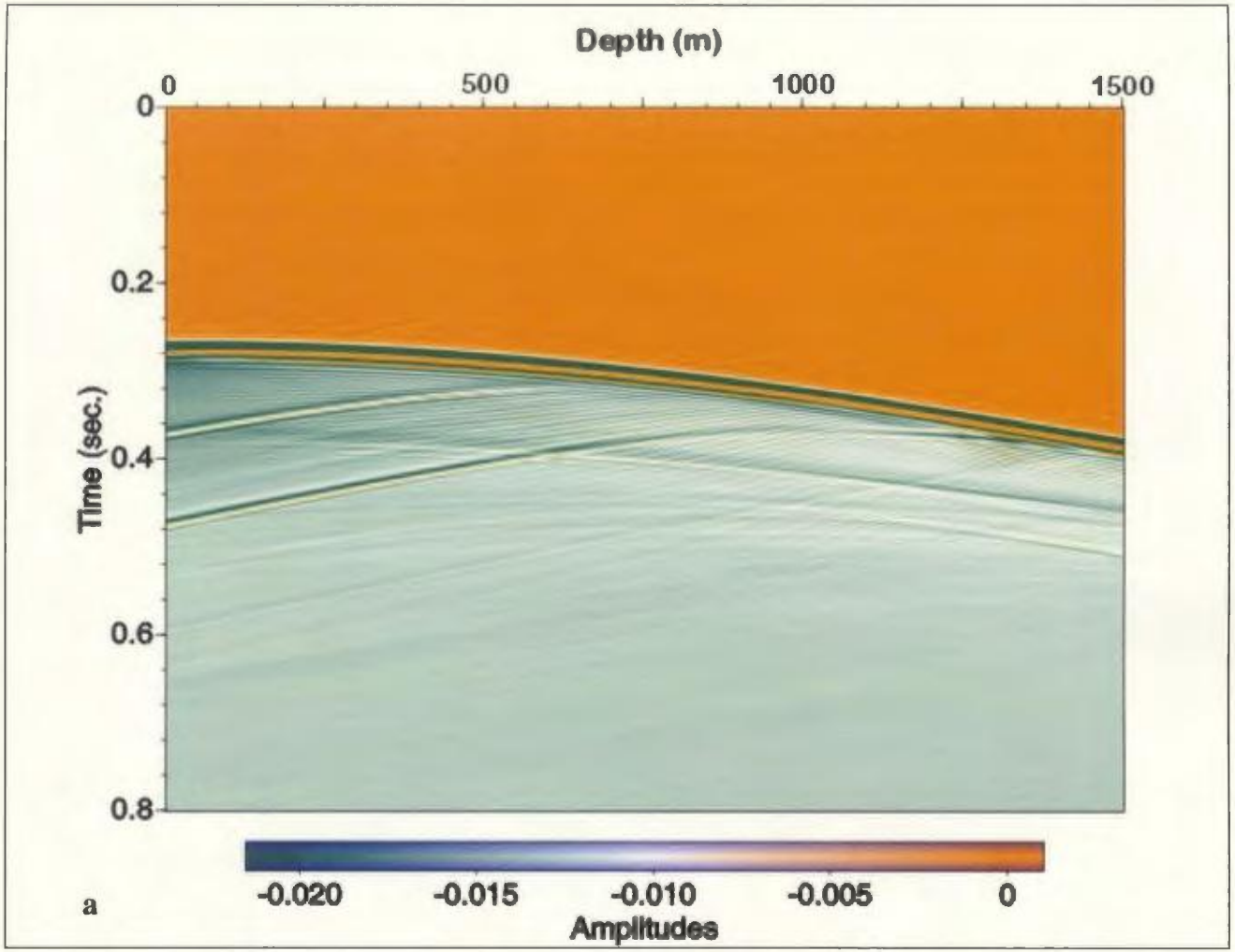

Figure 4.1.1-3: a) Shot gather from the right VSP, shot at 300 m. Note the high-amplitude zone on shallow traces. Note how on deeper traces, reflections combine with the direct wave, especially deeper than 1000 traces.

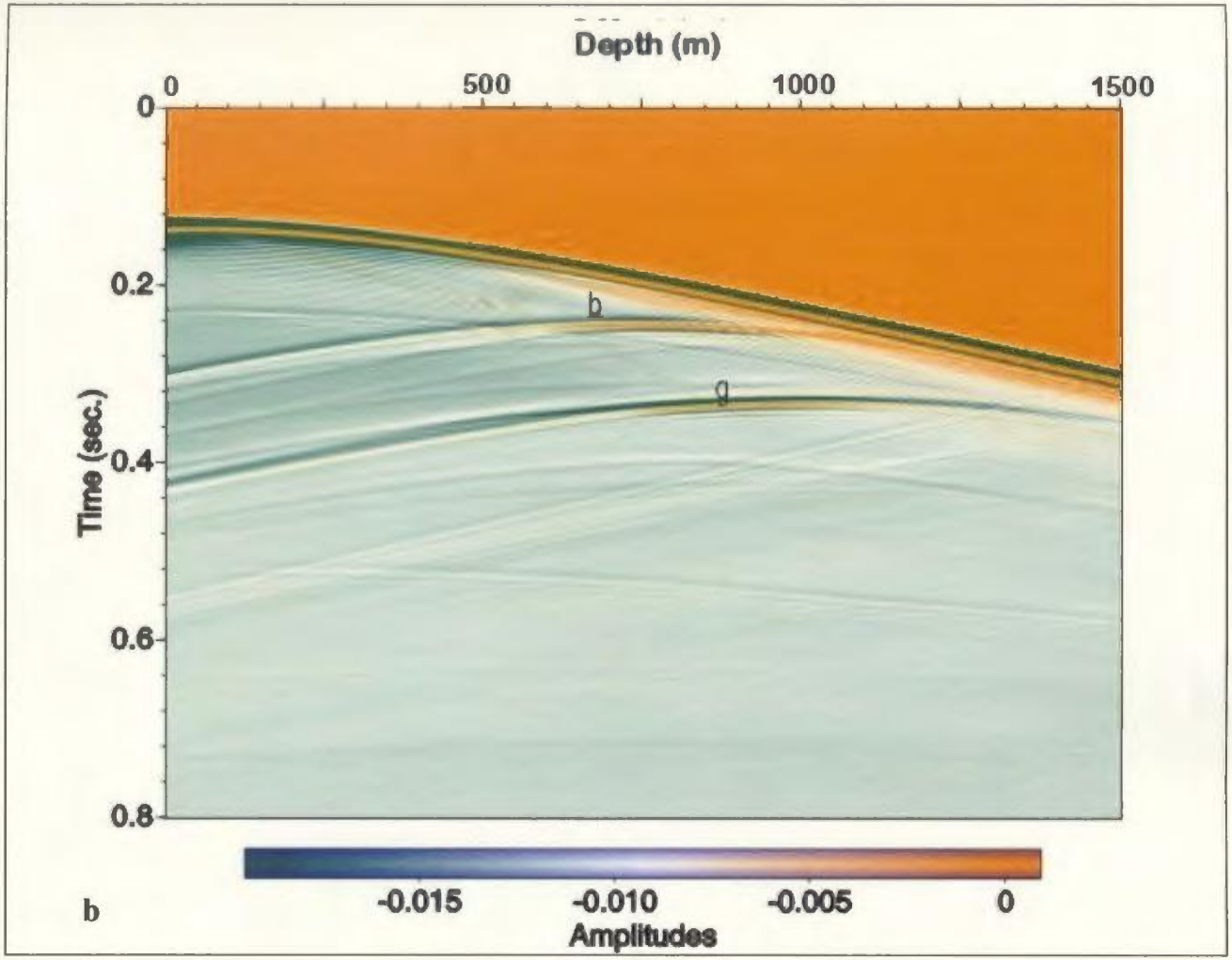

Figure 4.1.1-3: b) Shot gather from the right VSP with shot location at 1140 m. The strong reflections are interpreted to be from faces of the octagon (letters are indicated on Figure 4.1-1) with normals directed into the right VSP array.

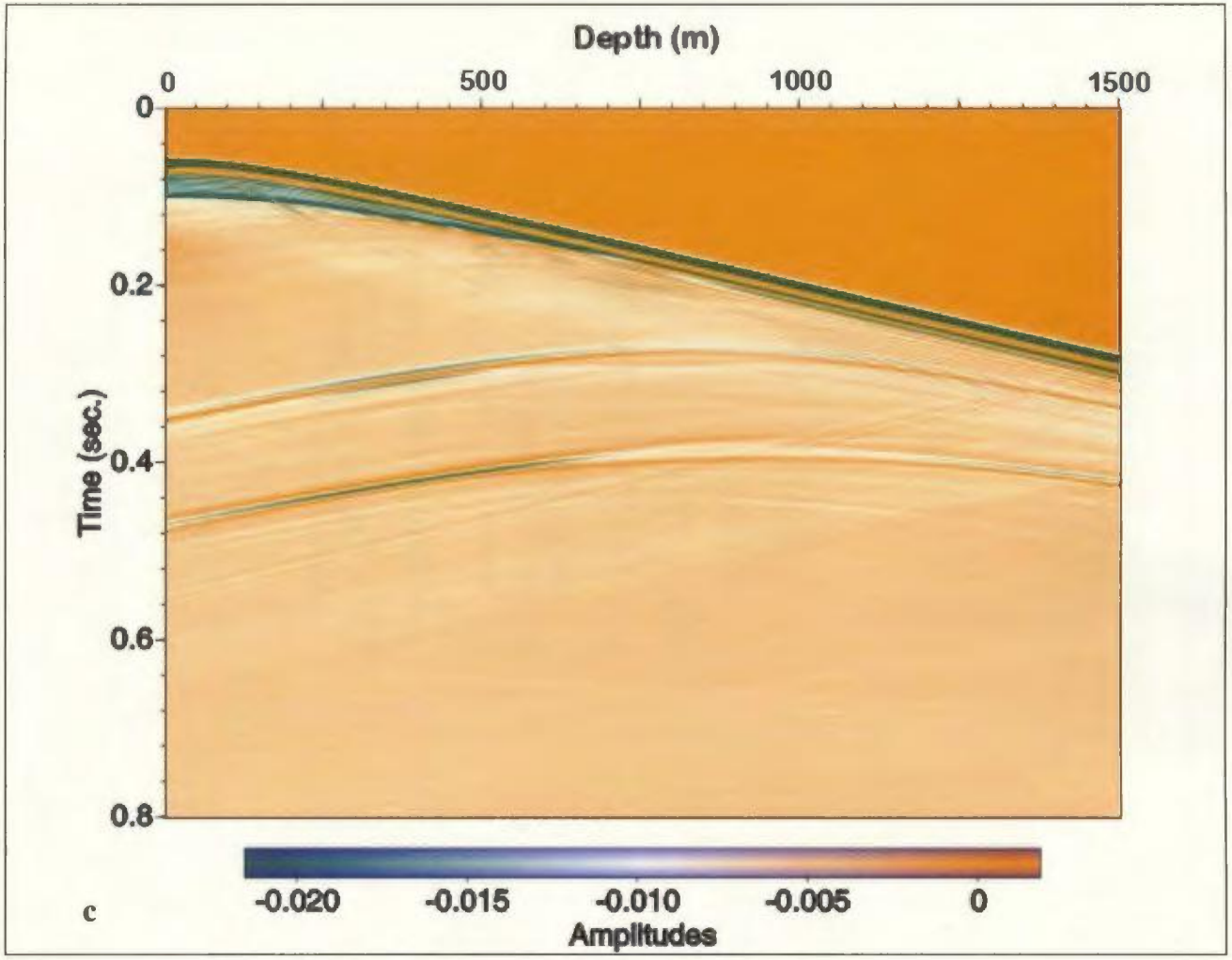

Figure 4.1.1-3: c) Shot gather from the right VSP with shot location at 1900 m.

The VSP records (see Figures 4.1.1-3b and 4.1.1-4) (at shotpoint=1140 m) from each side clearly show the direct wave, a weak reflection of the direct wave from the model edge (as a result of the imperfectly-absorbing boundary conditions), and reflections from the top near dipping flank and bottom far dipping flank that direct the energy into the seismic array (i.e., for the right VSP, they correspond to faces b and g from Figure 4.1-1, and for the left VSP, they correspond to faces e and j from Figure 4.1-1). Other, weaker diffractions are also visible but it is difficult to determine their origin. By using only the top 200 traces of the VSPs, we lose some information about the deeper dipping flank (either face e or g depending on which VSP is used) but clearly very little data is lost and is still usable as shown by comparing Figures 4.1.1-4 and 4.1.1-5.

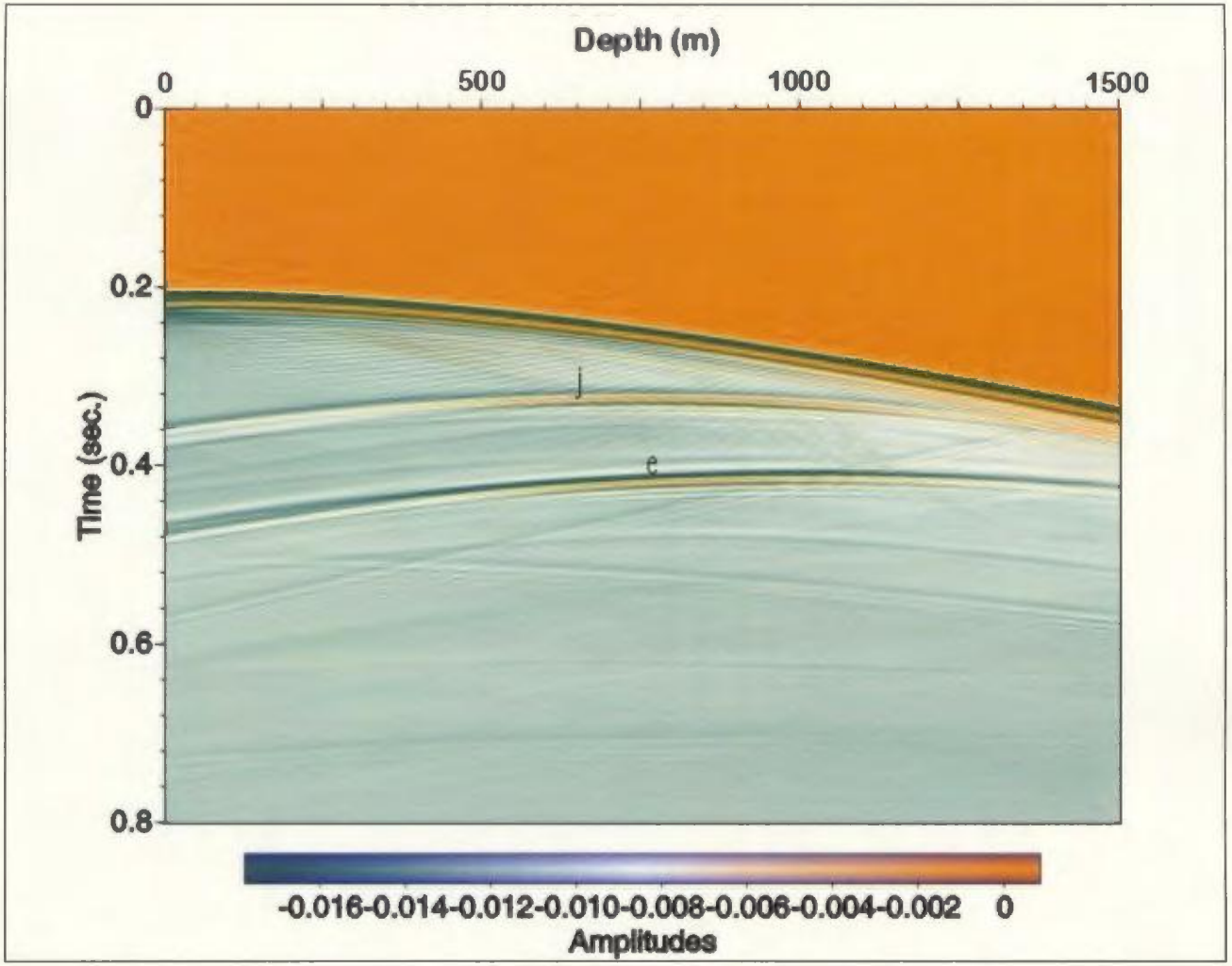

Figure 4.1.1-4: Raw shot gather from the left VSP, shot location at 1140 m. Letters indicate interpreted parts of the geometry from Figure 4.1-1.

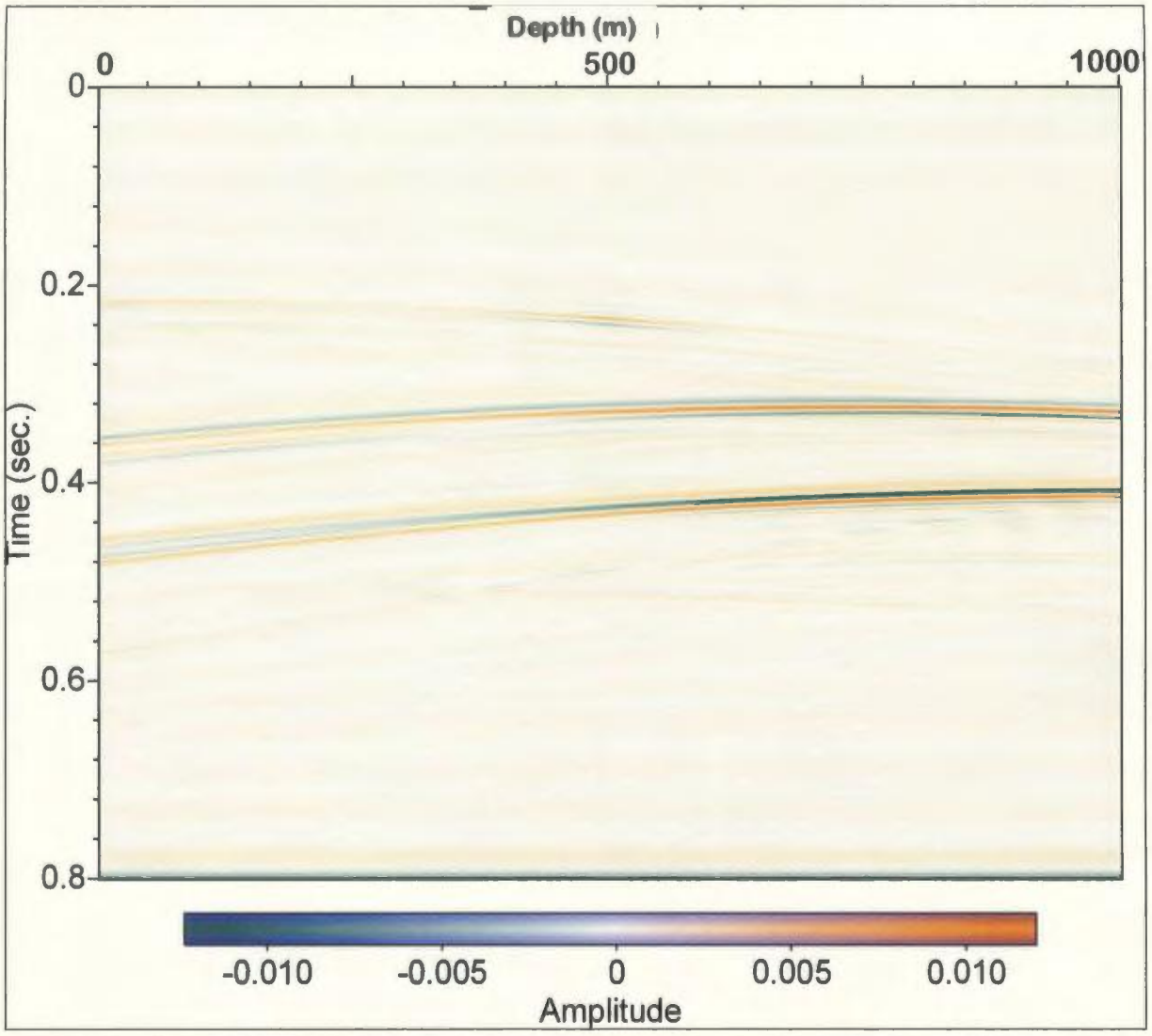

Figure 4.1.1-5: Processed shot record from the left VSP, shotpoint at 1140 m. Note the deepest 100 traces have been removed, compare this data with Figure 4.1.1-4.

Figure 4.1.1-6a is a pre-stack depth migrated image of the standard asymmetric octagon, using only 3 shotpoints (at 300 m, 1140 m, and 1900 m), the shallowest 200 traces from the VSPs, and the centre 200 horizontal profile sensors (from 500 m to 1500 m in the x-direction). The top and bottom of the octagon and all four of the dipping sides are well imaged, with the left-dipping sides being clearer than the right-dipping ones, and the vertical faces are missing altogether. Figure 4.1.1-6b is a pre-stack depth migrated image of the standard octagon using only horizontal profile records (as described above) and shows clearly the top and bottom of the octagon while the dipping faces are less well-defined, and the vertical faces are not imaged at all. Figure 4.1.1-6c is a pre-stack depth migrated image of the standard octagon using only the VSP records (as described above), clearly showing that all the dipping sides were well-imaged, while the top, bottom, and vertical sides are missing

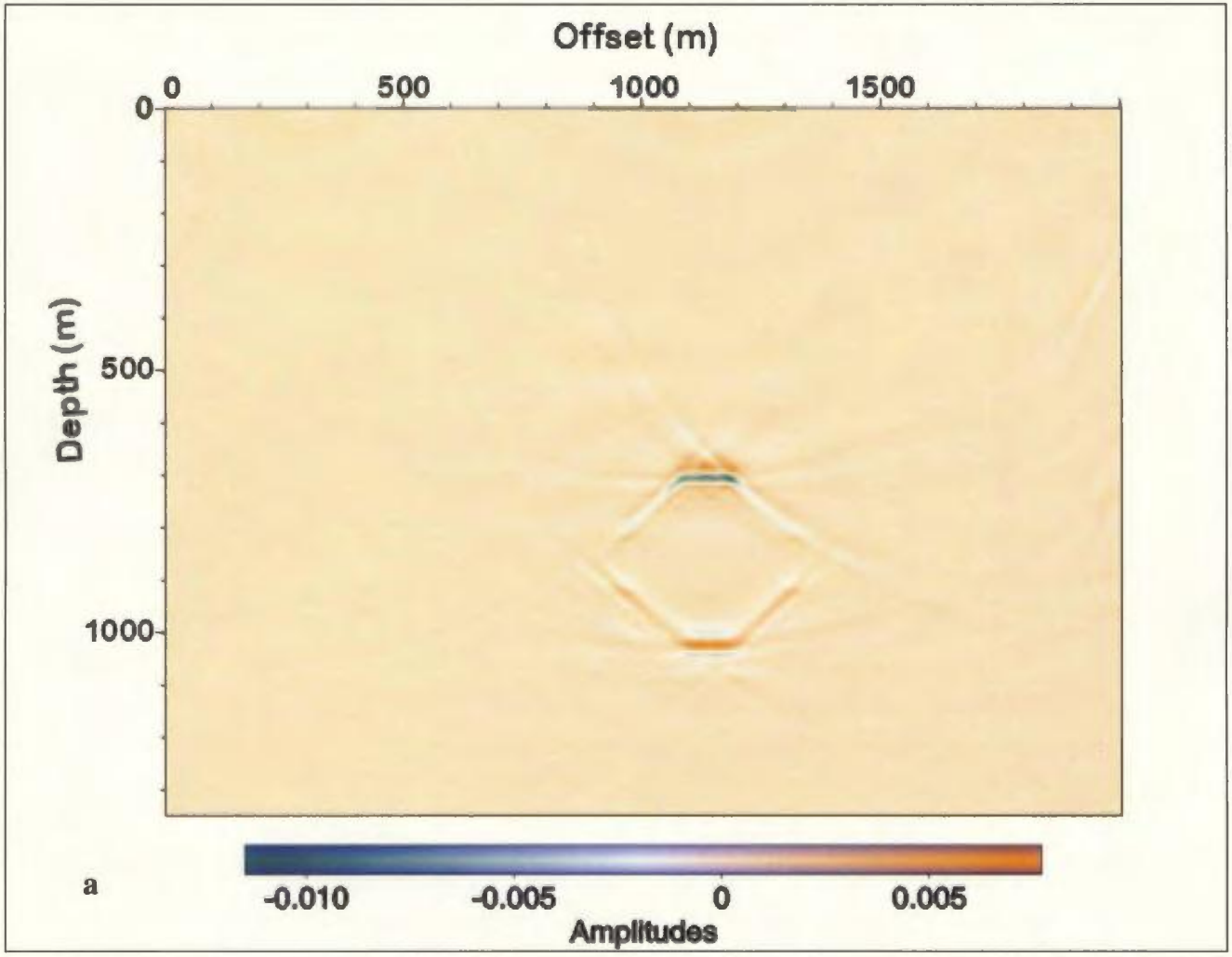

Figure 4.1.1-6: a) Migrated image of the octagon, using surface and VSP data together, from 3 shots across the model space.

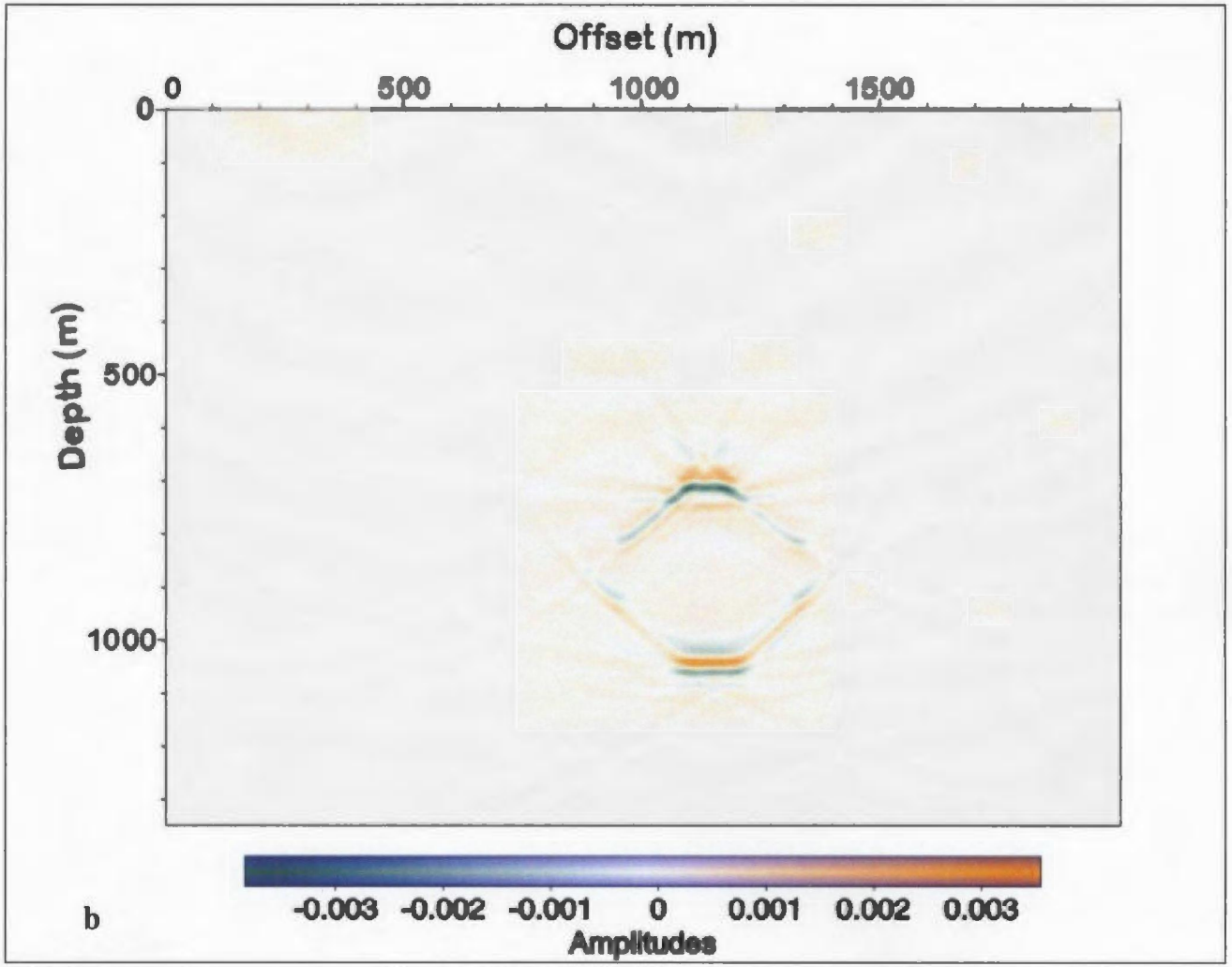

Figure 4.1.1-6: b) Migrated image of the octagon, using only data from the surface profile from 3 shots across the model space.

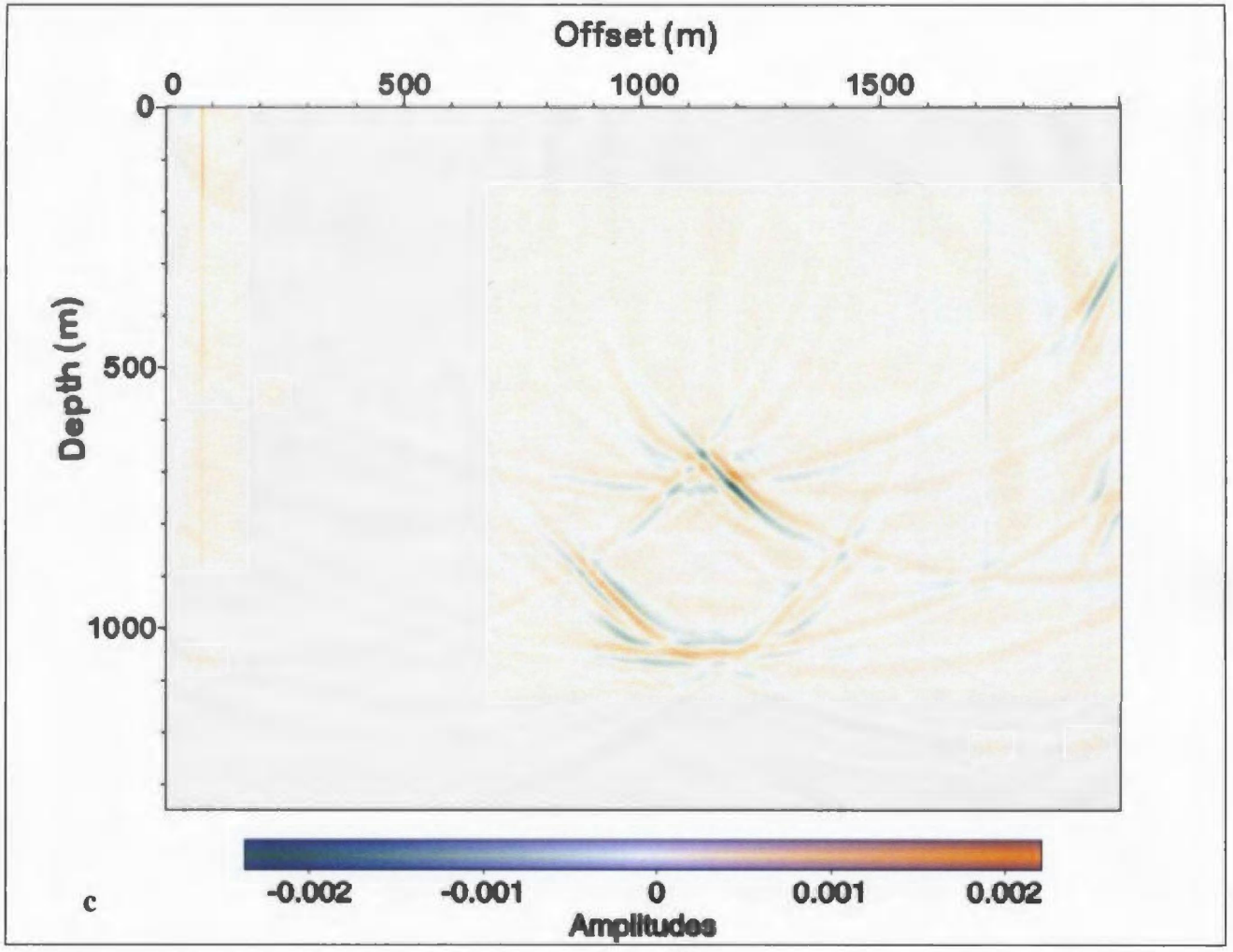

Figure 4.1.1-6: c) Migrated image of the octagon, using only data from the VSPs, from 3 shots across the model space. Note there is no significant difference in image quality between a) and b).

completely. Therefore, the horizontal profile is needed to image horizontal faces, and the long-offset on the left side of the target object allows the horizontal profile to catch energy from left-dipping faces, while the VSPs bring definition to all the dipping faces, especially the right-dipping ones that are not recorded as well in the horizontal profile (due to the shorter offset recording aperture). Figures 4.1.1-7a,b show a pre-stack depth migrated image of ten shots across the model space (at 200 m spacing) using only the horizontal profile (7a), and both horizontal and VSPs (7b). It should be noted that this migration took only 7 minutes of computational time running as a parallel code on 14 processors. Clearly from comparing Figures 4.1.1-7a and b, there appears to be no real advantage to including the VSP data in the pre-stack depth migration, which is disappointing and counter-intuitive. Perhaps the problem lay with the highly idealized model space and this possibility is examined further in Sections 4.1.5 and 4.1.6.

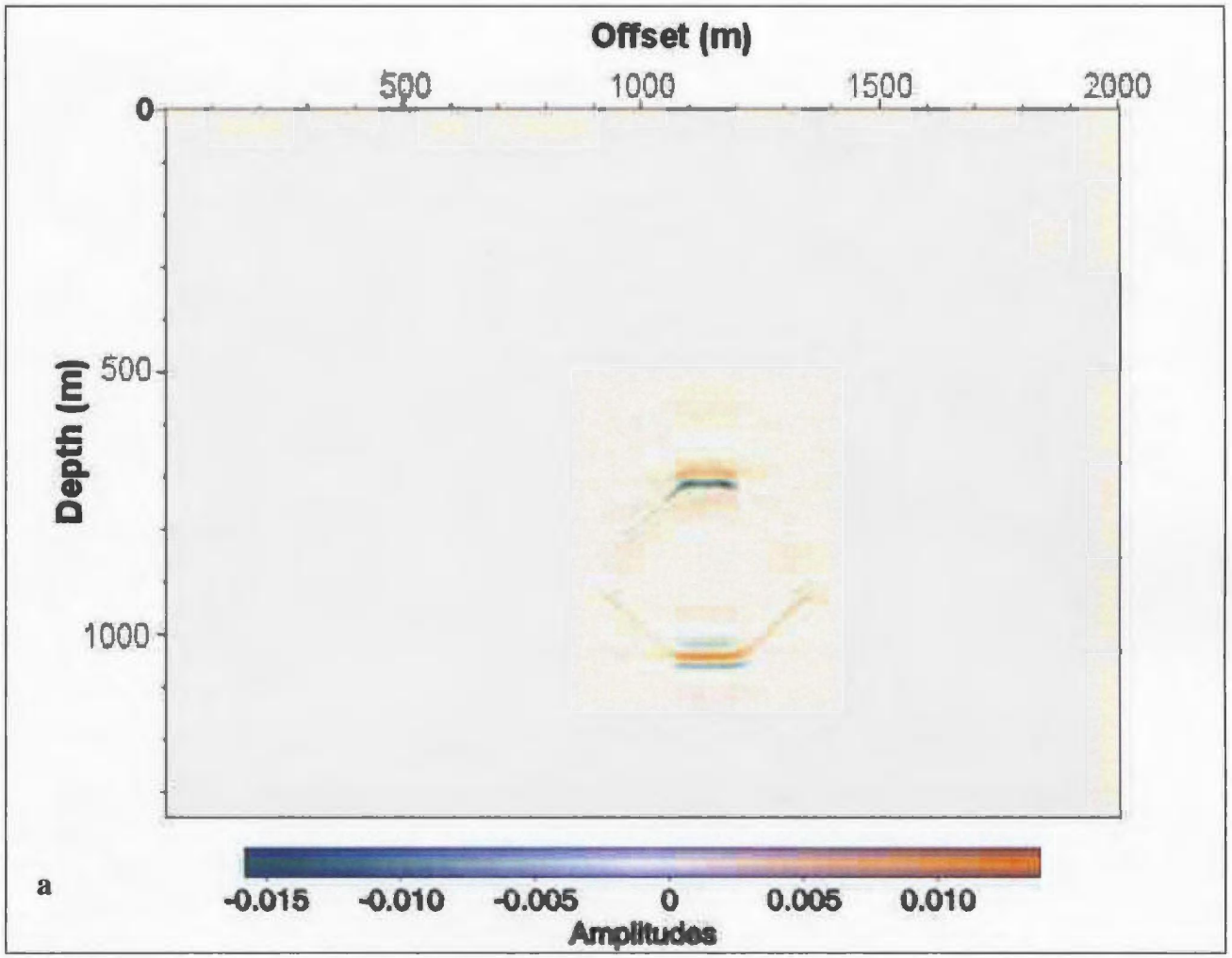

Figure 4.1.1-7: a) Migrated image of the octagon using 10 shots across the model and including only data from the surface profile.

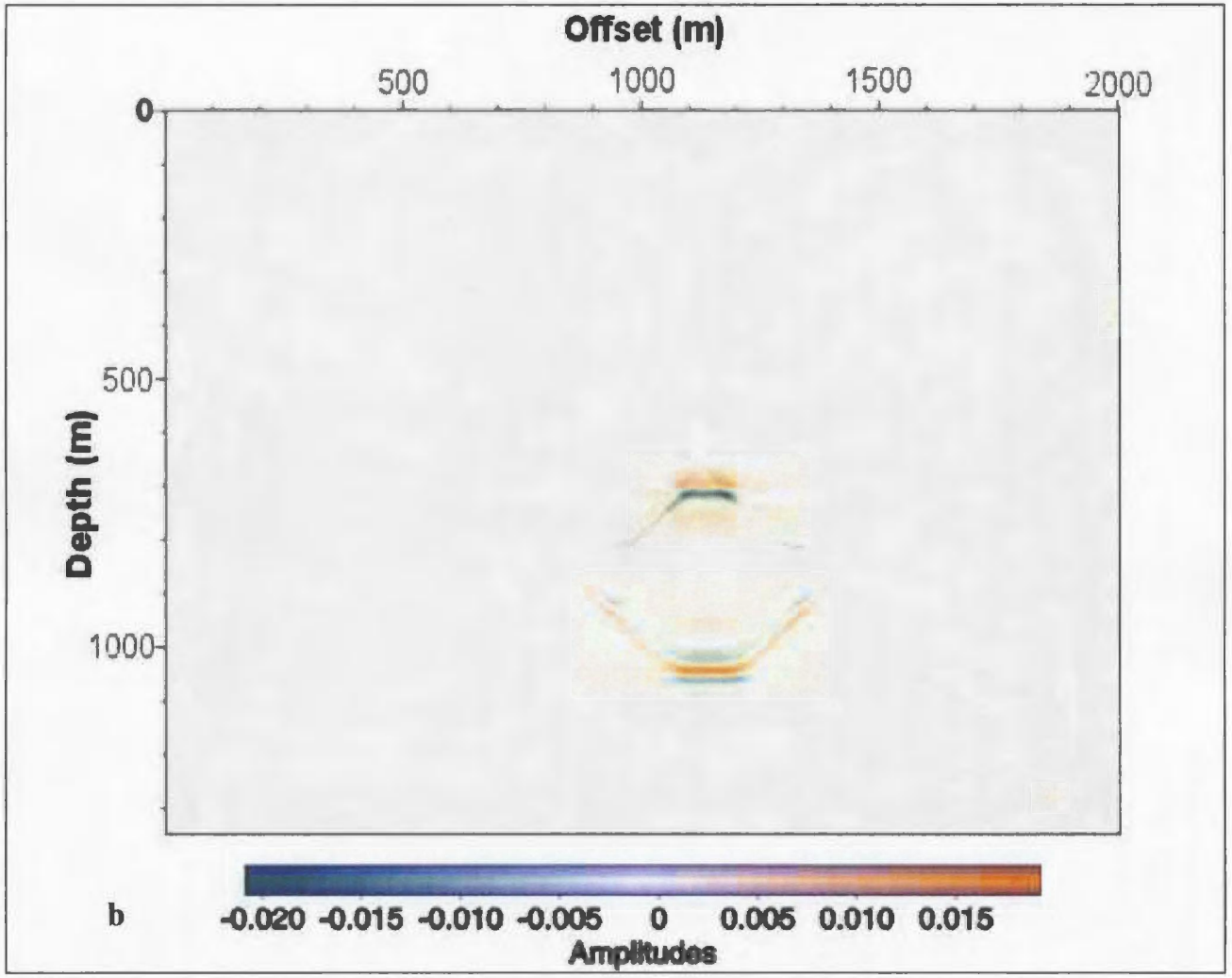

Figure 4.1.1-7: b) Migrated imaged of surface and VSP data for 10 shot locations across the model space. Note there is no significant improvement by including VSP data in the migration.

4.1.2 Standard Octagon Using Post-Stack Migration

As a comparison, a post-stack migration was performed on the synthetic data recorded from the standard asymmetric octagon. It is not a true comparison since it is not possible to stack data from VSPs and horizontal profiles together and migrate them simultaneously. Therefore, only data from the horizontal profile were used (from 10 shots across the model space). The data were filtered, the direct wave was muted out, and CDP stacked. The stacked data (see Figure 4.1.2-1) clearly show strong amplitude diffractions, probably from backscattered energy from the dipping flanks. Two different post-stack migration algorithms were used, T-K (time-wavenumber domain) and Gazdag (both SU modules), and both produced the same result (see Figure 4.1.2-2). The migration algorithms failed to collapse the top and bottom of the octagon and there is no evidence of the dipping flanks of the body. This poor-quality result may be because the geometry imaging may be controlled by data from weaker events (e.g., reflections from dipping flanks and diffractions from corners of the target object) that are destroyed during the stacking process. It should be noted that the post-stack migration took 40 minutes of computational time on a single processor, while the pre-stack migration runs as a parallel code on 14 processors (taking approximately 7 minutes of computational time).

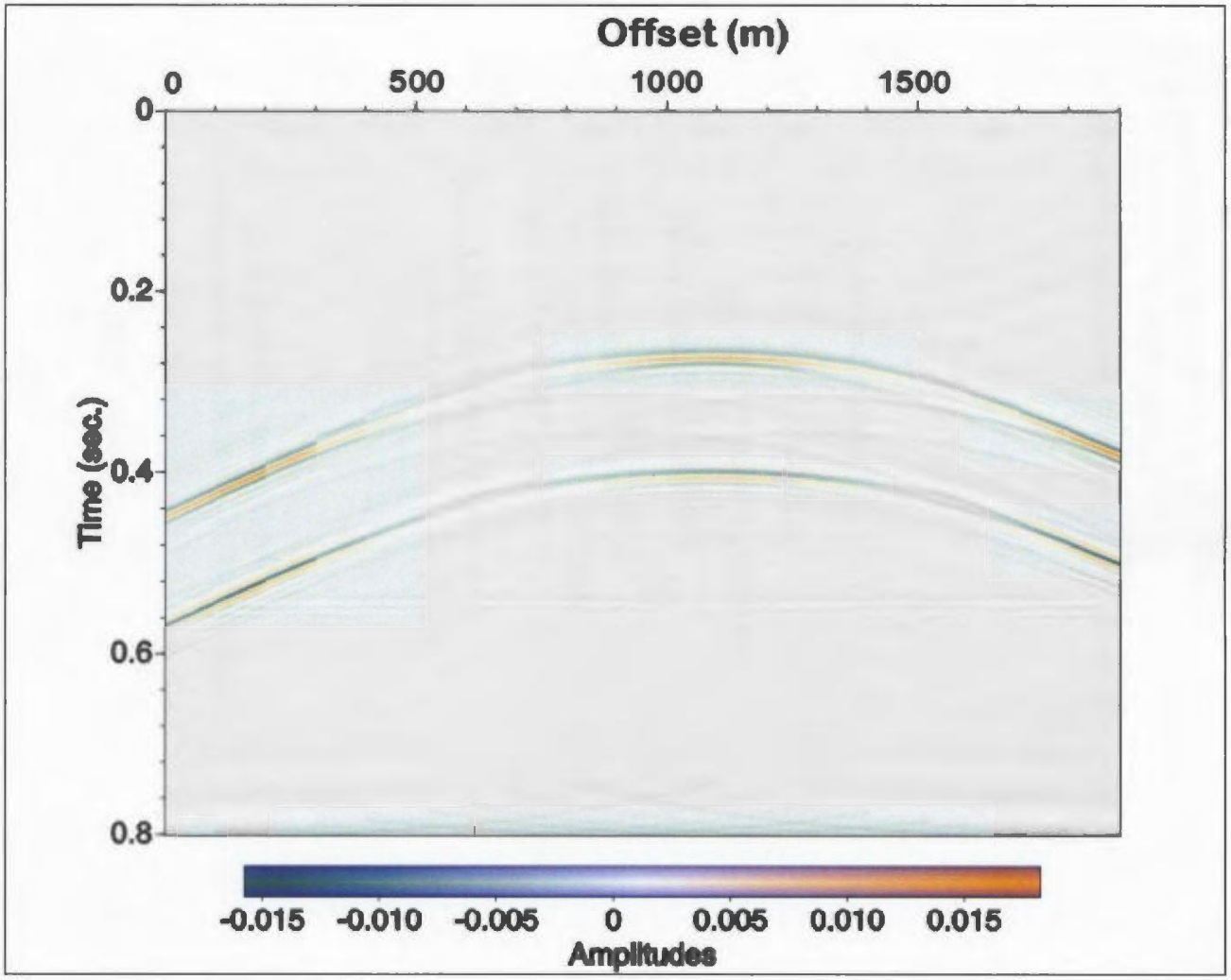

Figure 4.1.2-1: Stacked image of the standard octagon model.

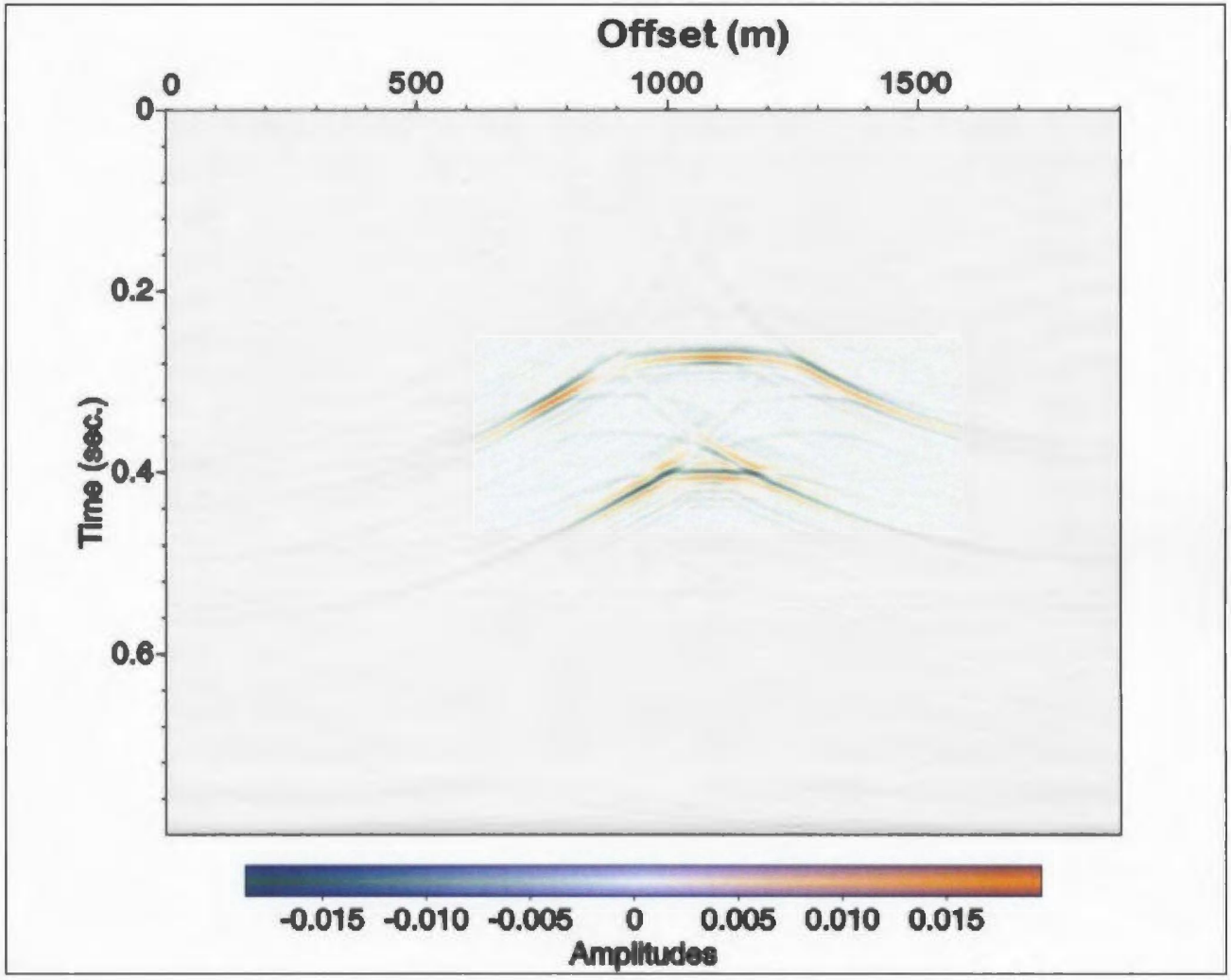

Figure 4.1.2-2: Post-stack migrated image of the standard octagon model.

4.1.3 Symmetric Octagon

To ensure that any differences in the right and left VSPs were due to offset from the target object and not a numerical artefact, a model was run with the standard octagon centred in the model space (the top face was at x=~1000 m, z=~700 m). The target object geometry and properties were identical to those used in Section 4.1.1, and three shots were taken over the body (at x=300, 1140, and 1900 m). The right and left VSPs (see Figures 4.1.3-1a,b) for a shotpoint at 1140 m appear to be identical to each other and a compromise between Figures 4.1.1-3b and –4, but still show all the same features as those in Figures 4.1.1-3b and –4.

The shots were processed as described in Section 4.1.1 and then pre-stack depth migrated, the results of which are shown in Figures 4.1.3-2a,b. The algorithm properly located the target object and there was no apparent difference between including the VSP data or not. In addition, the upper right dipping face has been imaged (compare with Figures 4.1.1-6a,b,c) probably due to the larger number of surface sensors that recorded data.

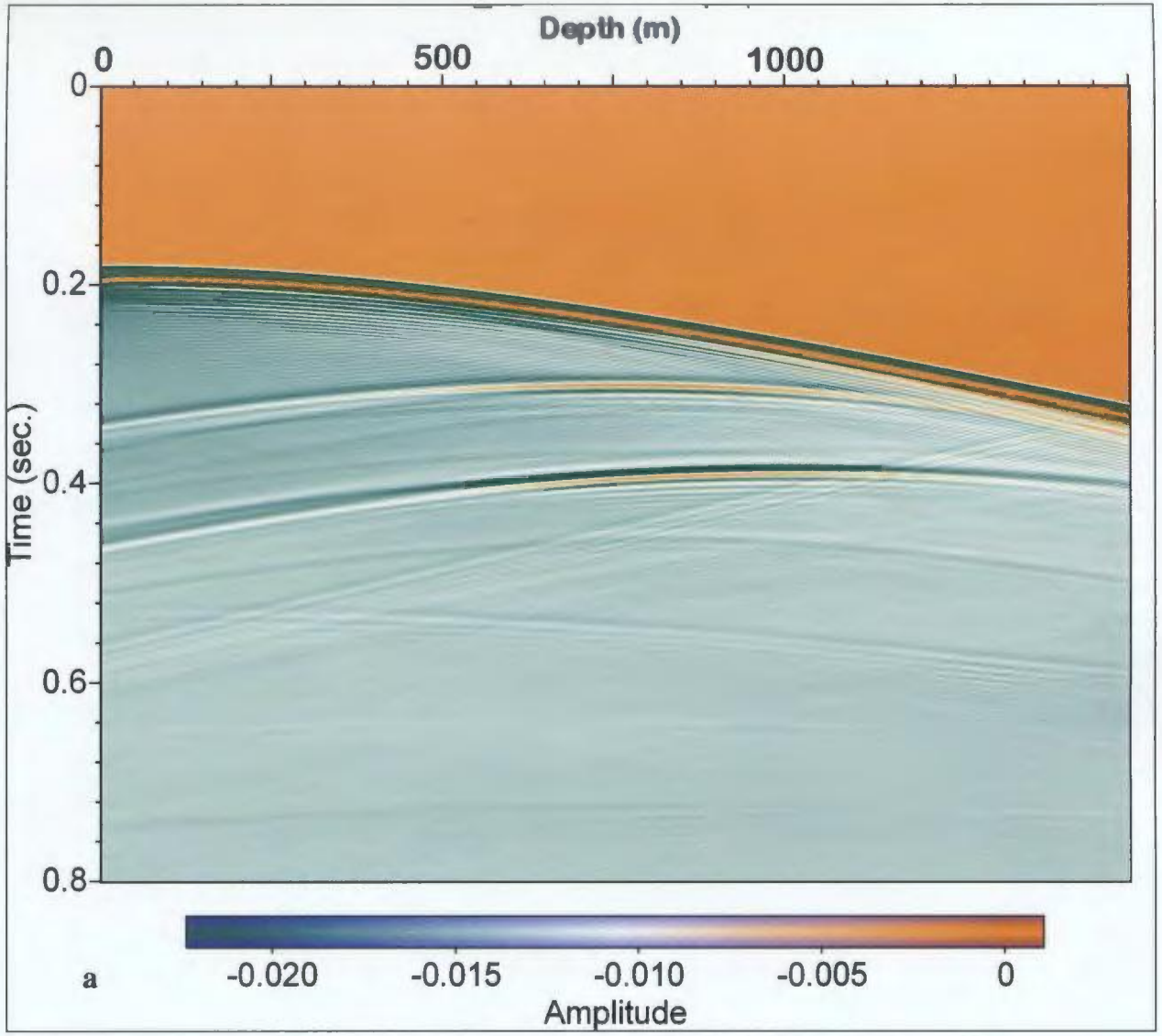

Figure 4.1.3-1: a) Raw shot gather from the left VSP over the symmetric octagon model space, shotpoint at 1140 m.

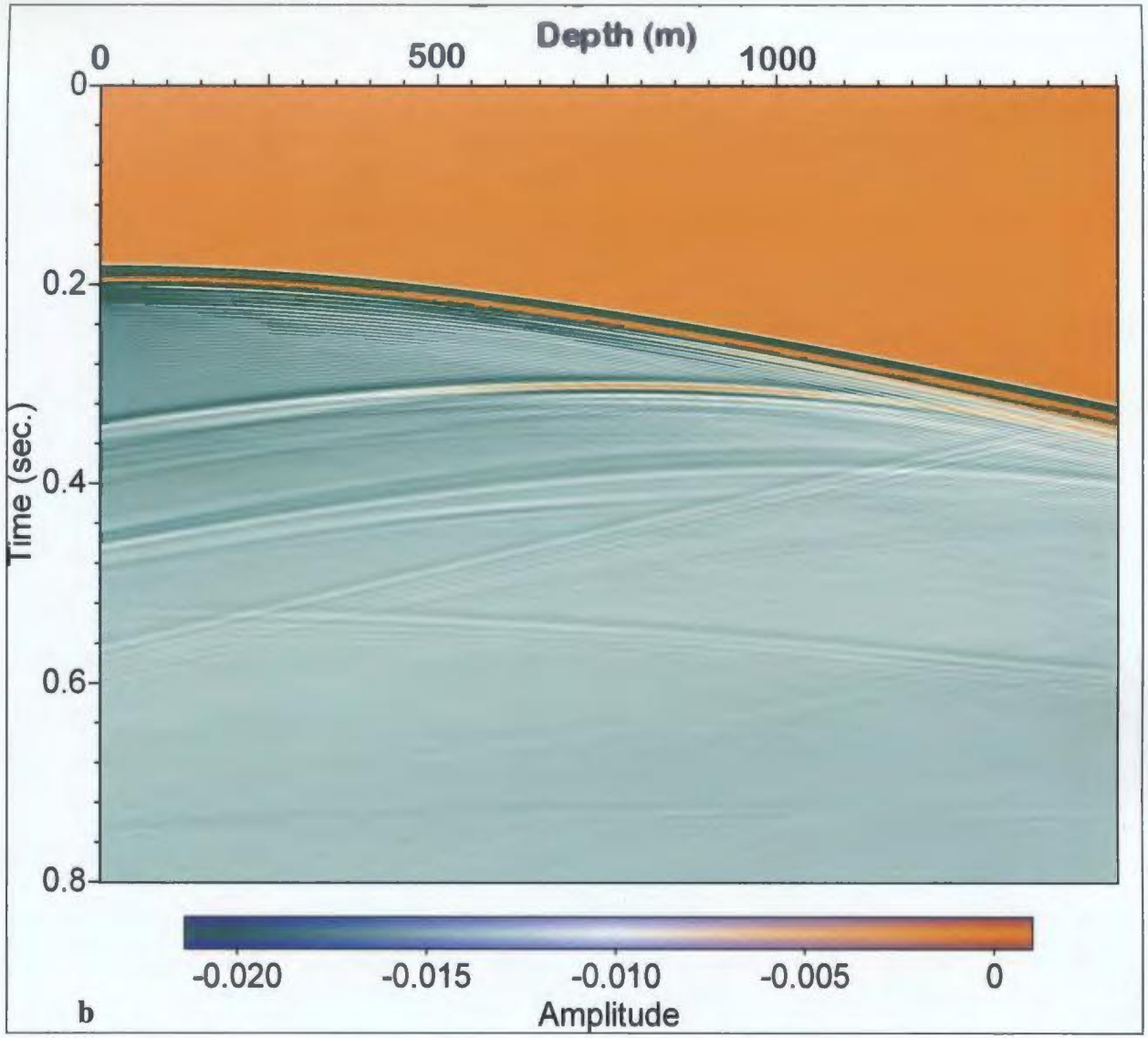

Figure 4.1.3-1: b) Raw shot gather from the right VSP over the symmetric octagon model space, shotpoint at 1140 m. The lack of difference between a) and b) indicates differences observed between right and left VSPs over the asymmetric octagon model is a result of the different VSP offsets.

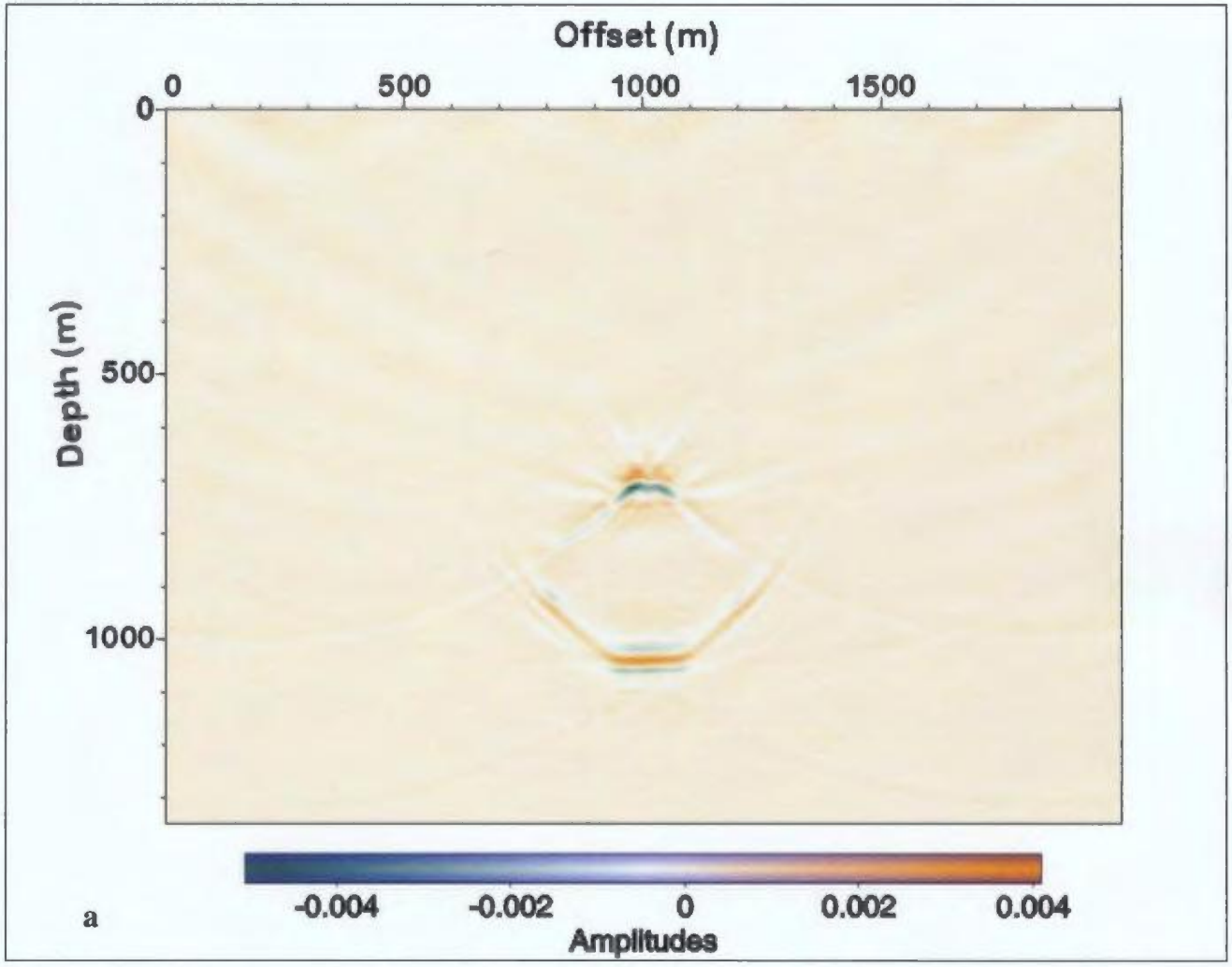

Figure 4.1.3-2: a) Migrated image of the symmetric octagon space using data from the surface array only.

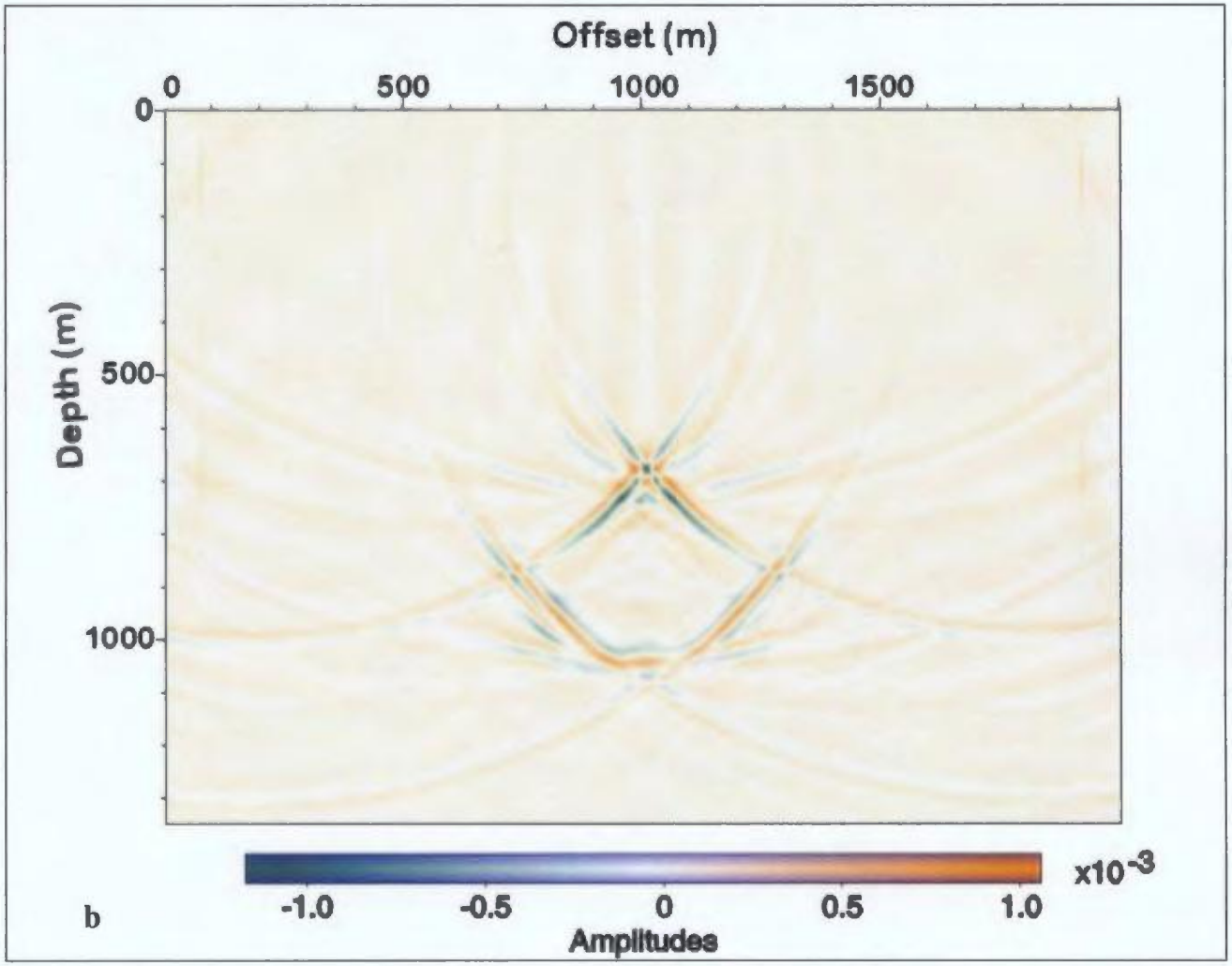

Figure 4.1.3-2: b) Migrated image of the symmetric octagon space using data from the VSPs only.

4.1.4 Wavefield Separation

To determine where most of the usable energy in the wavefield is coming from and to remove noise, wavefield separation was conducted on 3 shots (at x=300, 1140, 1900 m) from the standard asymmetric octagon model. The data were converted to SEG-Y format and imported into Vista™ processing software package where it was f-k filtered to separate the upgoing and downgoing wavefields. The amplitude spectra of the separated wavefields clearly show the downgoing wavefield has a higher amplitude and peak frequency than the upgoing wavefield. Figure 4.1.4-1a,b,c,d illustrates the superiority of the upgoing signal compared with the downgoing signal quality for the right and left VSPs. To further illustrate this point, the pre-stack depth migrated images (see Figures 4.1.4-2a,b) produced from the wavefield-separated data show that the downgoing wavefield contributes almost no usable information to image the target object but the upgoing wavefield gives a much clearer result.

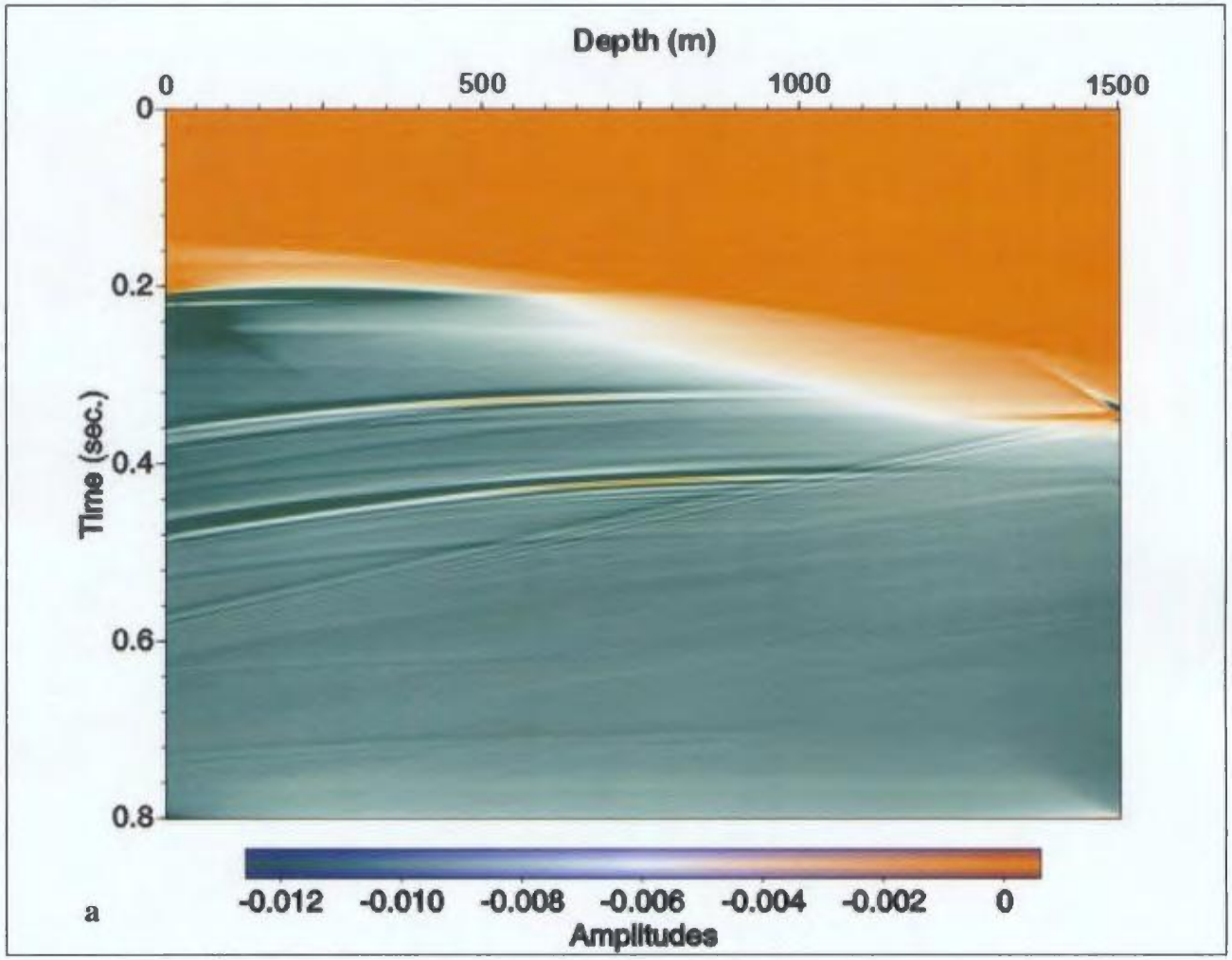

Figure 4.1.4-1: Shot gather with shotpoint at 1140 m. a) Left VSP, upgoing wavefield.

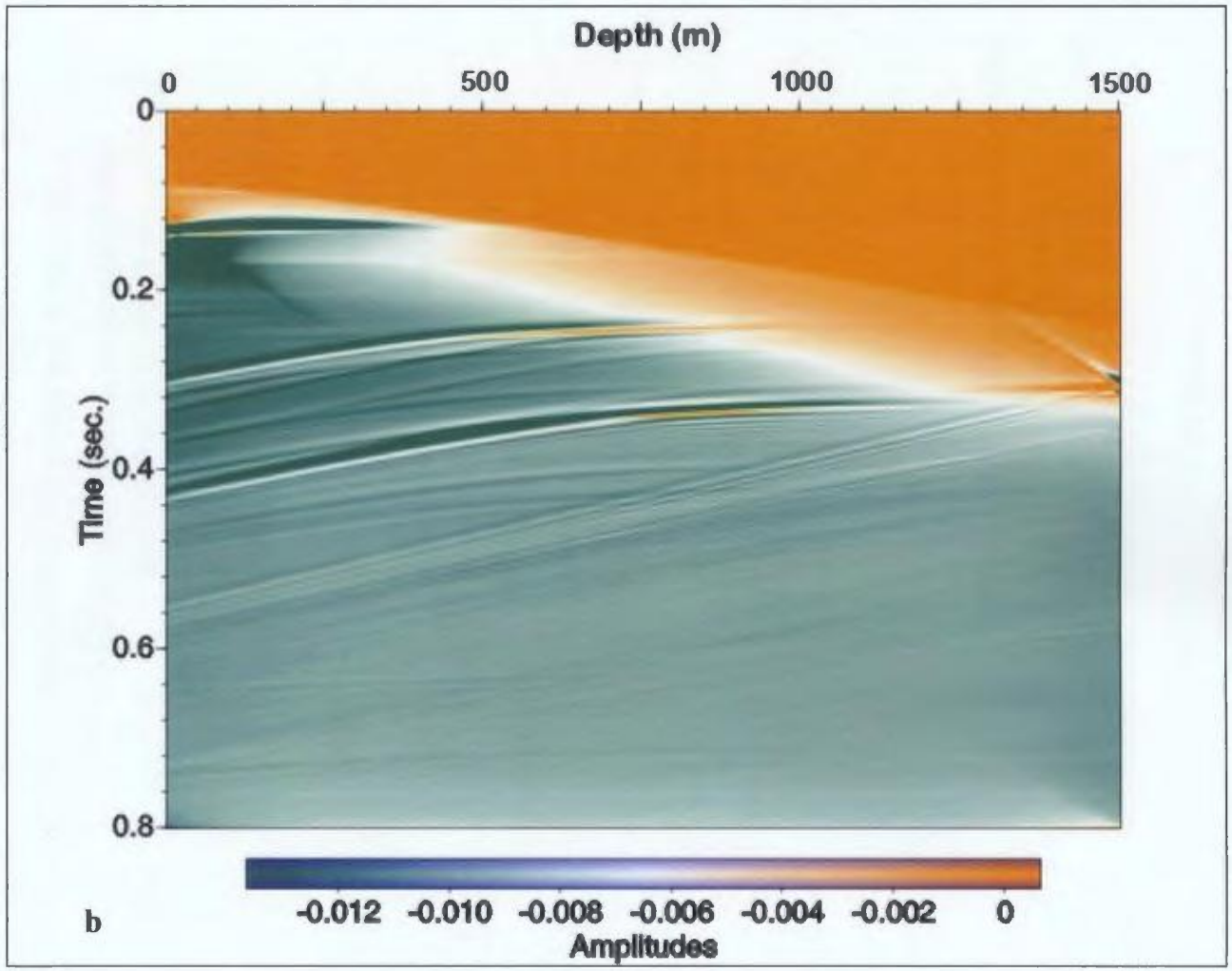

Figure 4.1.4-1: Shot gather with shotpoint at 1140 m. b) right VSP, upgoing wavefield.

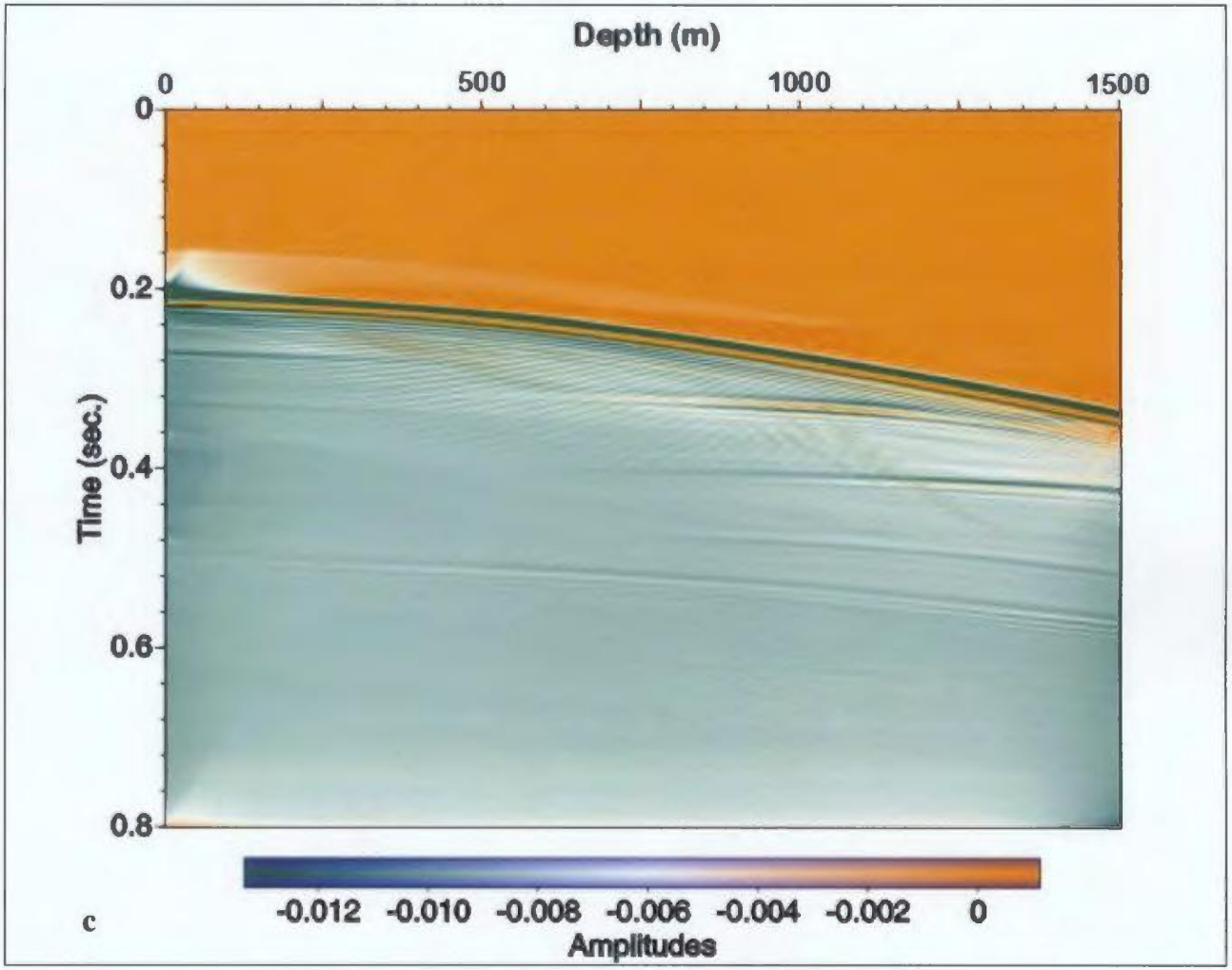

Figure 4.1.4-1: Shot gather with shotpoint at 1140 m c) left VSP, downgoing wavefield. Note the lack of strong reflections.

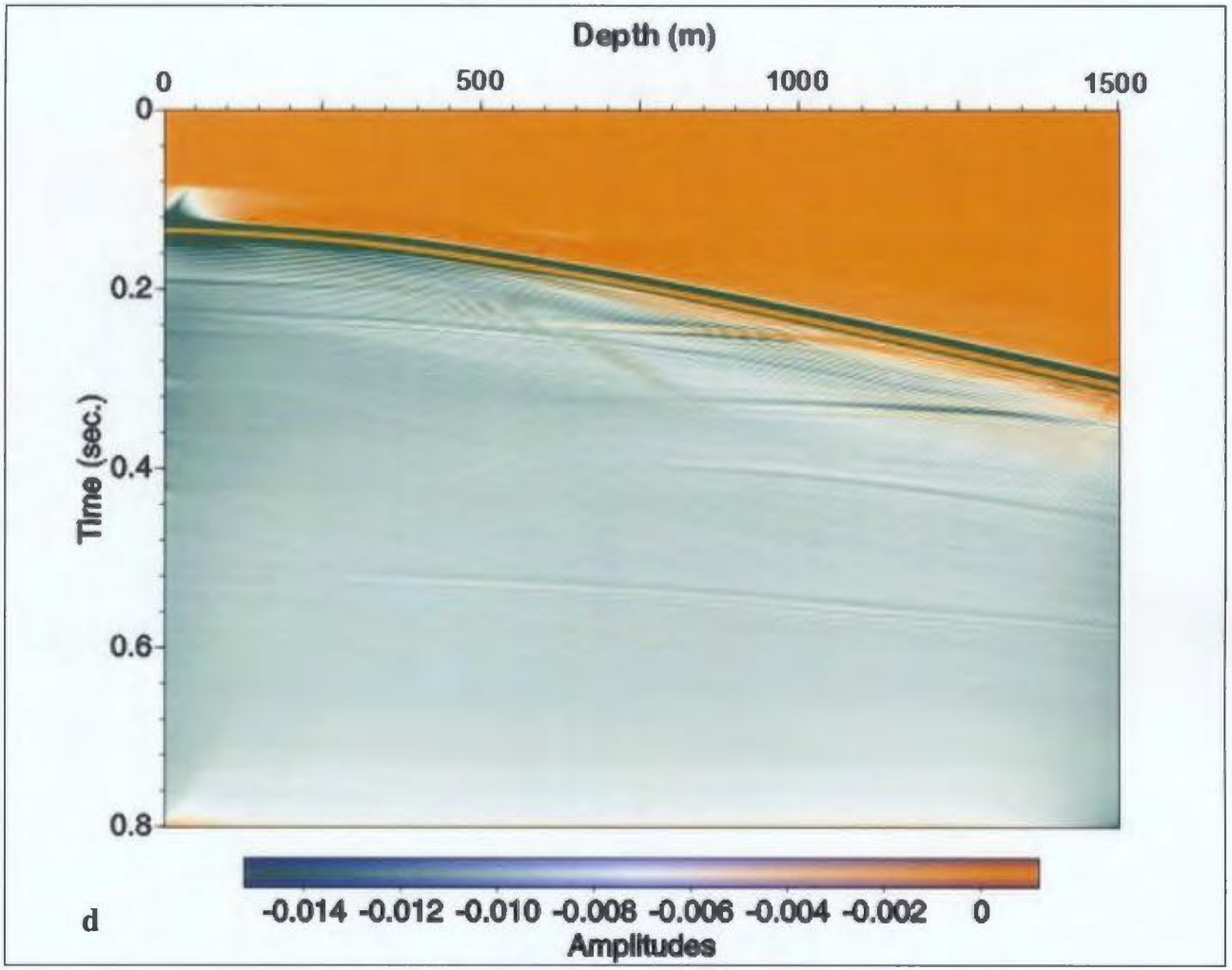

Figure 4.1.4-1: Shot gather with shotpoint at 1140 m. d) right VSP, downgoing wavefield. Note the lack of strong reflections.

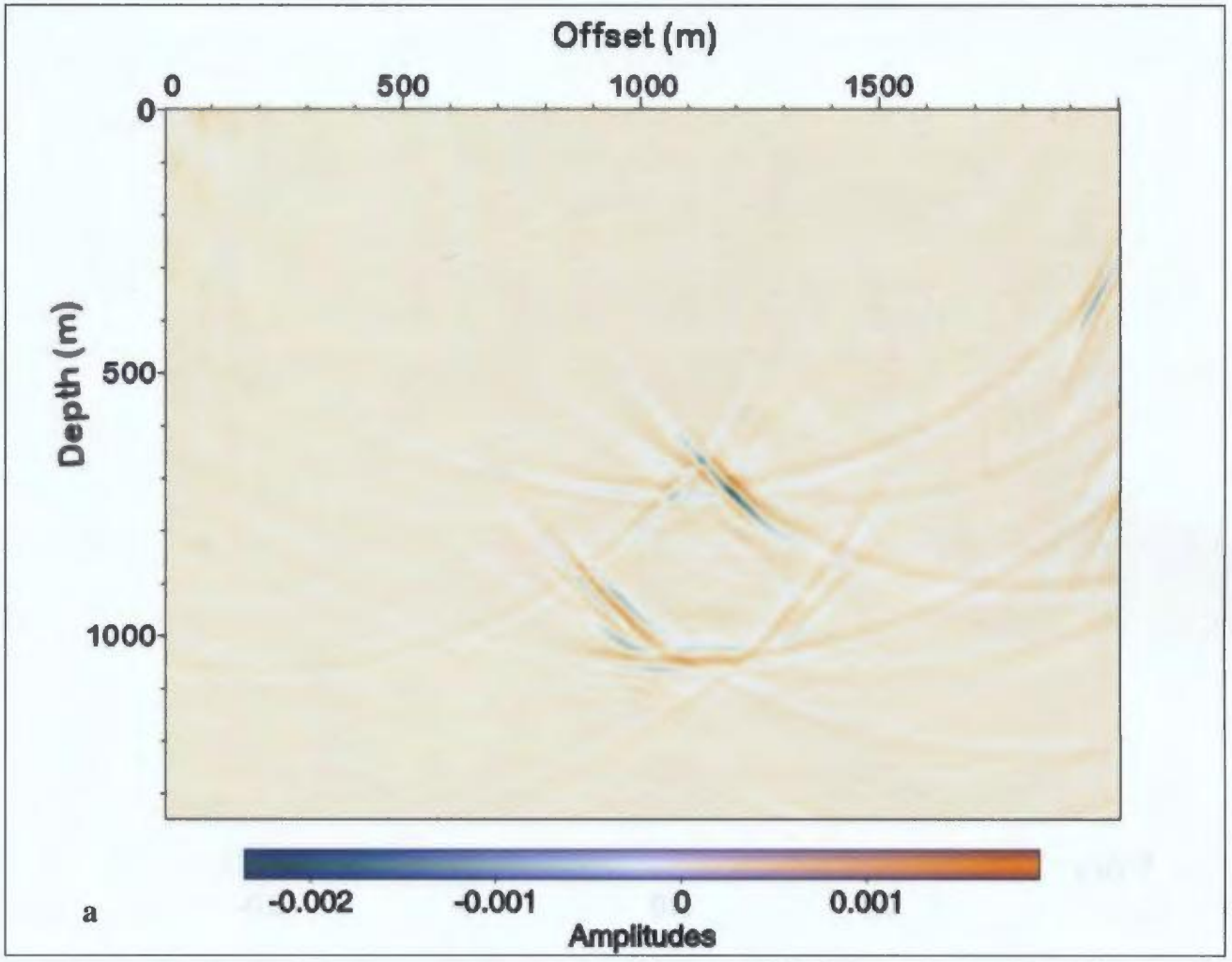

Figure 4.1.4-2 a) Migrated image of the standard octagon model space using upgoing wavefield VSP data only.

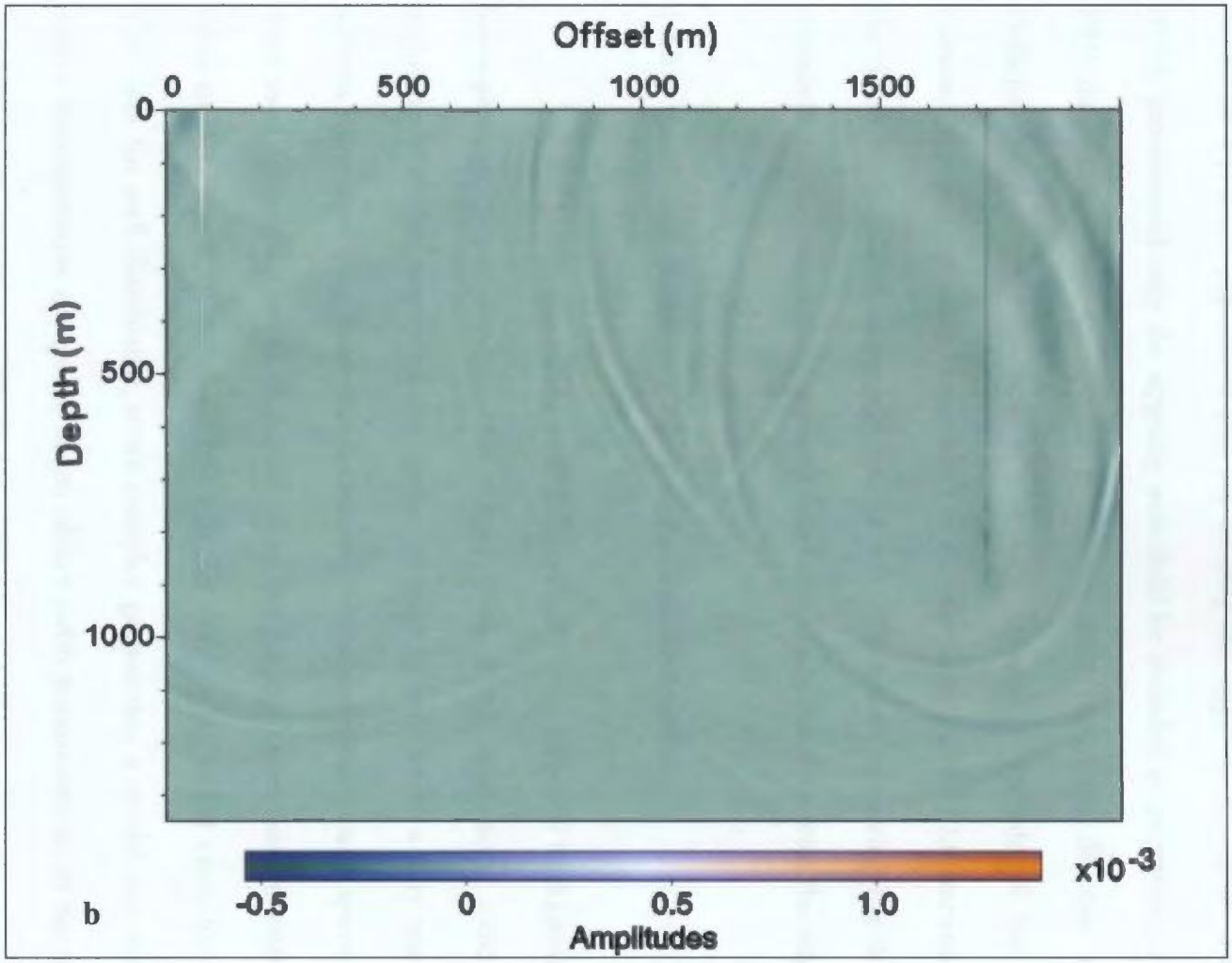

Figure 4.1.4-2 b) Migrated image of the standard octagon model space using downgoing wavefield VSPs only.

As a result of these observations, a recommended step in data processing would be wavefield separation and use of only the upgoing wavefield. Payne *et al.* (1994) recommend only the upgoing wavefield be included in migration of standard VSP data to improve the quality of the resultant image (to decrease artefacts). Perhaps the downhole aperture is not wide enough to include all the forward-scattered energy, and what is recorded at the deep end of the VSP becomes part of the direct wave that is eventually muted out. Therefore, removing the downgoing wavefield will (by association) remove noise that could interfere with the migration.

4.1.5 Randomly-Scattering Media: Background Only

To this point, modelling included a simple homogeneous background with a homogeneous target object. The results from these simulations indicated that including VSP data improved the quality of imaging only when a very sparse set of sources were used (the three shot locations), but when more closely-spaced sources were used (providing better illumination of the target), there was no visible added value to including VSP data. To test whether there is no added value for including VSP data for well-illuminated, more complex geometries, a model was investigated with a homogeneous octagonal target object (with parameters as in Section 4.1.1) within a random-scatter media background (the velocity matrix was random, while the density matrix was homogeneous). Although it was stated above that the seismic response of massive sulphide minerals is more sensitive to their large density contrast compared with host rock, only the velocity matrix was randomized because the

mineralisation is hosted in silicate rock, which lies on the Nafe-Drake curve (see Figure 2.3-1) and therefore is equally sensitive to velocity and density contrasts. The code used to create the background velocity matrix was developed by Hurich (personal communication, 2001). The parameters for the velocity matrix were chosen according to Holliger's (1996) values for the Abitibi greenstone belt and are as follows: ρ=2.7 g/cm^3, $V_{Pavg\ host}$=5800 m/s, 3% RMS velocity variation, a Hurst number of 0.18, and an autocorrelation length of 40 in the x-direction and 20 in the z-direction (see Figure 4.1.5-1). Ten shots were taken across the array at 200 m intervals (starting at 100 m). Only the shallowest 200 traces on each VSP and the centre 200 traces on the horizontal profile were used for migration. The data were muted and filtered using the same parameters as for the standard asymmetric octagon (see Section 4.1.1 for more details). The downgoing wavefield was not removed to maintain continuity for comparison with the original asymmetric octagon model results.

Figures 4.1.5-2a,b,c show the shot gathers of the horizontal and VSP arrays for a shot located at 1140 m (centred over the target object). In Figure 4.1.5-2a, the horizontal profile, the top and bottom of the target object show up as strong reflectors but the diffraction tails are much shorter than in the homogeneous model, and the corners (c,d,h,i in Figure 4.1-1) are still identifiable, but not as strong. Figures 4.1.5-2b and c, the right and left VSP shot gathers, appear very similar to shot gathers over the original model but the amplitudes are not as large.

The data were pre-stack depth migrated using a constant velocity of 5800 m/s first using only 3 shotpoints (at 300 m, 1140 m, 1900 m), and then using all 10

shots. The 10 shotpoint pre-stack depth migration (see Figures 4.1.5-3a,b,c) is an improvement over the results obtained from using only 3 shots. The migration using horizontal data only clearly images the top, bottom, top left face and bottom right face, but the top right face and bottom left face are poorly imaged. The asymmetry of the model allows the left-dipping faces to be well-imaged by the horizontal data because the longer recording offset on the left side of the target object will catch reflections from dipping faces. The migration from VSP data only (Figure 4.1.5-3b) images the top right, lower left and bottom faces clearly; the bottom right face less clearly; and the top left face poorly while the vertical sides of the target object are not imaged at all. In this case, the left-dipping faces are less well-defined probably because they are farther away from the left VSP and only the top part of the left VSP would record reflections from left-dipping faces while the upper half of the right VSP can record energy from right-dipping faces. This effectively decreases the recording aperture and degrades the migrated image. The combined VSP and horizontal pre-stack depth migration shows definite improvement over the horizontal data-only migration. The right-dipping faces (upper right and lower left faces) are better defined using combined data, and the top, bottom, and bottom right faces are all clearly defined. It appears that the upper left face is less well-defined than in the horizontal data-only migration, but it may be a case of relative amplitudes.

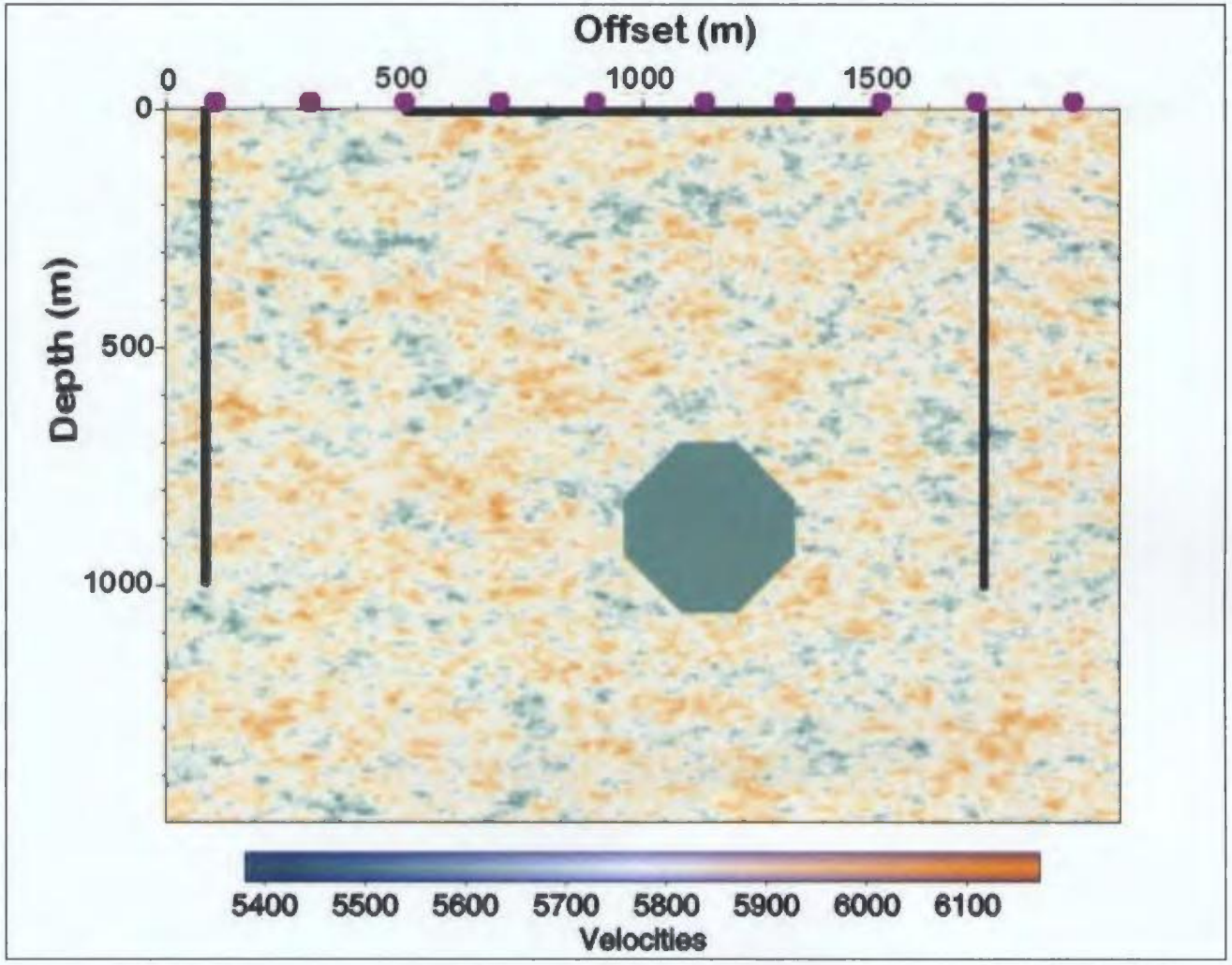

Figure 4.1.5-1: Model space of solid, standard octagon in a scattering media background.

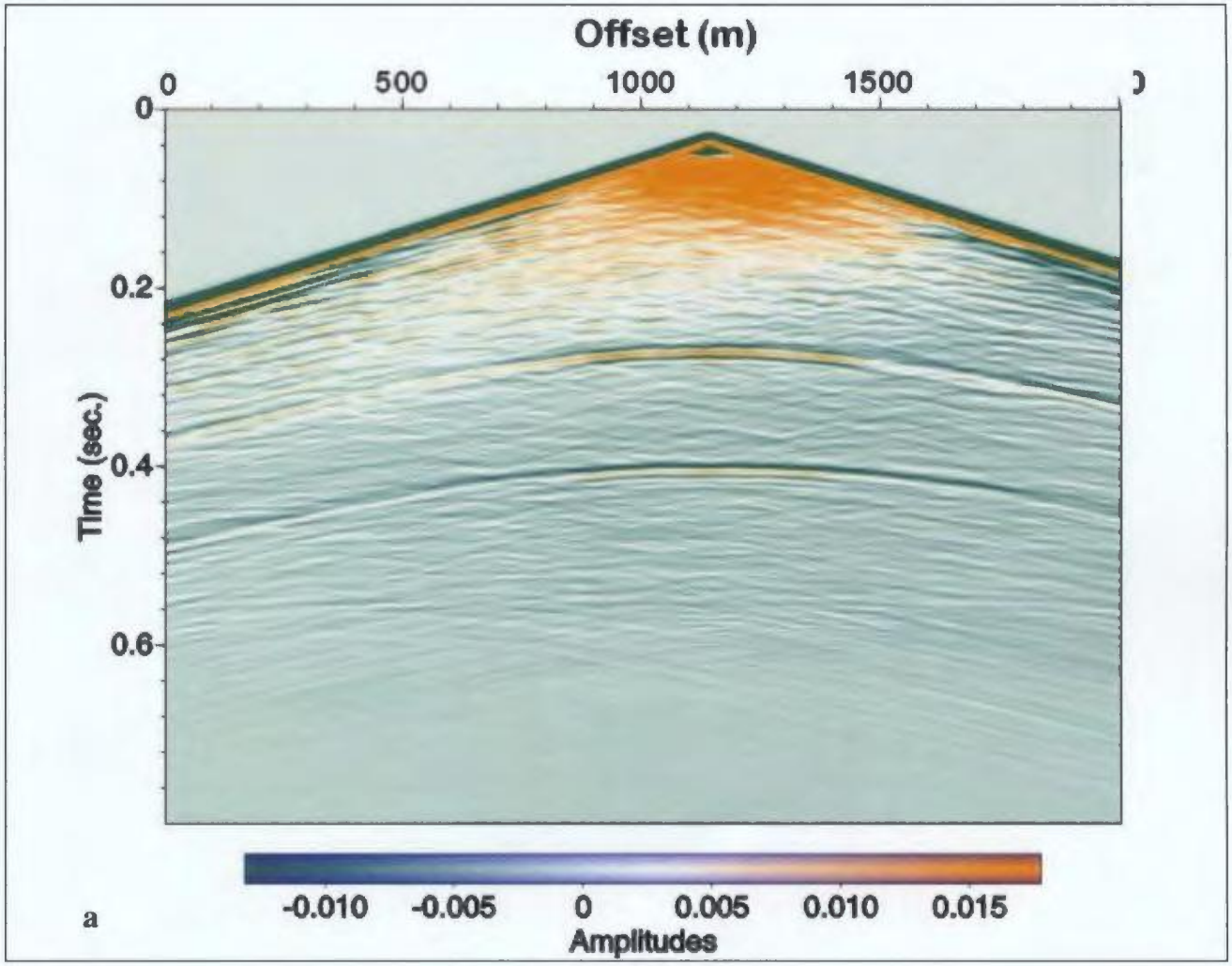

Figure 4.1.5-2: a) Raw surface seismic shot gather, shotpoint at 1140 m, over solid octagon in scattering host. Compare with Figure 4.1.1-1a—the strong reflections from faces of the octagon are still identifiable.

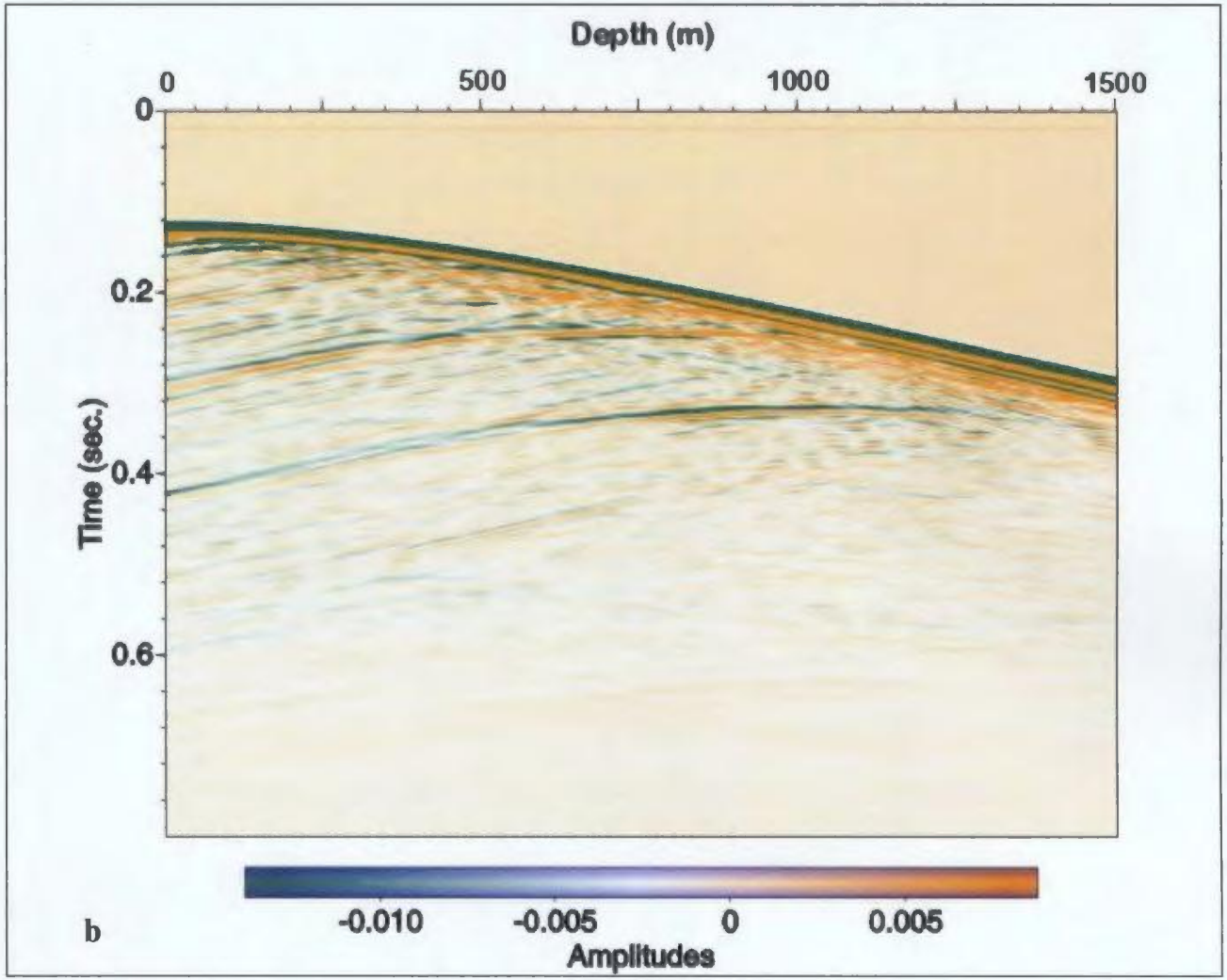

Figure 4.1.5-2: b) Right VSP raw shot gather, shotpoint at 1140 m, over solid octagon in scattering host. Compare with Figure 4.1.1-3b—the strong reflections from faces of the octagon are still identifiable.

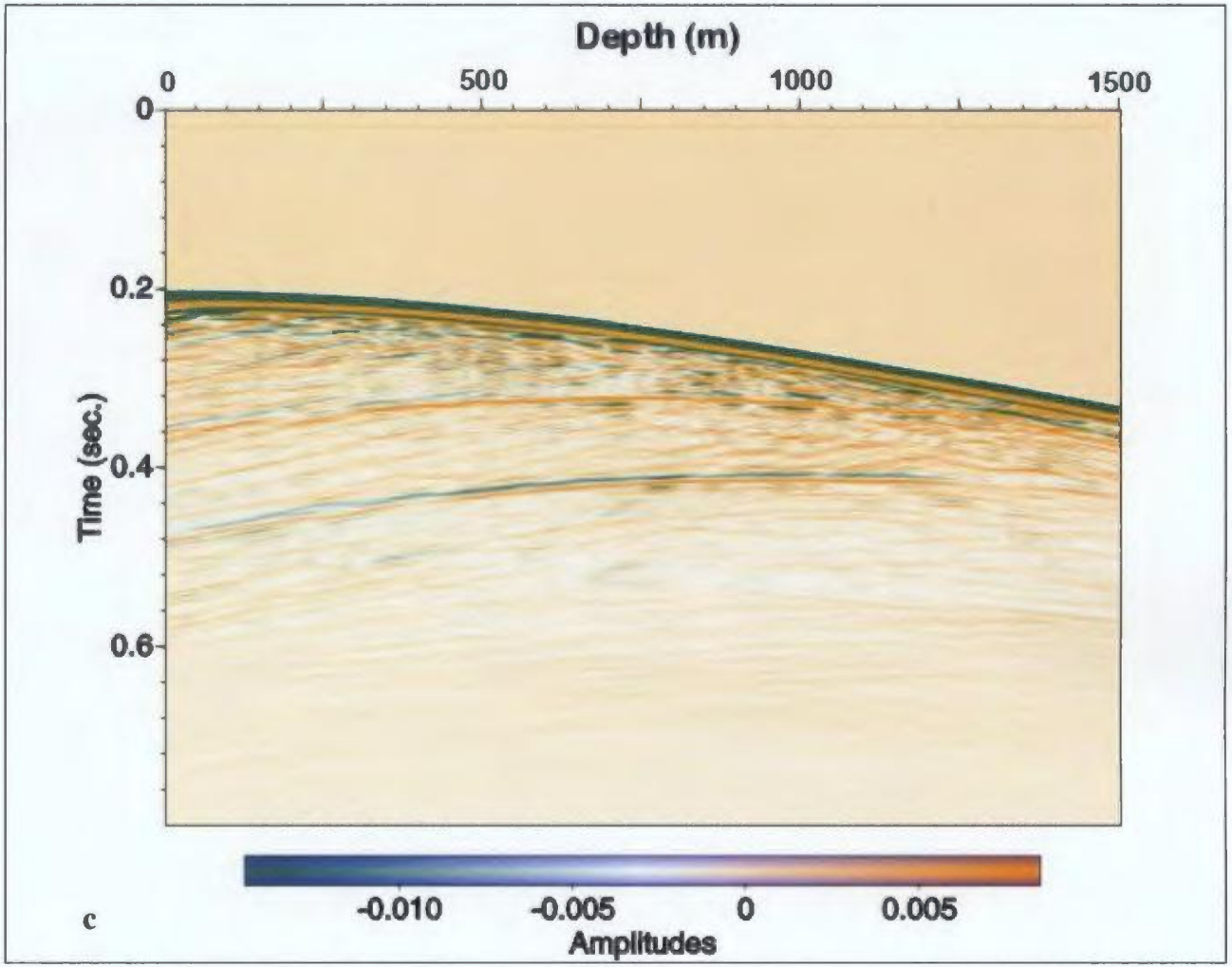

Figure 4.1.5-2: c) Left VSP raw shot gather, shotpoint at 1140 m, over solid octagon in scattering host. Compare with Figure 4.1.1-4, the strong reflections from faces of the octagon are still identifiable.

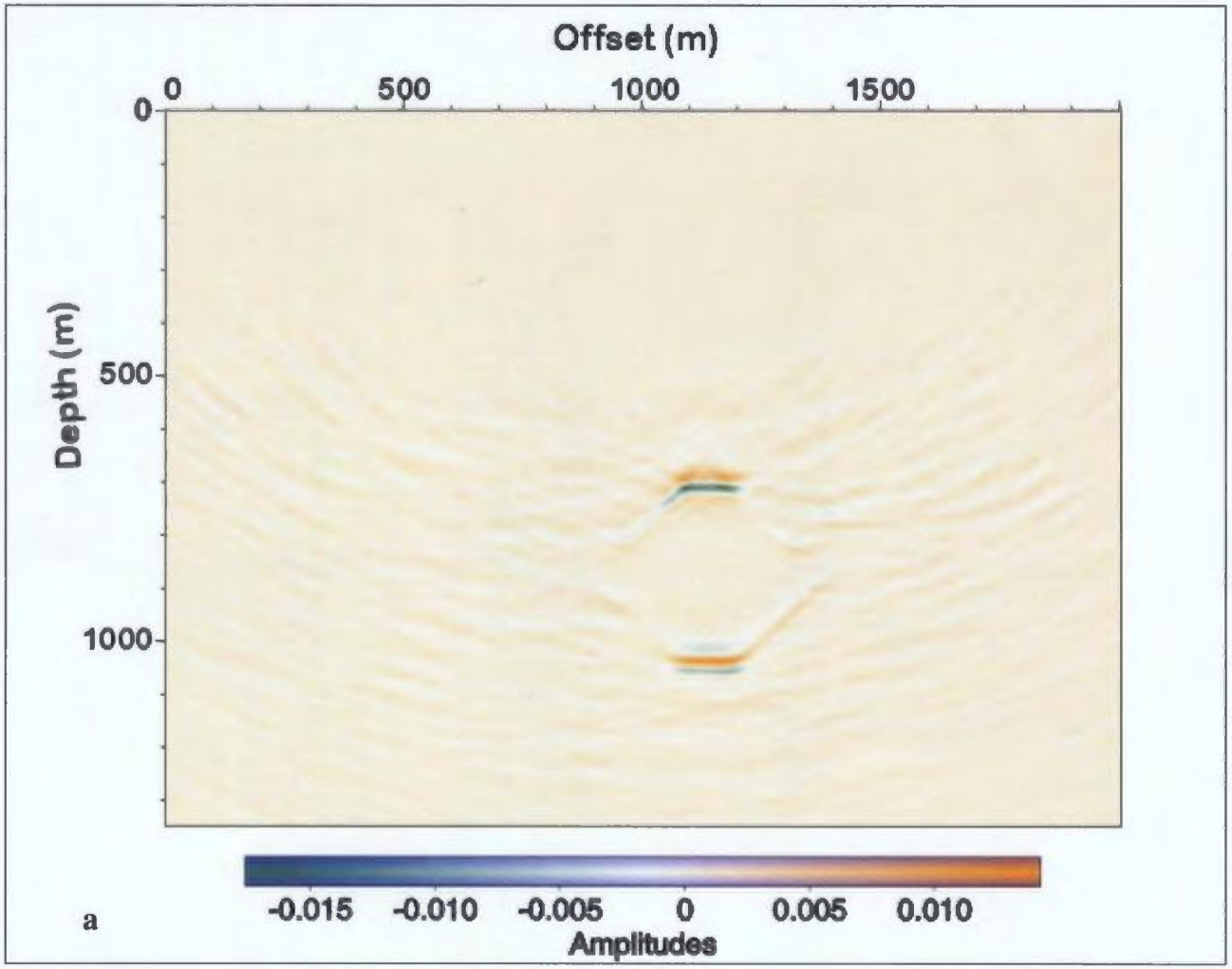

Figure 4.1.5-3: a) Migrated image of solid octagon in scattering background media using surface seismic data and only 10 shots across the model space.

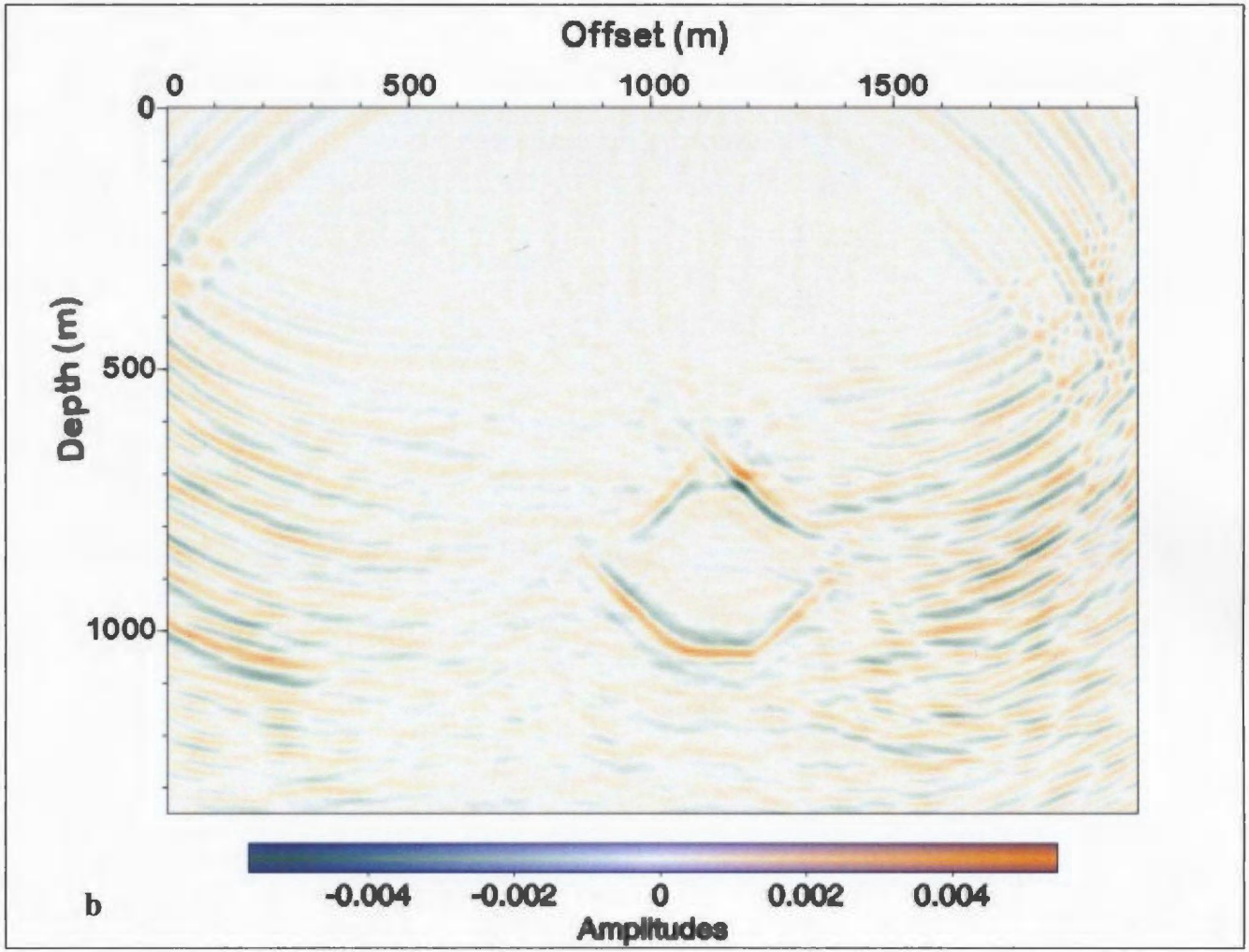

Figure 4.1.5-3: b) Migrated image of solid octagon in scattering background media using VSP data only and 10 shots across the model space.

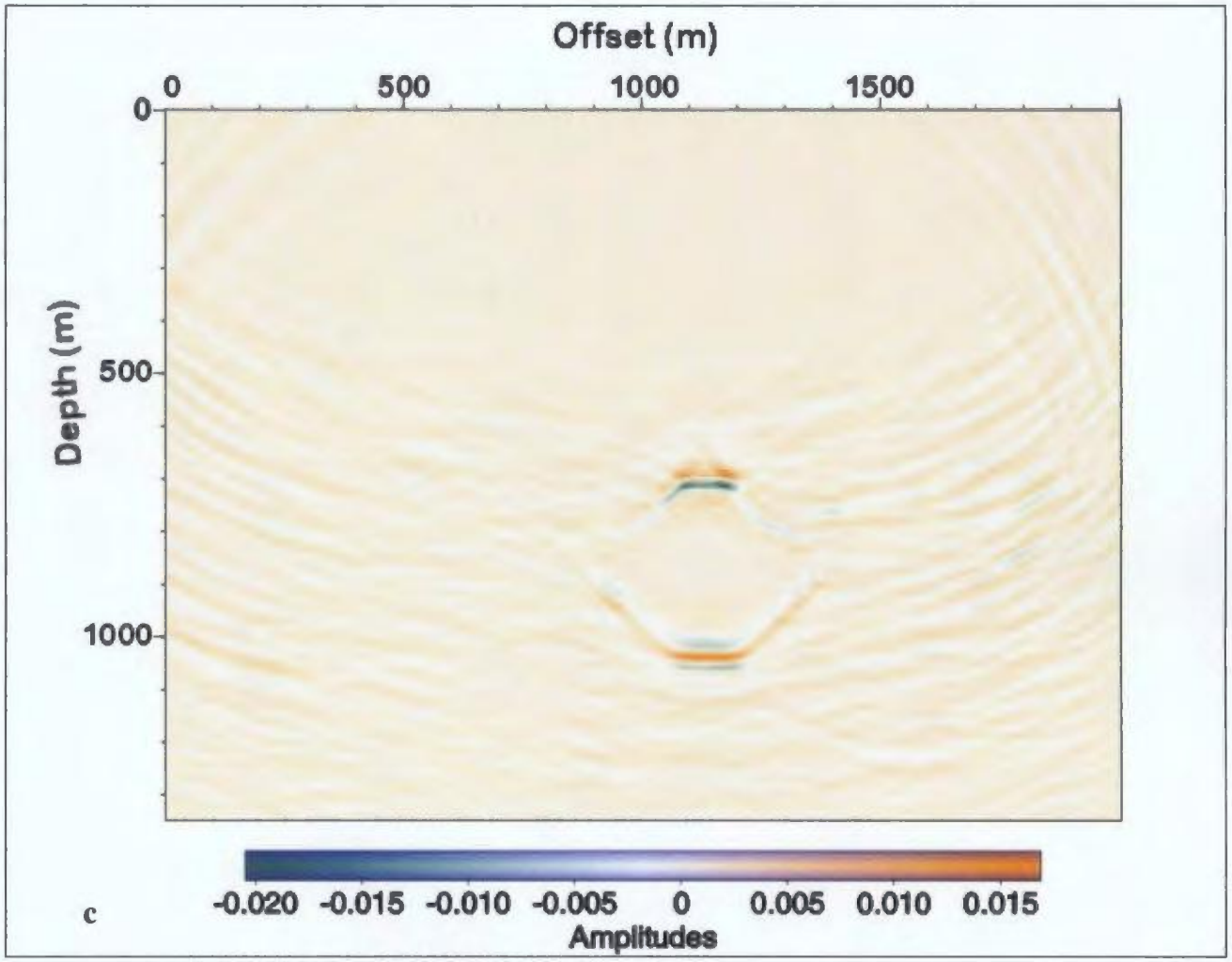

Figure 4.1.5-3: c) Migrated image of solid octagon in scattering background media using both surface and VSP data together and 10 shots across the model space. Note there is a slight improvement in image quality when VSP and surface seismic data are used together.

4.1.6 Randomly-Scattering Media: Target Object and Background

The findings from the previous section were intriguing enough to extend the complexity of the model by simulating the most realistic case of velocity variation—both host material and target object are random scatter media. Using the same model parameters as Section 4.1.5, with the addition of $V_{Pavg\ target}$=5250 m/s and ρ_{target}=4.03 g/cm^3, two random scatter media velocity matrices were created (one for the host and one for the target object) and combined for the model space. The resulting velocity matrix (see Figure 4.1.6-1) shows good variation in velocity for both host and target object. The shape and positioning of the target object was the same as the standard asymmetric octagon and this was identifiable in the velocity matrix, but not as clearly as in the homogeneous case.

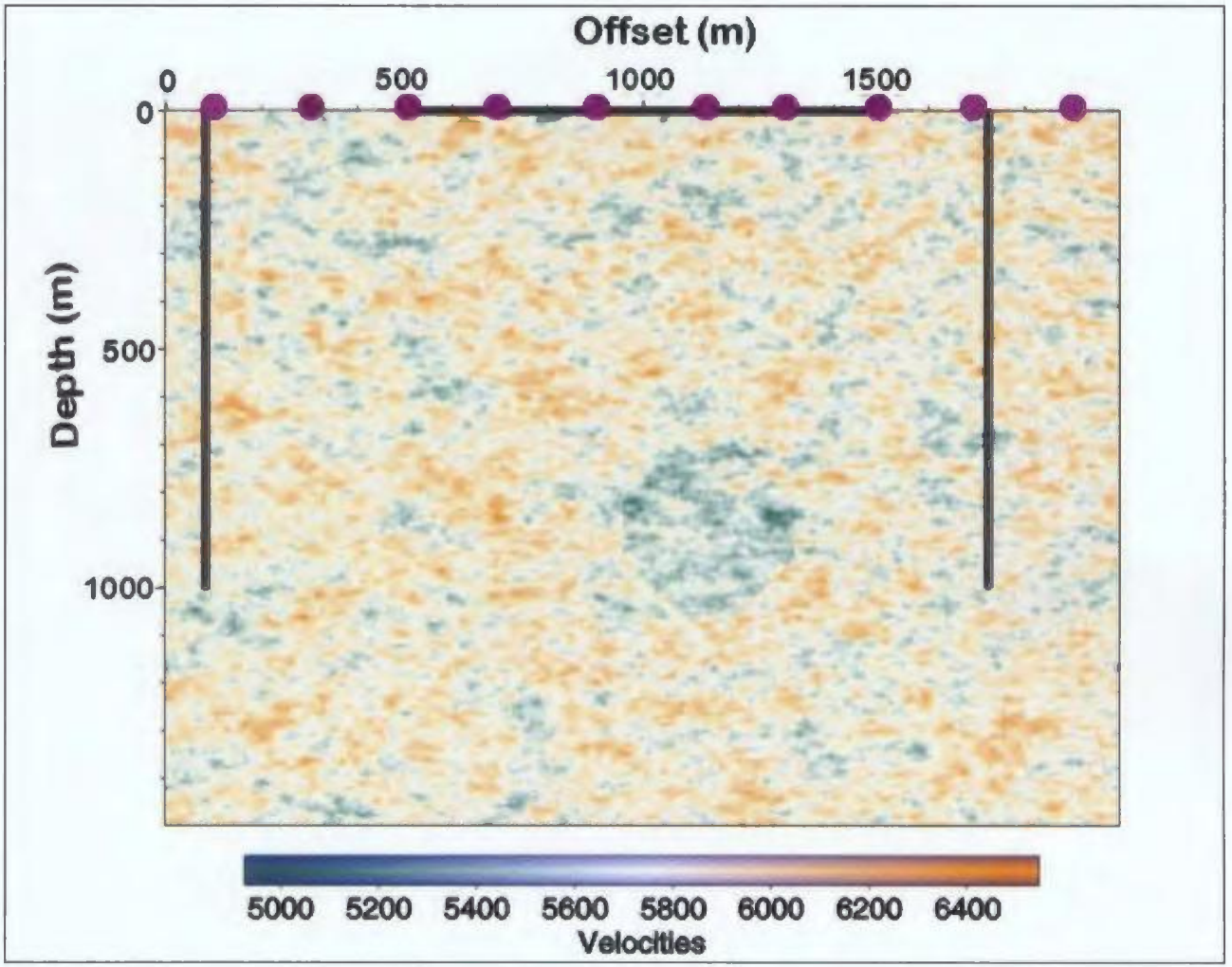

Figure 4.1.6-1: Model space of the octagon and background, both of scattering media. Violet circles indicate shot points, black lines indicate seismic array locations.

There were 10 shotpoints used for this model and example shot gathers are shown in Figures 4.1.6-2a,b,c. The horizontal profile clearly shows the reflections from the top and bottom of the target object, but the amplitude of this reflection dies off quickly with increasing offset compared with the observations from the standard octagon (see Figure 4.1.1-1a). It is interesting to note that the amplitude of the reflection from the bottom face dies off slower than that of the top face, and that no other reflections or diffractions are obvious in the gather. The left VSP shot gather shows clearly the reflections from the upper left and lower right faces, but the reflections decrease rapidly in amplitude with offset and no other reflections/diffractions are obvious. The right VSP shot gather is similar to the left, clearly showing reflections from the upper right and lower left faces, but nothing else.

The raw data was muted and filtered as for the standard octagon, and was pre-stack depth migrated using a constant velocity (V_p=5800 m/s). Figures 4.1.6-3a,b,c show the pre-stack depth migration from 3 shotpoints. The migration using horizontal profile data only shows very clearly the top and bottom faces, while the top left face and lower right face are adequately imaged and the upper right face and lower left face are less well-defined. Using only the VSP data, the migration shows clearly the upper right face and lower left face (that direct energy into the right VSP), while the lower right face, upper left face and bottom are poorly defined and the top is not imaged at all. The migration that includes both VSP and horizontal profile data shows an improvement over the two options described above. The top, bottom, lower left face and upper right face are clearly imaged; the upper left and

lower right faces are also well-defined (but not as clear as the other faces). Only the vertical faces are not imaged at all.

Figures 4.1.6-4a,b,c show the migrated images using horizontal profile data only, VSP data only, and a combination of horizontal and VSP data for 10 shots across the model space. The horizontal data-only migrated image shows the top and bottom of the octagon very clearly while the left-dipping faces are poorly defined and the right-dipping and vertical faces do not appear at all (they are below the detection level). The VSP data-only migrated image shows well-defined dipping faces, but the bottom face is poorly defined and the vertical and top faces are below the detection level. The best migration result is obtained by the combined use of horizontal and VSP data and results in clearly-defined top and bottom faces, well-defined upper right and both lower faces, while the upper left face is poorly-defined. The absence of the upper left face in this migration image has not yet been explained satisfactorily but may be some kind of interference between the VSP and horizontal data, or it could possibly be an effect from the velocity matrix itself (the boundary may not be a strong enough contrast). Even with the unexplained missing upper left face, this demonstrates that the added aperture of combined surface and VSP recording provides a better migration result than either method alone when diffraction tails are obscured by noise (scattered energy, in this case). Therefore, the blend of surface and VSP data shows great promise for application in crystalline environments where large velocity variations and high noise levels are possible.

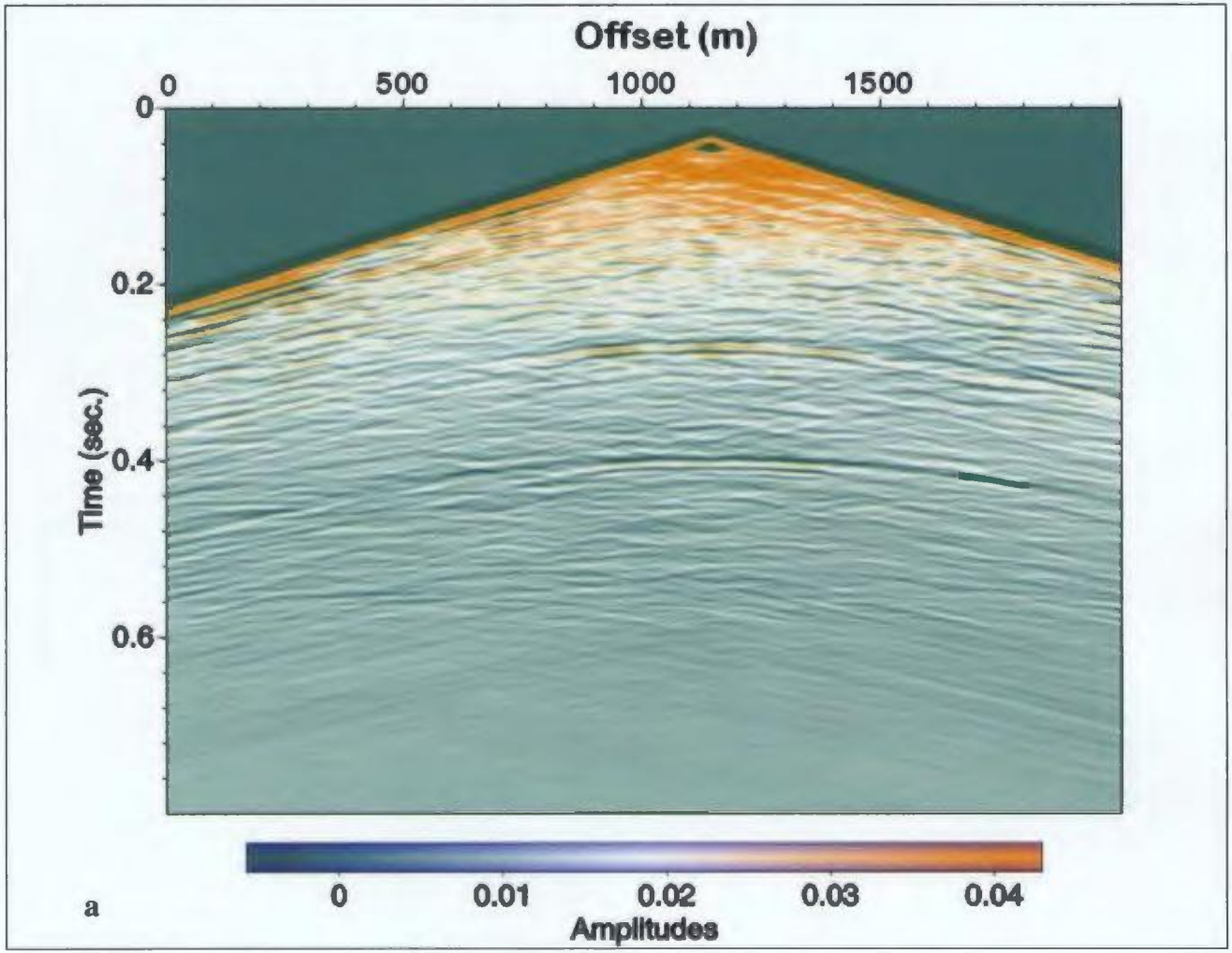

Figure 4.1.6-2: a) Surface seismic shot gather (shotpoint at 1140 m) over the scattering media octagon in scattering media host.

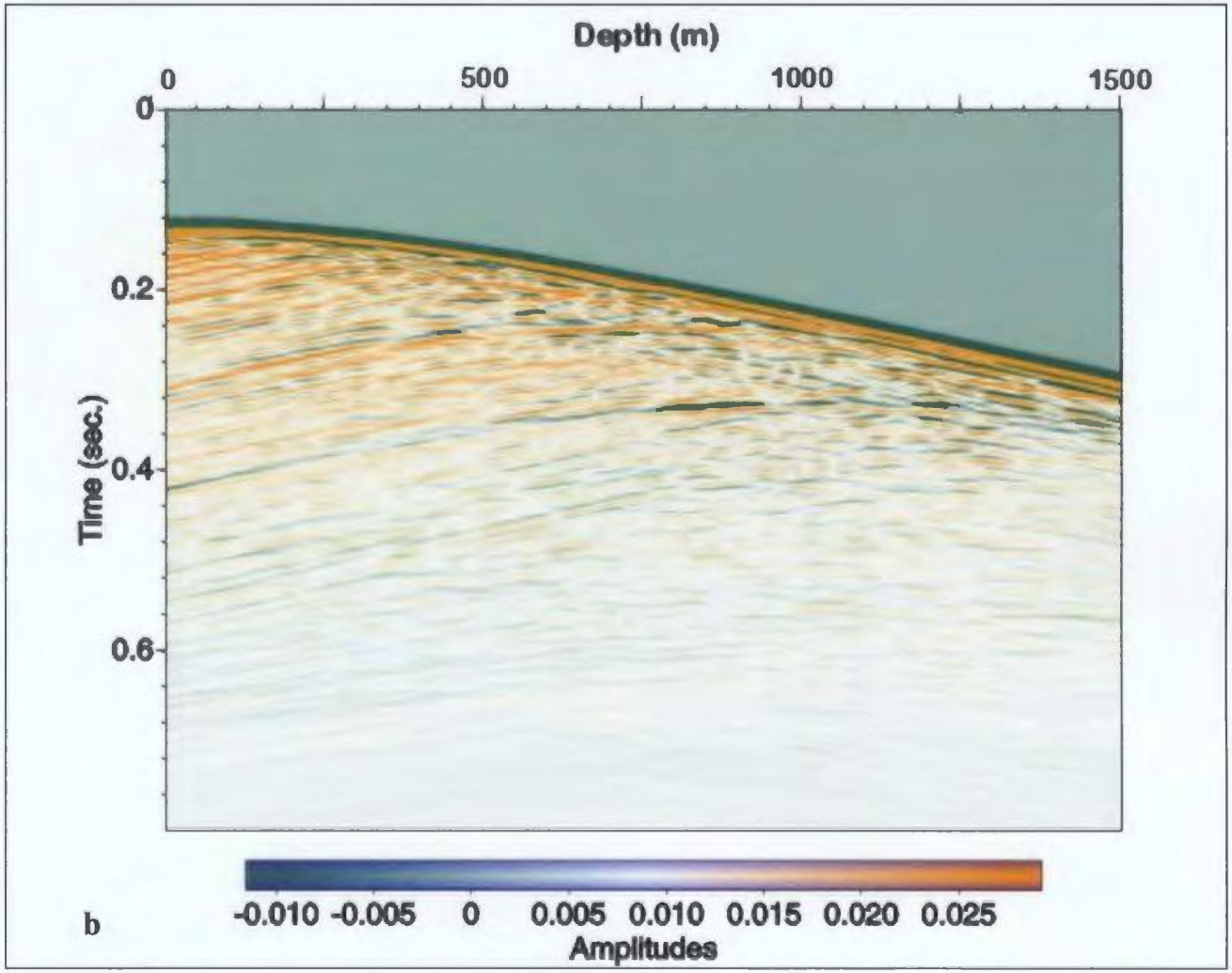

Figure 4.1.6-2: b) Right VSP raw shot gather (shotpoint at 1140 m) over the scattering media octagon in scattering media host.

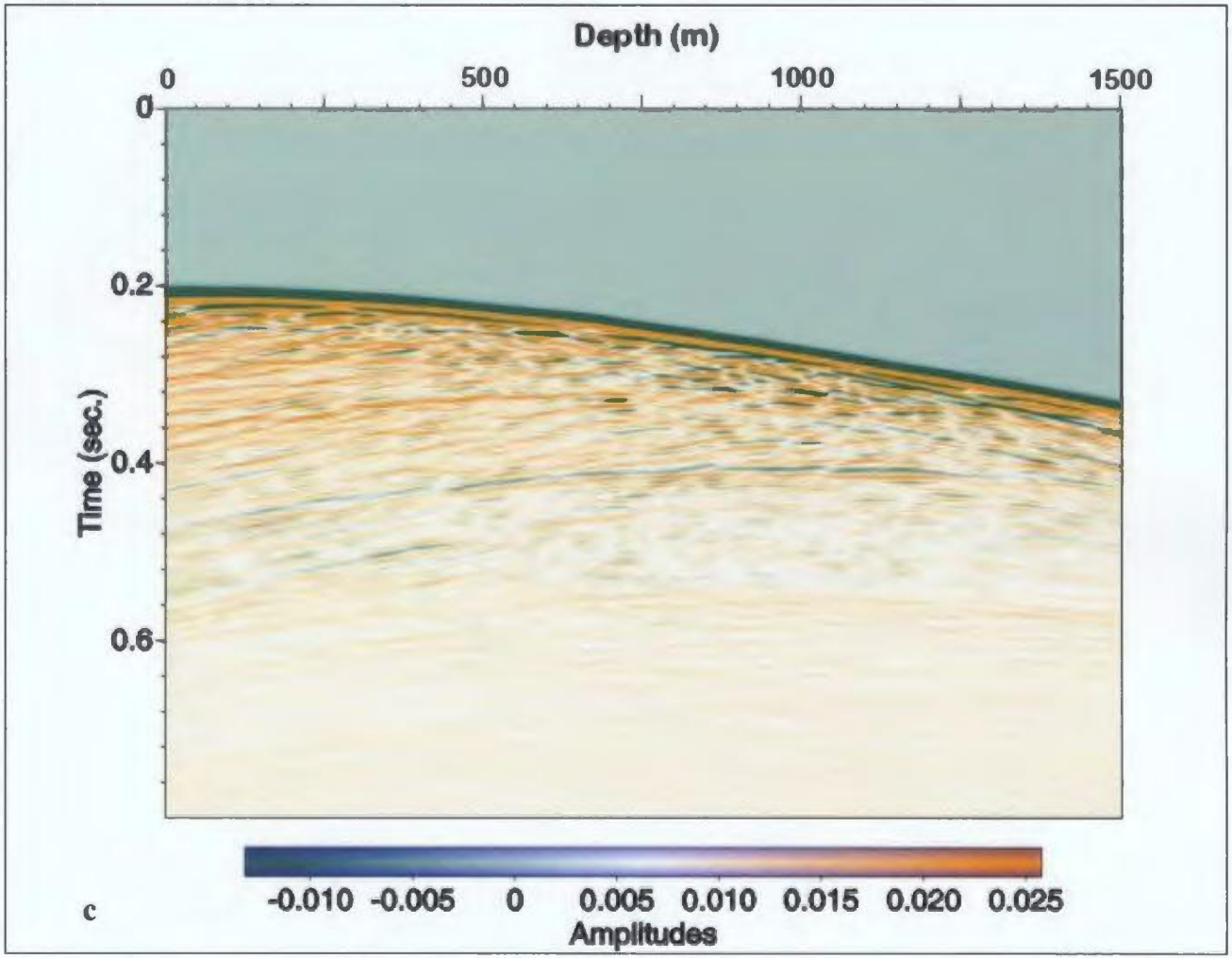

Figure 4.1.6-2: c) Left VSP raw shot gather (shotpoint at 1140 m) over the scattering media octagon in scattering media host.

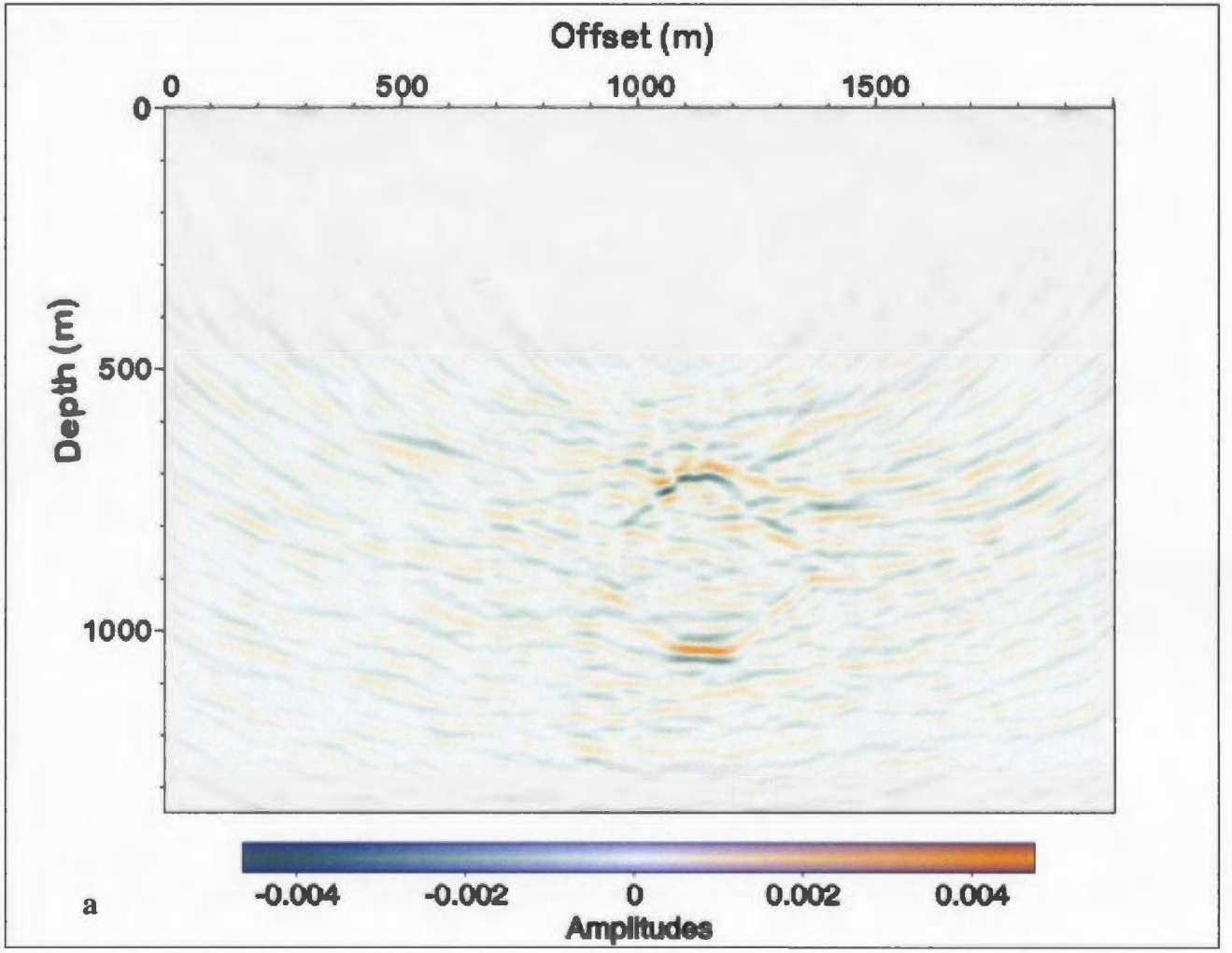

Figure 4.1.6-3: a) Migrated image of the scattering media octagon in scattering media background, using surface data only and 3 shots across the model space.

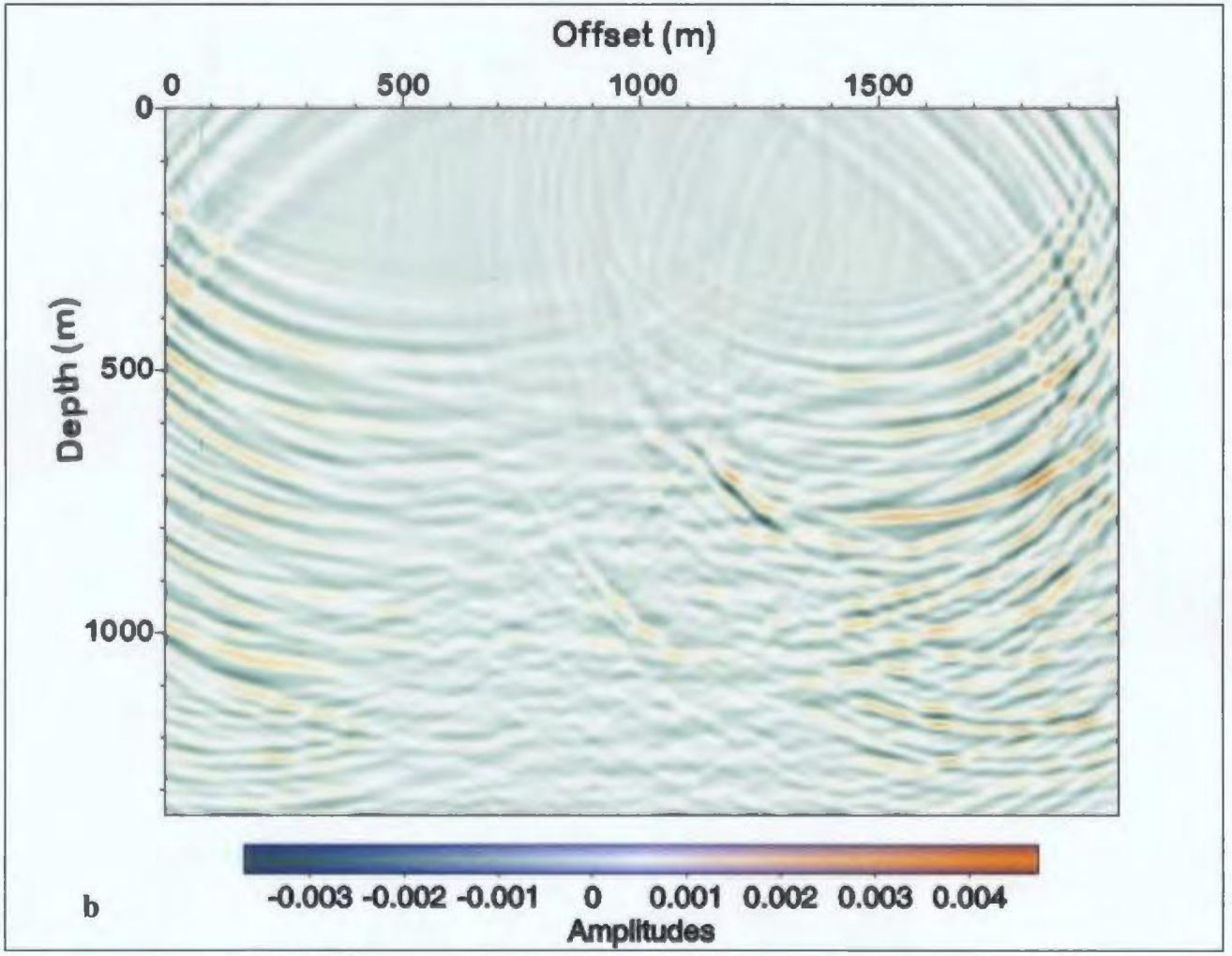

Figure 4.1.6-3: b) Migrated image of the scattering media octagon in scattering media background, using VSP data only and 3 shots across the model space.

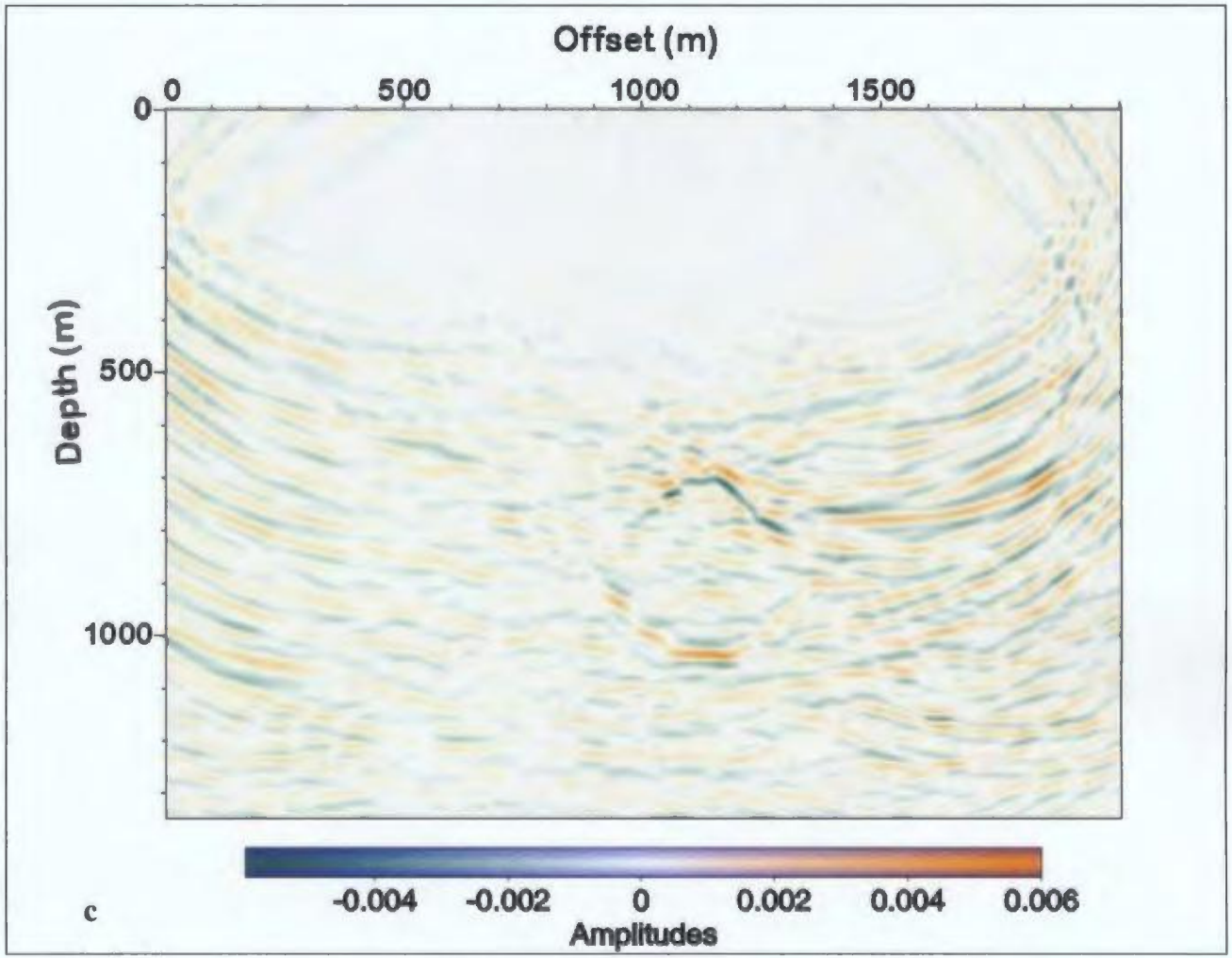

Figure 4.1.6-3: c) Migrated image of the scattering media octagon in scattering media background, using both surface and VSP data together and 3 shots across the model space. Notice that c) is a slight improvement over a) and that right-dipping faces are imaged much better than left-dipping ones due to the smaller offset to the right VSP.

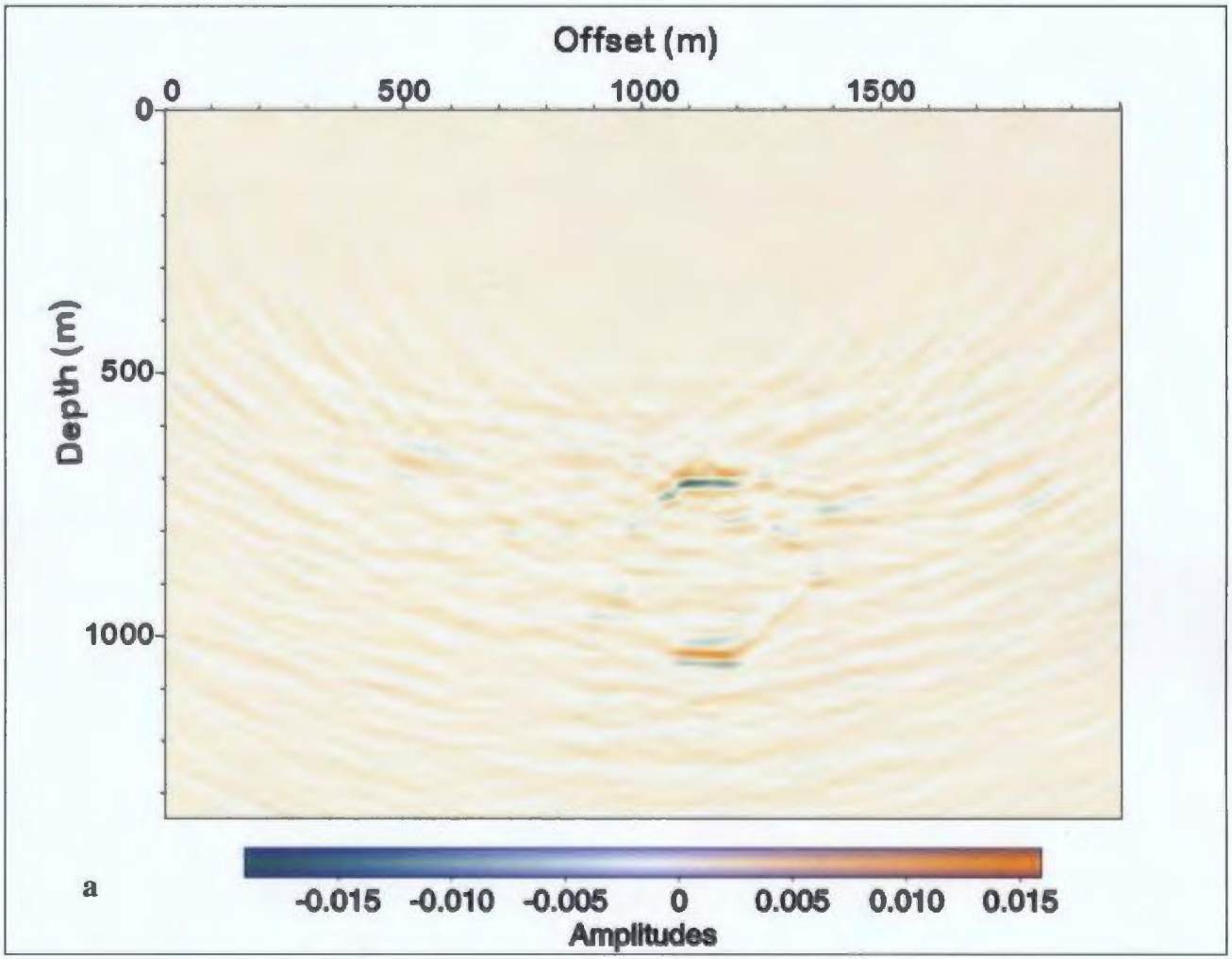

Figure 4.1.6-4: a) Migrated image of scattering media octagon in scattering media background, using surface data only and 10 shots across the model space. Compare with Figure 4.1.6-3a) and notice that the result using 10 shots gives better definition of the sides of the target object.

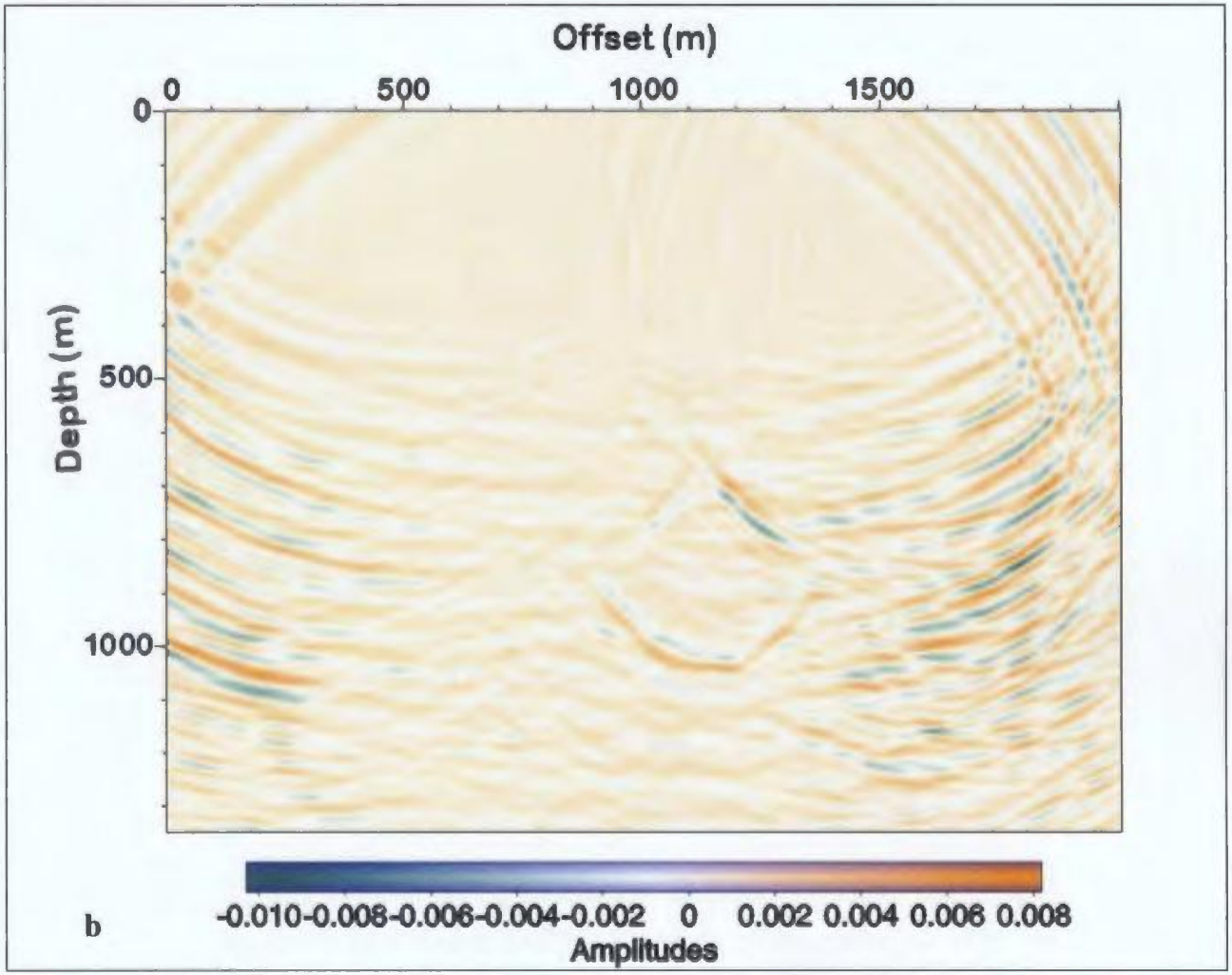

Figure 4.1.6-4: b) Migrated image of scattering media octagon in scattering media background, using VSP data only and 10 shots across the model space. Compare with Figure 4.1.6-3b) and notice that the result using 10 shots gives better definition of the sides of the target object.

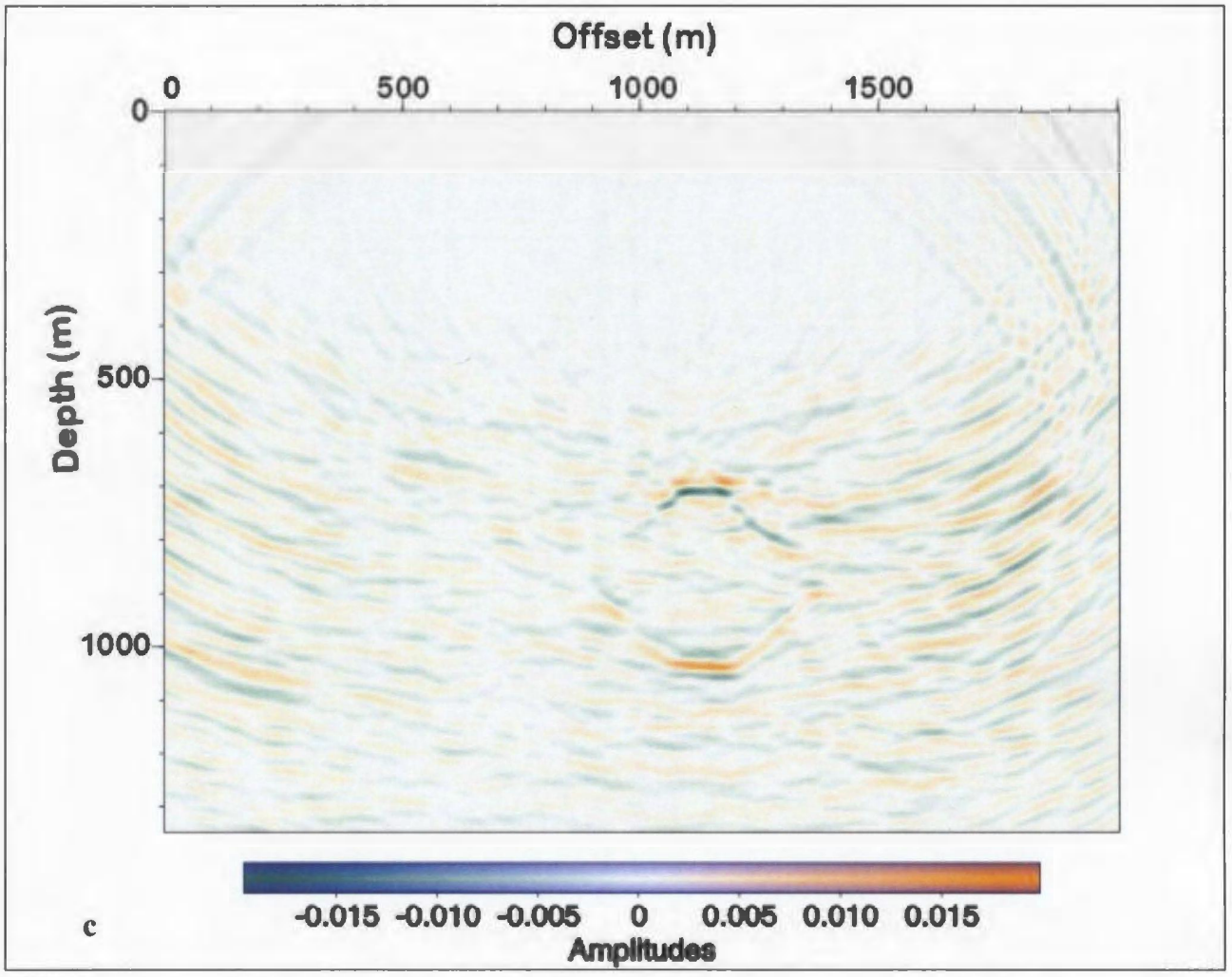

Figure 4.1.6-4: c) Migrated image of scattering media octagon in scattering media background, using both surface and VSP data together and 10 shots across the model space. Compare with Figure 4.1.6-3c) and notice that the result using 10 shots gives better definition of the sides of the target object. There is significant improvement in image quality of dipping faces in c) compared with a) due to the inclusion of VSP data in the migration.

4.1.7 Examination of Imaging Qualities of the Model Space

To examine the coverage of the model space that is provided by two boreholes and one surface array (see Figure 4.1.7-1), models were run with the standard octagon located at 8 positions. For each position, 3 shot locations were used (300 m, 1140 m, 1900 m) and the synthetic data were processed (1st breaks were muted, band-pass filtered 20/25-120/125) and then pre-stack depth migrated to evaluate the level of detection at each of the 8 positions. The detection level for each position was evaluated by awarding it a number out of 8 with one point given to a clearly-imaged side, and ½ point awarded for each face that was poorly-imaged (considered to be the detection threshold).

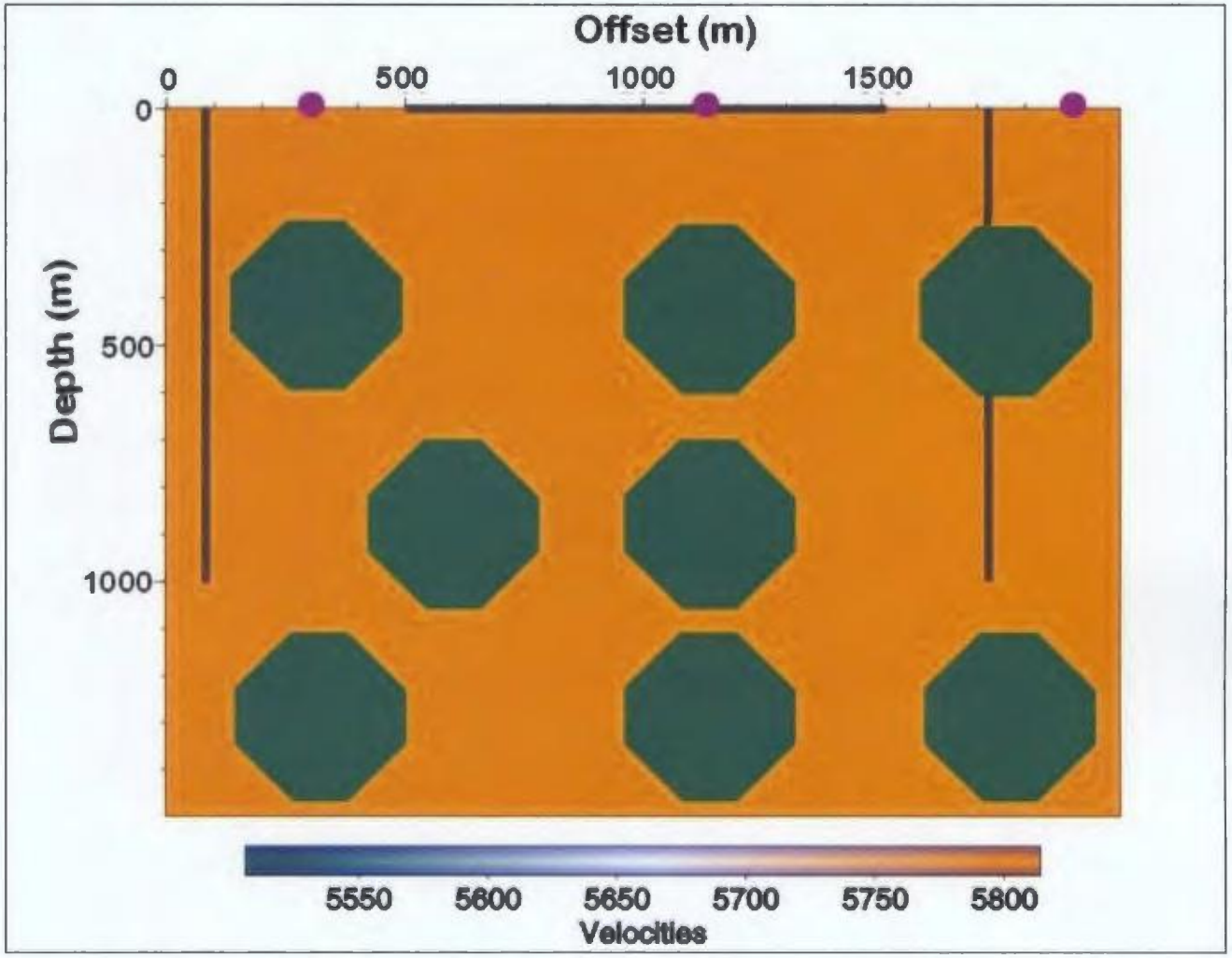

Figure 4.1.7-1: Model space showing the positions of octagons for examining the imaging capability of a combined surface and double VSP array. Violet circles indicate shotpoint locations, black lines indicate seismic array locations.

Figure 4.1.7-2 shows the compilation of results where the percentage in the octagon indicates the level of imaging and the imaged faces are highlighted. Clearly, the best imaging occurs when the target is located between the boreholes and above the bottom of the VSP array and the worst detection occurs when the target object is located beneath the boreholes and toward the outside of the array. The ability to image an target object drops off significantly when it lies close to, or is cut by one of the boreholes. In addition, if the target lies close to one of the boreholes and a shot location is at a relatively far offset (e.g., octagon A and shot location at 1900 m), the reflections from upper faces arrive simultaneously with the direct wave in VSP data. When the direct wave is muted during processing there is very little usable data left that can contribute to the final migrated image. Therefore, for the best possible imaging, choose boreholes away from the target object, use a surface spread that connects the boreholes (and/or a line perpendicular to the plane they lie in) and locate shots carefully so that it maximises the amount of usable data collected.

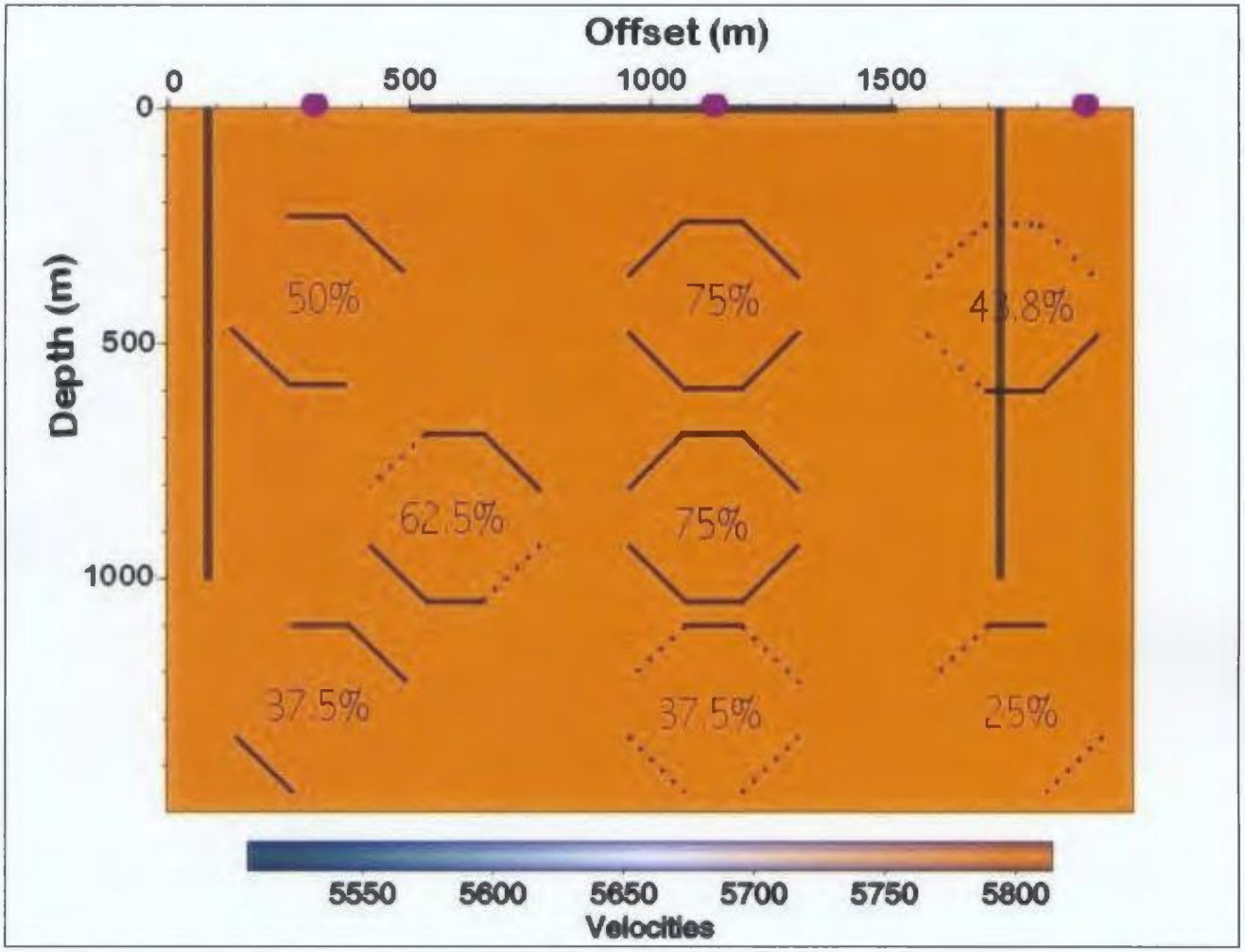

Figure 4.1.7-2: Results of examining the imaging qualities of the model space. Solid segments of octagon faces indicate faces that were well-imaged, dotted faces were poorly-imaged, missing faces were not imaged at all. Percentages indicate how much of the octagon was identifiable for each position. The best positioning is for the VSPs to be on either side of the target object and to extend to the depth of the target object.

4.2 Other Geometries

To experiment with the effectiveness of this tool on more complex geometries than an octagon, more numerical models were run. These were not done in an effort to achieve a more realistic target object, but merely as a test of the robustness of the method. For each of these models, the shot locations; recording positions for VSPs and surface profiles; target object position; and the velocities and densities were identical to those used for the standard asymmetric octagon model.

4.2.1 Standard Sputnik

This geometry (see Figure 4.2.1-1) was named for its resemblance to old satellites and was created by placing a box-shaped protuberance on each flat face of the standard asymmetric octagon. Doing this created many corners and small faces with size on the order of the dominant (peak) wavelength ($\lambda_{dom} \cong 77$ m) thereby increasing the number of possible diffractors and decreasing the number of specular reflectors. This model used 10 shots across the horizontal array and was processed similar to the standard octagon. Figure 4.2.1-1b shows the labelled faces of the "sputnik" target that are identifiable in shot records (compare with Figure 4.2.1-2b).

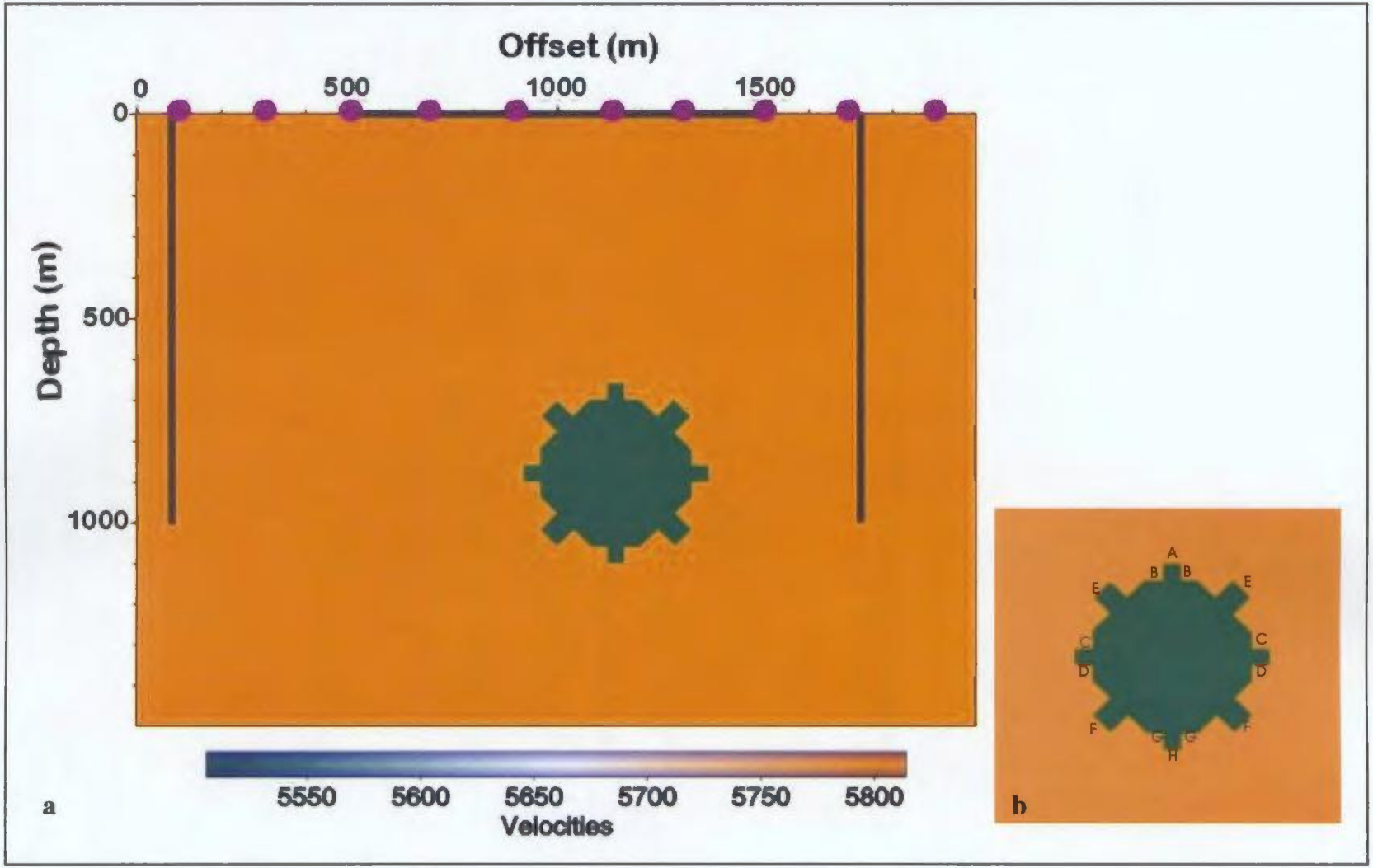

Figure 4.2.1-1: a) Model space for the irregular target object shape "sputnik"; b) labelled faces of identifiable reflections in shot gathers (see Figure 4.2.1-2b).

Figures 4.2.1-2a,b,c show a horizontal-profile zero-offset shot gather (a) over the target (shot location at 1140 m), while (c) shows a left VSP shot gather (again, the shot location was at 1140 m). The horizontal shot gather shows a large number of well-separated diffractions (approximately 14), most of which can easily be related to a part of the target object and have qualitatively larger amplitudes than those of the VSP (see Figure 4.2.1-2b). The VSP also shows a large number of diffractions but other than the nearest and farthest faces of the target object (compare with Figure 4.1.1-1a, and Figure 4.1.1-3b), it is difficult to distinguish them from each other.

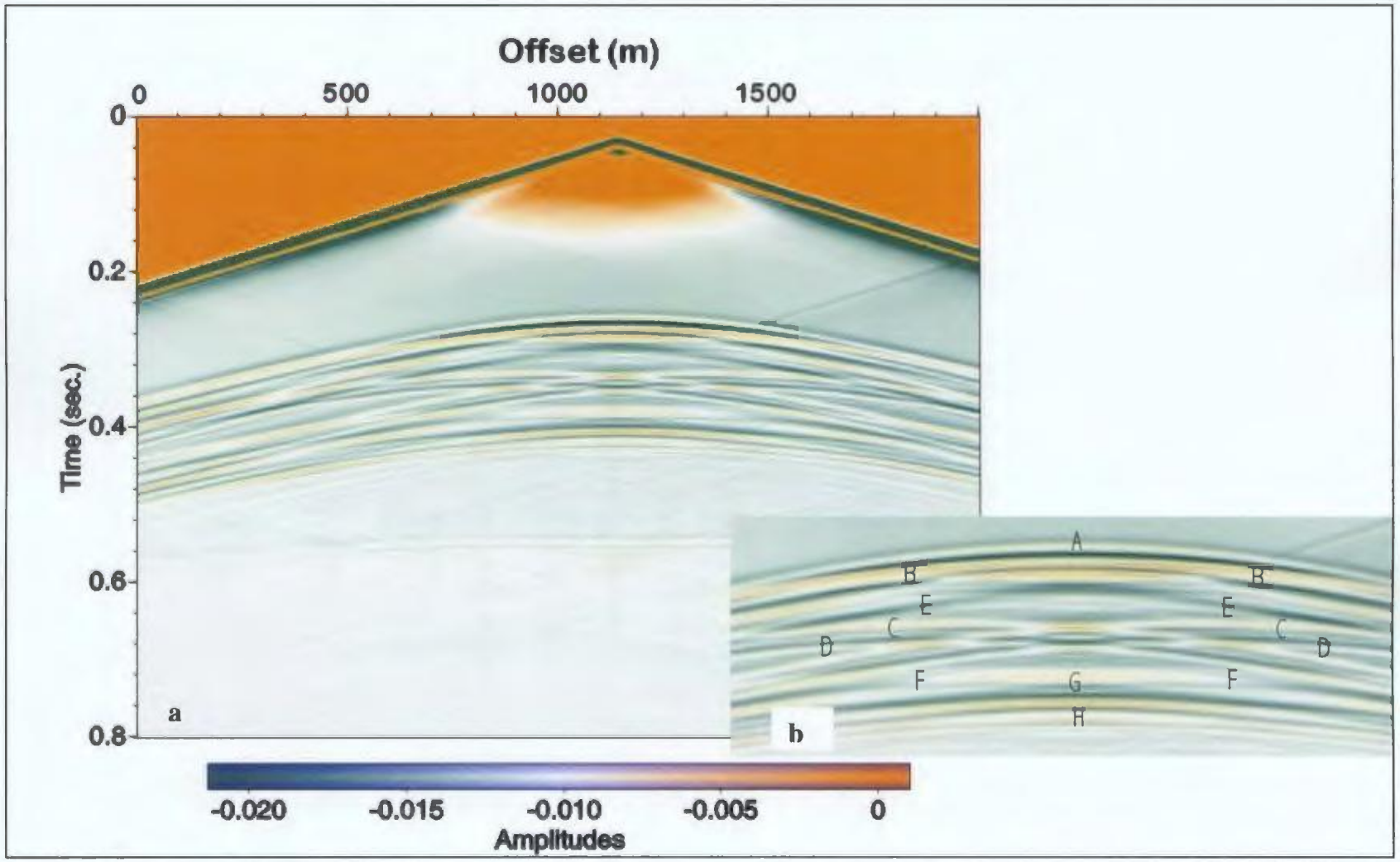

Figure 4.2.1-2: a) Raw shot gather over the "sputnik" model; b) enlargement of a) with labelling corresponds to faces that created the reflections (compare with Figure 3.2.1-1b).

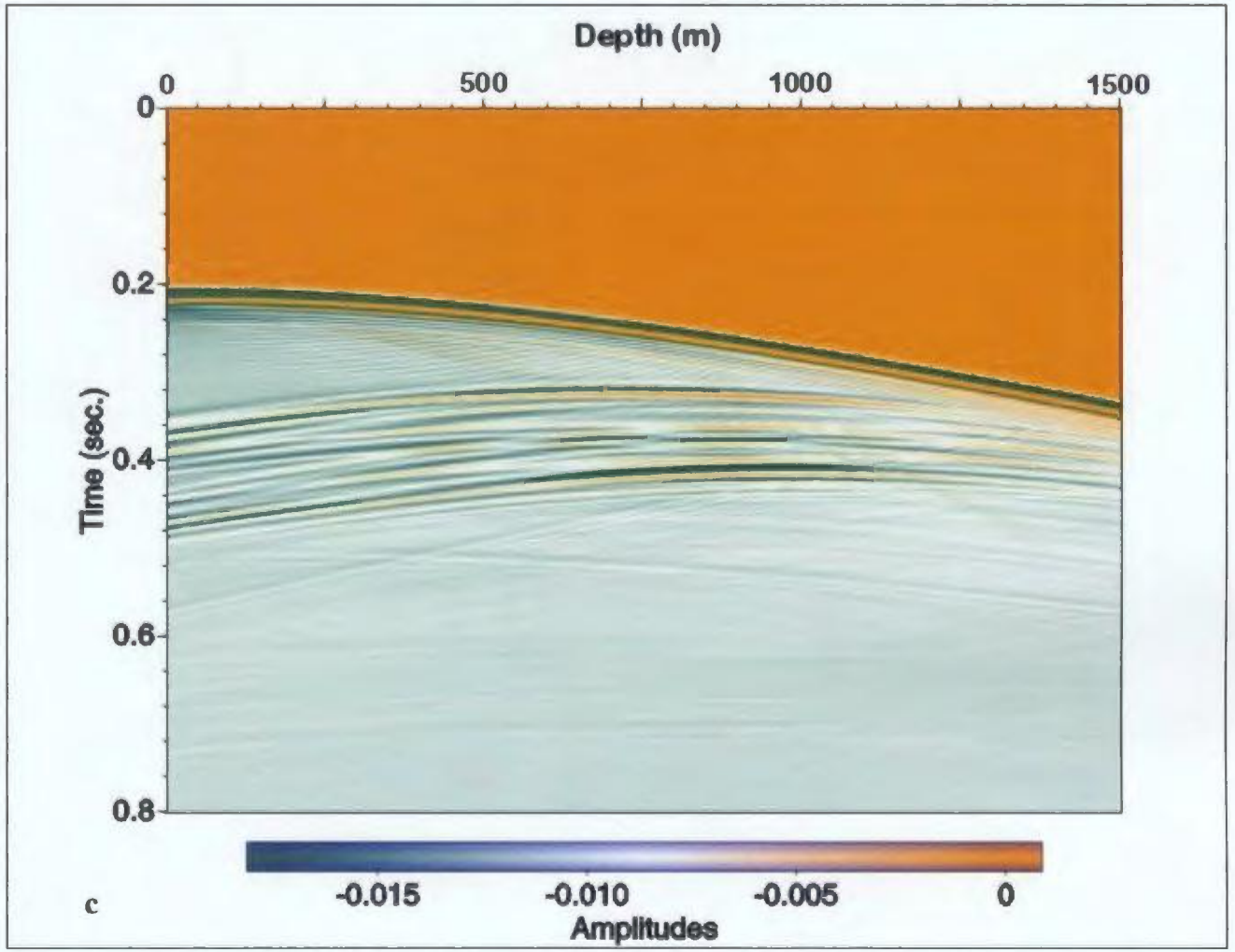

Figure 4.2.1-2: c) Raw shot gather from the left VSP over the "sputnik" model, note that it is difficult to identify the specific surface (see Figure 4.2.1-1b) that produced the reflections .

Figures 4.1.2-3a,b,c show the pre-stack migrations of sputnik using, respectively, horizontal data only; VSP data only; and horizontal and VSP data together. The horizontal-only migrated image shows a well-defined anomaly with good images of most faces. It appears that corners facing upward created more problems for the migration algorithm than flat faces by the fact that their diffractions are not completely migrated. Looking closely, the left side of the image is of higher quality than the right, which can be attributed to the wider aperture available for energy returning from the left side of the target object (to the horizontal array) compared to the right side. The VSP-only migration is clearly dominated by the energy collected by the right VSP and images right-dipping faces well, but left-dipping and horizontal ones are poorly constrained. The migration using both horizontal and VSP data looks very similar to that using horizontal data only, and is probably dominated by the energy collected by the horizontal array, with one difference: the right and left sides of this image are of an identical quality. Therefore, the inclusion of VSP data improved the imaging of the target object to a level where its geometry was represented clearly.

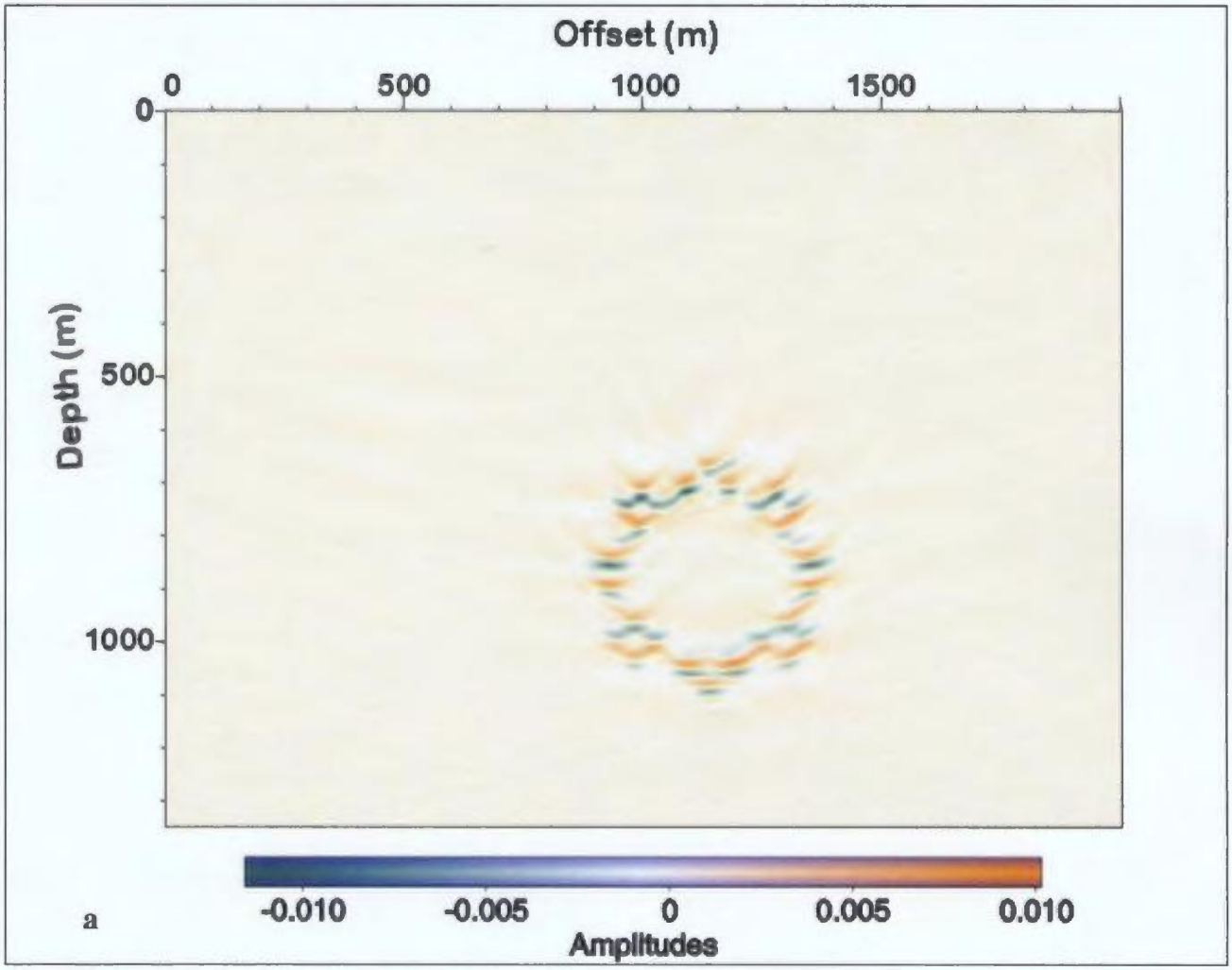

Figure 4.2.1-3: a) Migrated image of the "sputnik" target object using surface seismic data only.

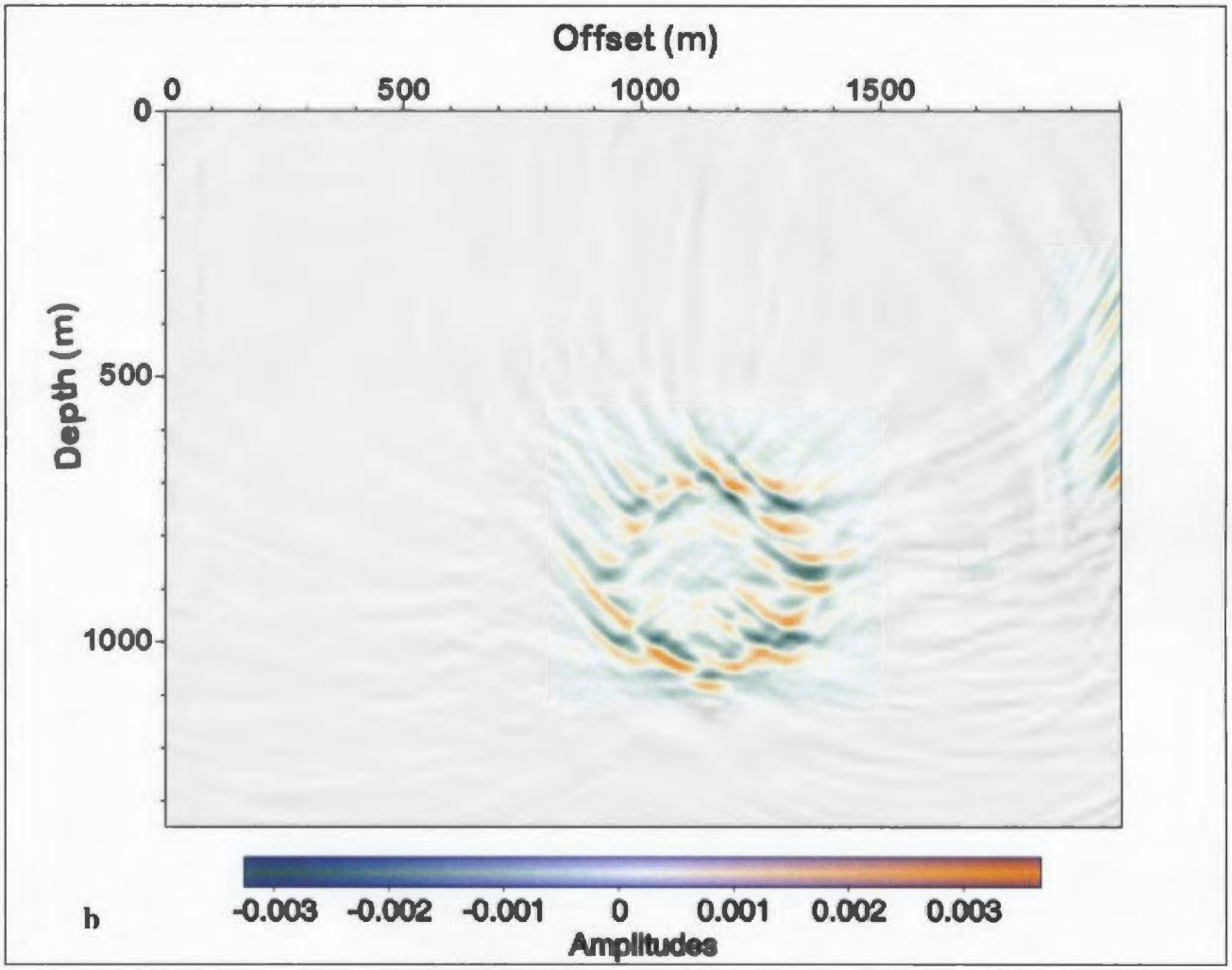

Figure 4.2.1-3: b) Migrated image of the "sputnik" target object using VSP data only.

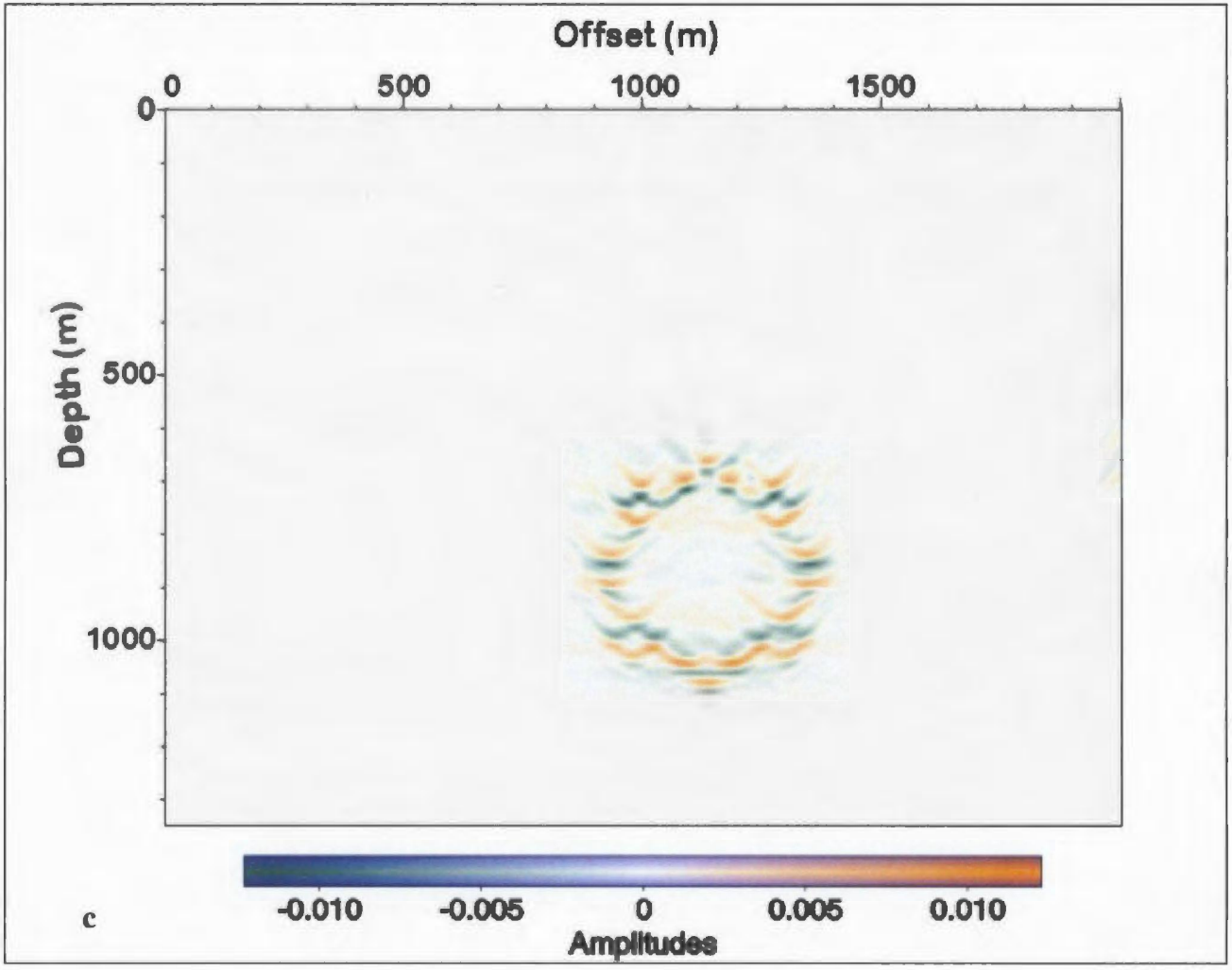

Figure 4.2.1-3: c) Migrated image of the "sputnik" target object using a both surface and VSP data, notice there is no significant improvement in the migrated image by including VSP data.

4.2.2 Randomly-Scattering Media: Target Object and Background

Wishing to test the robustness of the findings of Section 4.2.1, a more complex case was created. Using parameters identical to those in Section 4.1.6, a sputnik of random-scatter media was created inside a random-scatter media host (see Figure 4.2.2-1) and synthetic seismograms were calculated.

Figures 4.2.2-2a,b show the raw shot gathers from the horizontal profile and left VSP, respectively. Despite the scattering media, the horizontal profile still clearly shows reflections from the top and bottom of the target object, but other diffractions do not appear at all. Similarly, the left VSP shows approximately 3 reflections (probably from the near, upper and far, lower left-dipping sides), but they are not as clear as those from the horizontal profile, and other diffractions that were evident in the homogeneous case do not appear at all.

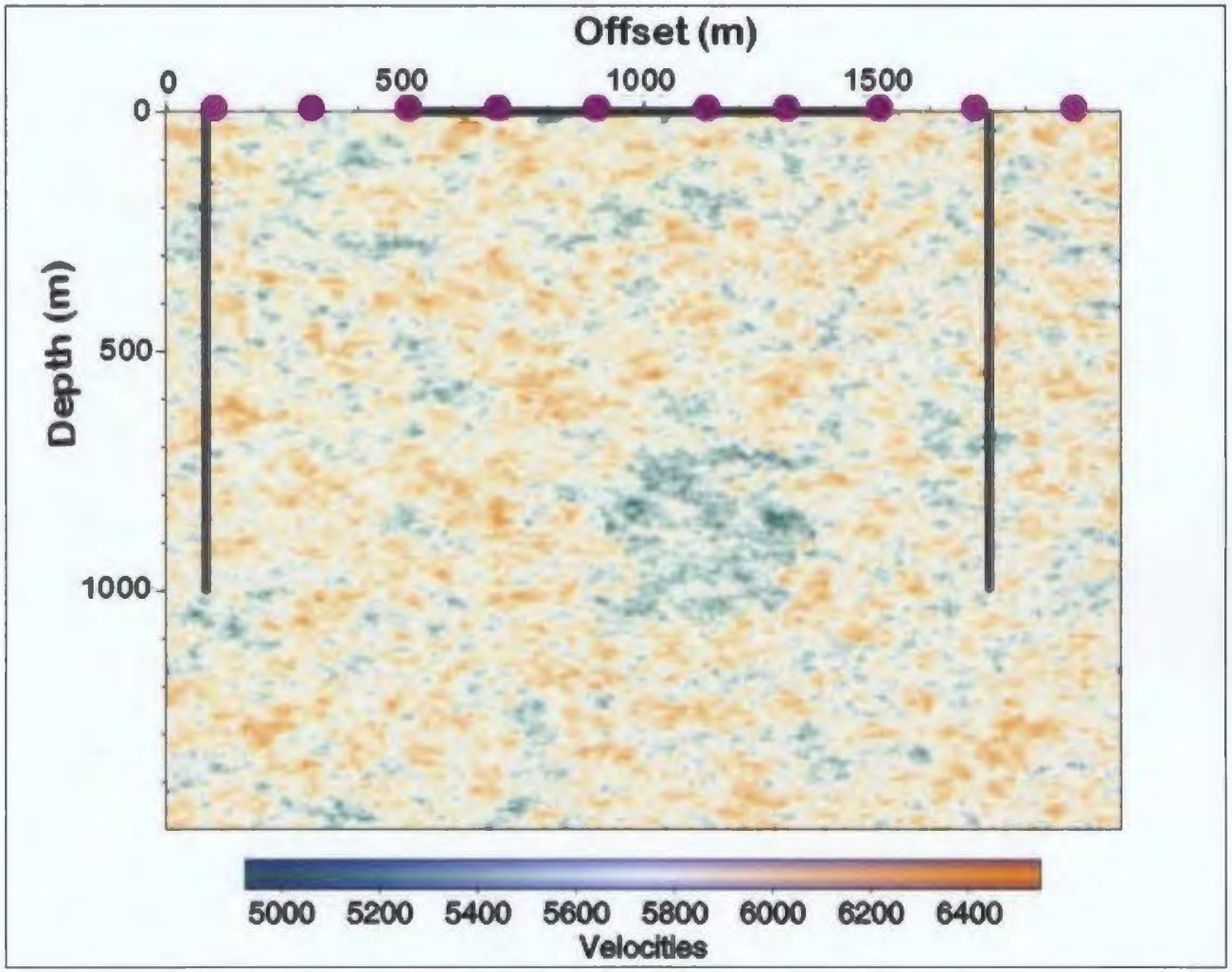

Figure 4.2.2-1: Model space of scattering media "sputnik" model in scattering media background. Violet circles indicate shot point locations, and black lines indicate seismic survey locations.

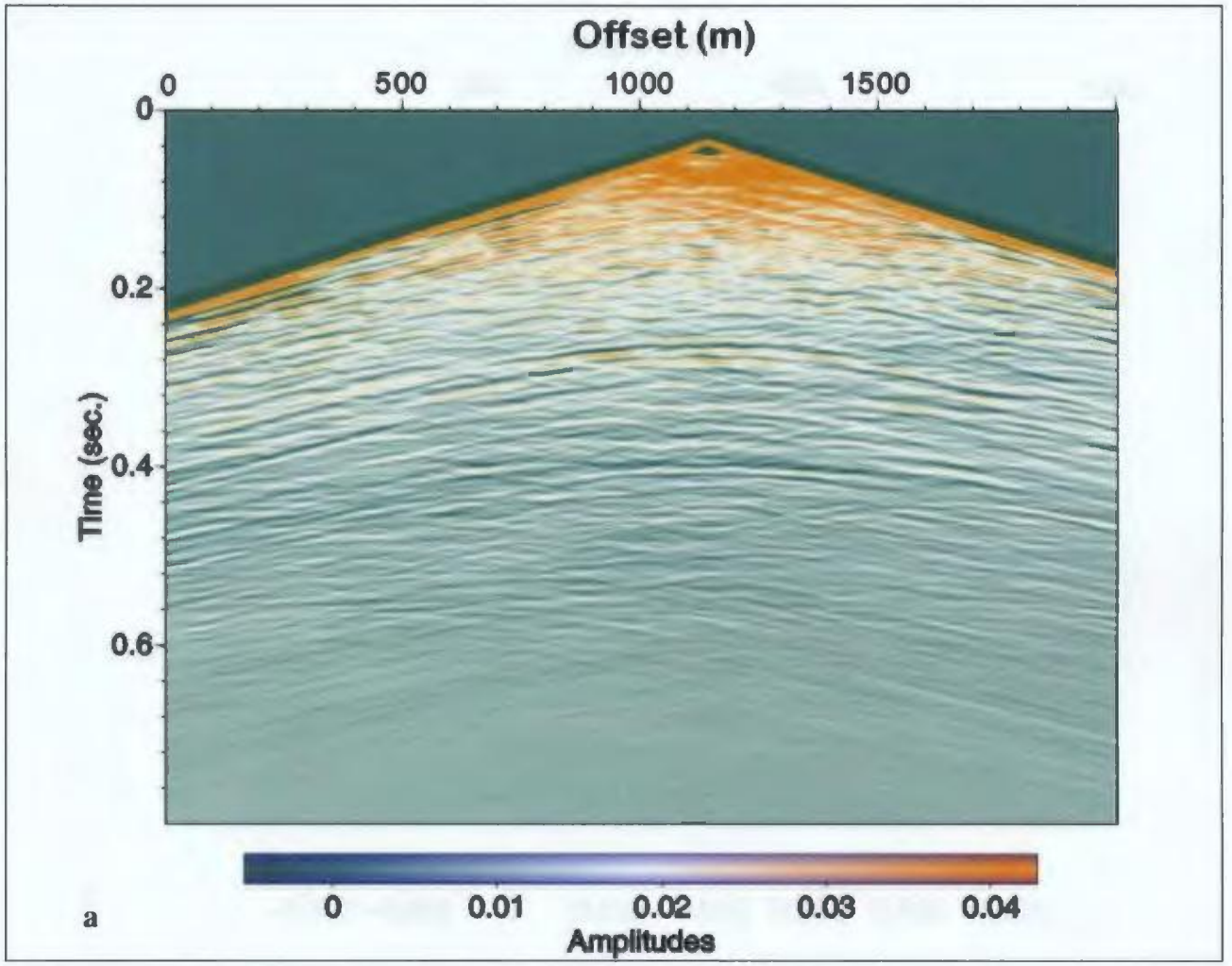

Figure 4.2.2-2: a) Raw shot gather from a surface seismic array over the scattering "sputnik" target object in scattering media background, shot at 1140 m. Notice that reflections that were evident in Figure 4.2.1-2a are barely visible here.

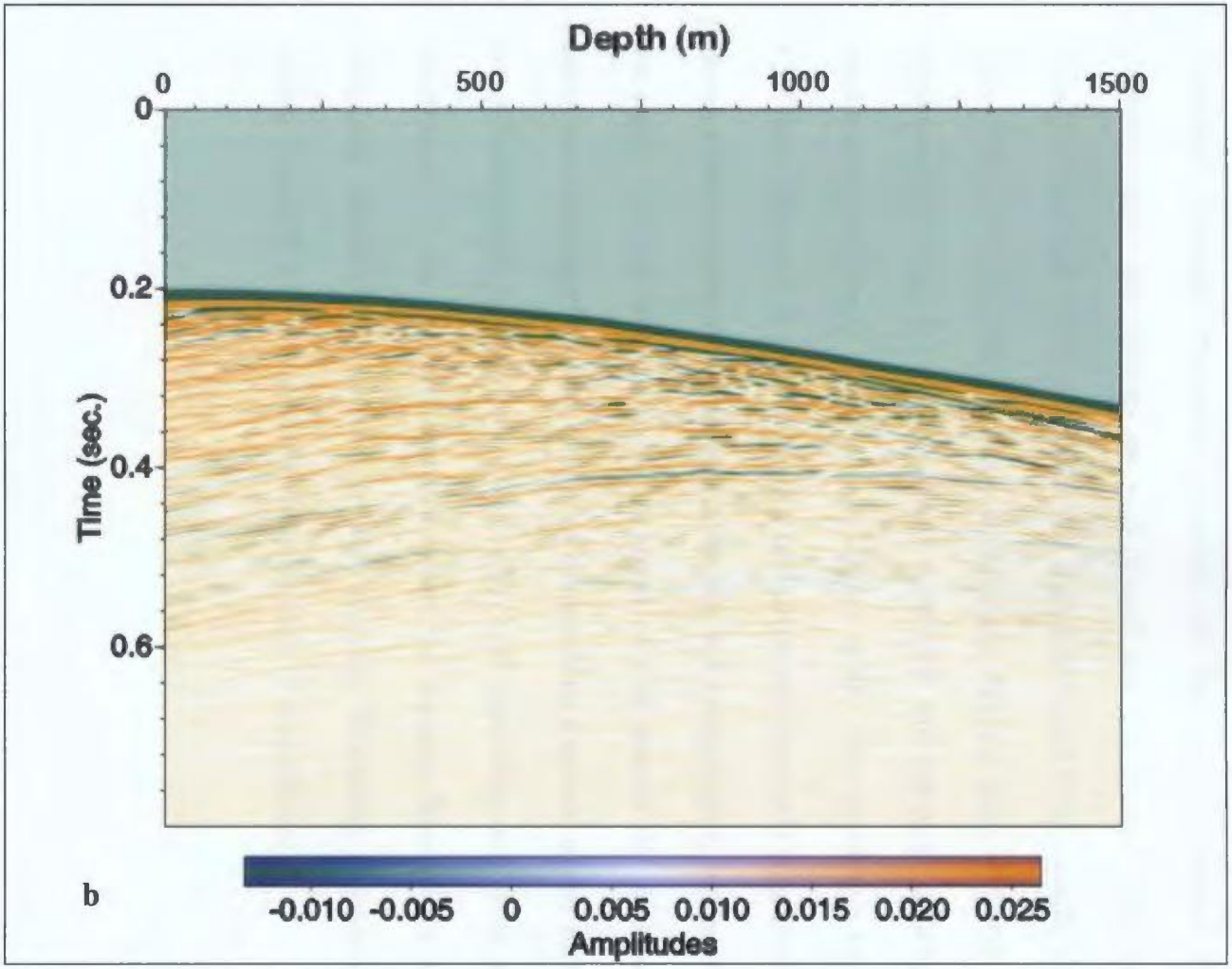

Figure 4.2.2-2: b) Raw shot gather of the left VSP over the scattering "sputnik" target object in scattering media background, shot at 1140 m,. Notice that reflections that were evident in Figure 4.2.1-2c are barely visible here.

The data were migrated and the results are shown in Figures 4.2.2-3a,b,c (horizontal data only, VSP data only, horizontal and VSP data together). The horizontal data-only migration is similar to that of the original sputnik—the horizontal faces and corners are well imaged and the general shape of the target object is detectable, but the left side has a slightly higher image quality than the right side. The VSP data-only migration shows right-dipping faces well and seems to be dominated by energy recorded from the right VSP, but left-dipping faces are poorly-resolved and horizontal faces do not appear at all. The combined horizontal and VSP data migration is very similar to the horizontal data-only migration, and it still shows some asymmetry in image quality (the left being slightly better resolved than the right). This indicates that the inclusion of VSP data in the migration does not contribute significantly to the quality of the resulting migrated image and is therefore not advantageous in this geometry. The VSP data may not have a significant contribution to the migrated image because the dipping faces of the target object were not adequately illuminated by the sources, illustrating a main challenge to seismic acquisition over irregularly-shaped zones of mineralisation.

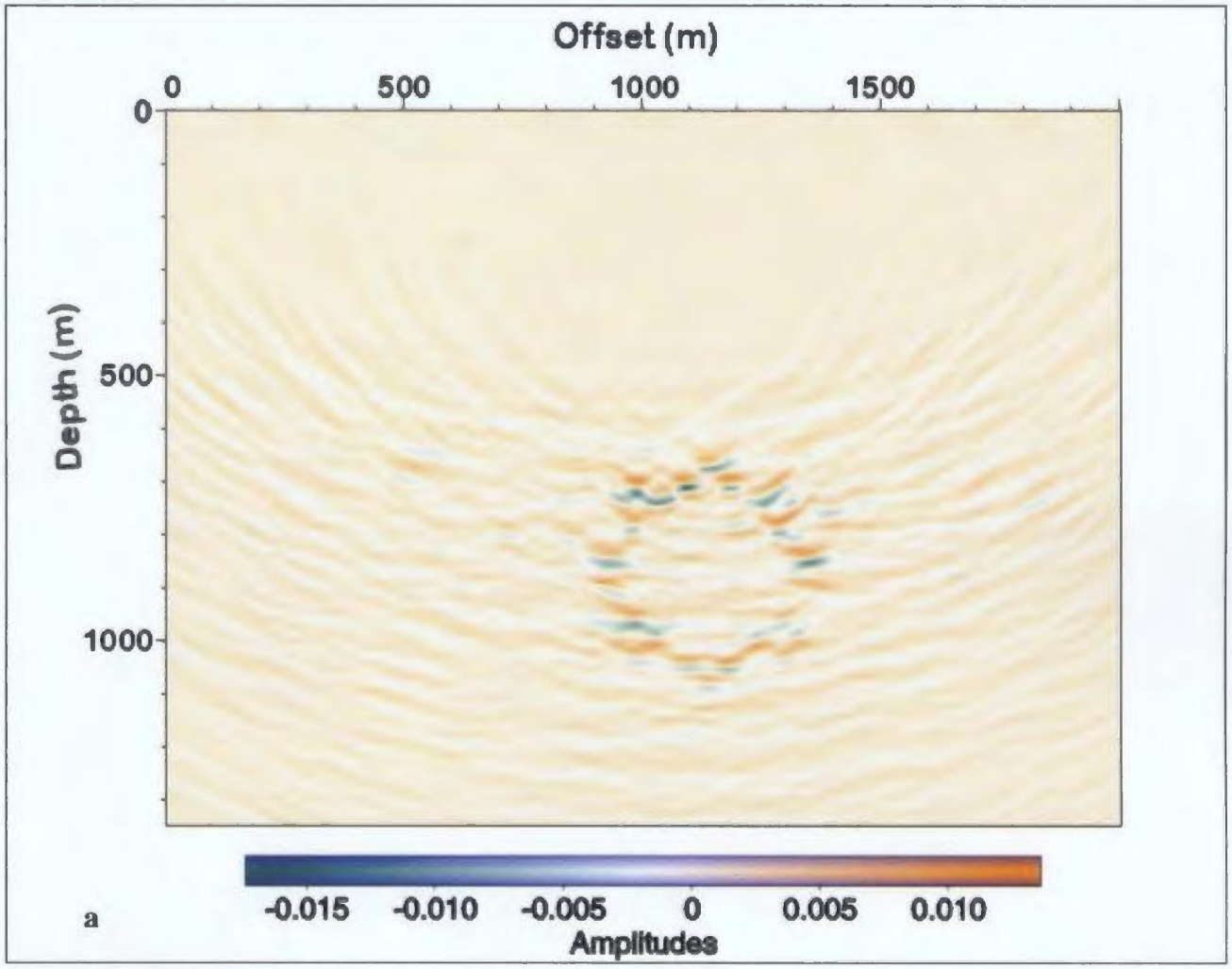

Figure 4.2.2-3: a) Migrated image of the scattering "sputnik" target object in scattering background media, using surface data only.

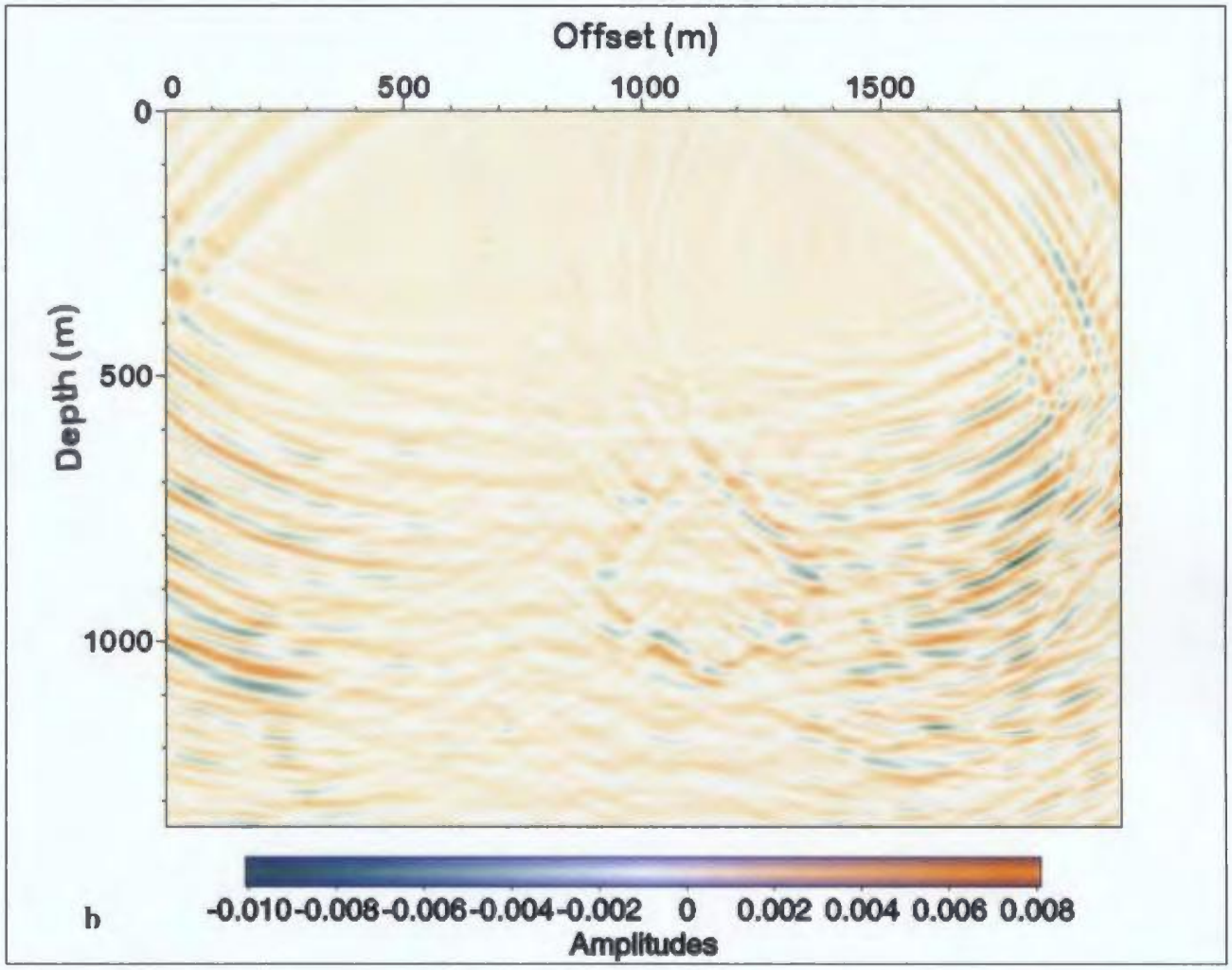

Figure 4.2.2-3: b) Migrated image of the scattering "sputnik" target object in scattering background media, using VSP data only.

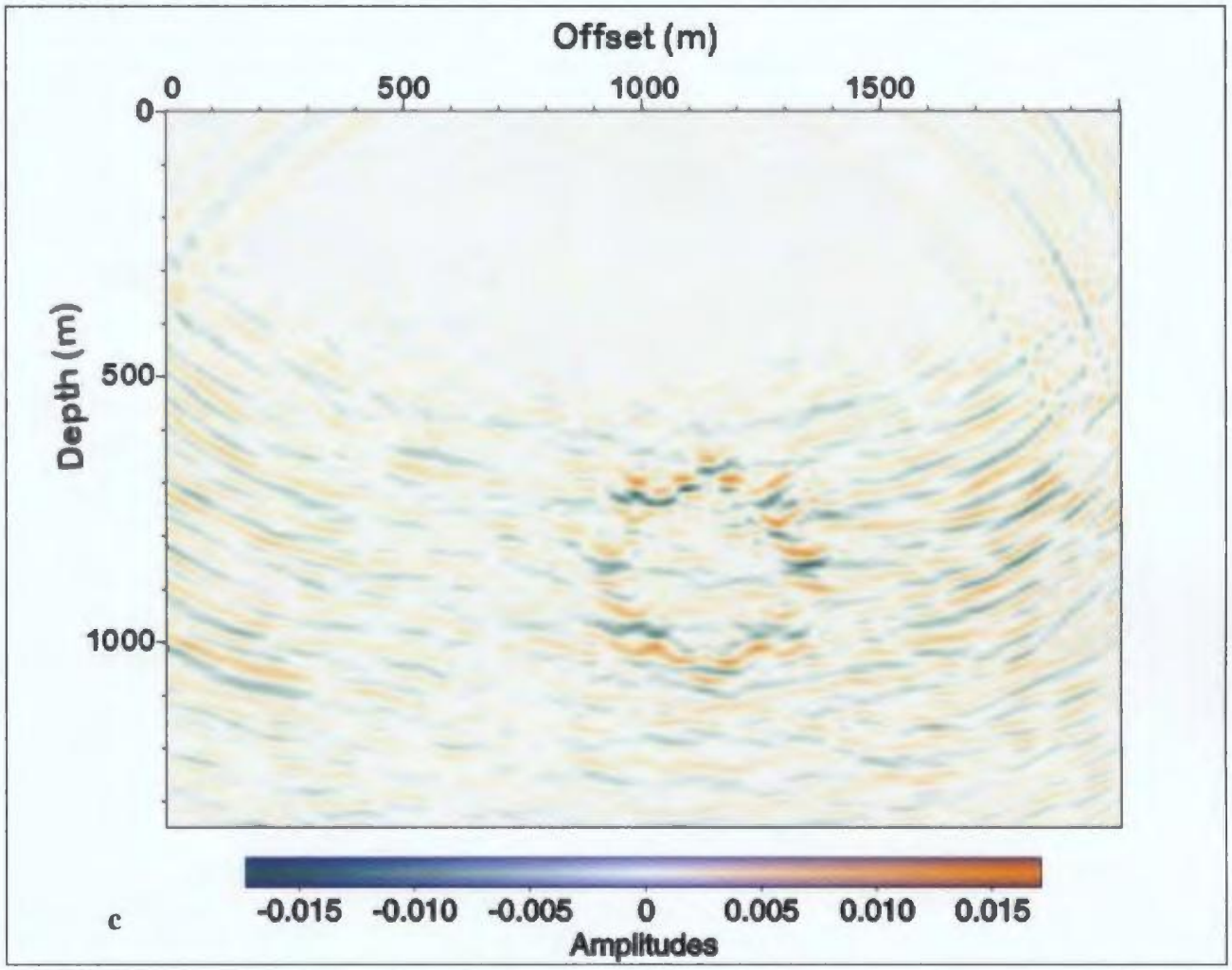

Figure 4.2.2-3: c) Migrated images of the scattering "sputnik" target object in scattering background media, using both surface and VSP data.

Chapter 5. Conclusions and Recommendations for Future Work

Limitations of seismic applications to mineral exploration include the following: the cost of acquiring and processing data; lack of experience in data acquisition and processing; cost of borehole re-opening; locations of existing boreholes; non-unique solutions to subsurface anomalies; and the level of success depends upon a priori knowledge of the subsurface (e.g., target object size, shape, depth, mineralisation type and properties, and host rock properties).

The integration of surface and VSP data effectively widens the recording aperture and the inclusion of VSP data decreases problems with the variable near-surface low-velocity layer. The results from this investigation have demonstrated there is improved seismic imaging by including simultaneously-recorded borehole seismic (VSP) data with surface data. In the most realistic model case, where both the mineralisation target and host rock were created from scattering media, the migrated seismic section showed noticeable improvement after integrating surface and borehole seismic data, compared with using surface seismic data alone. All horizontal faces and almost all dipping faces were clearly imaged (the remaining dipping faces were at the detection level) in the integrated surface and VSP migrated images. But the VSP arrays are limited in aperture and do not collect useful reflection data from horizontal or sub-horizontal lenticular bodies. Having a larger number of well-spaced source locations appears to better illuminate the important aspects of the target's geometry thereby increasing image quality. As indicated by Eaton (1999), the scattered energy for this type of mineralisation was at a maximum in the backward direction, and the dipping faces were primarily imaged by energy recorded from the VSPs (which were optimally oriented to

record energy from dipping features), while horizontal faces were primarily imaged by energy recorded from the surface array. For best results, the VSP wavefield should be separated during processing to remove downgoing waves and pre-stack migration algorithms should be used if possible.

Agreeing with field results of Gingerich *et al.* (2000), this research indicates that massive sulphide deposits greater than 500 m in depth can be detected directly by seismic surveying. This technique shows great promise for use in crystalline terrains and for dipping and/or complex structures in any geological setting. For optimal imaging purposes using two VSP arrays and a surface array, the VSPs should be placed on either side of the target and extend to the depth of interest, while the worst imaging quality occurs when the VSPs cut through the target, or the target lay directly beneath one of the VSP arrays.

Future work should include the following: 1) finite difference modelling using different target object geometries to determine the benefit of integrating surface and VSP seismic data; 2) finite difference modelling to include a near-surface low-velocity layer; 3) ray-trace modelling to investigate the possibility of destructive interference in recorded data; 4) elastic wave modelling to examine the added value (and complexity) that S-waves offer; 5) experimenting with different layouts of boreholes and surface profiles to categorize strengths and weaknesses of each respective geometry; and 6) a field test over a known mineral deposit with well-known geometry and lithology using close receiver spacing and shot spacing that adequately illuminates the major aspects of the mineralisation geometry.

References

Adair, R.N. 1992. Stratigraphy, Structure, and Geochemistry of the Halfmile Lake Massive-Sulfide Deposit, New Brunswick. Exploration Mining Geology, Vol. 1, No. 2, pp. 151-166.

Adam, E., Arnold, G., Beaudry, C., Matthews, L., Milkereit, B., Perron, G., Pineault, R. 1997. Seismic Exploration for VMS Deposits, Matagami, Québec. In "Proceedings of Exploration 97: Fourth Decennial International Conference on Mineral Exploration" edited by A.G. Gubins. pp. 433-438.

Bellefleur, G., Müller, C., Snyder, D., Matthews, L. 2002. Downhole Seismic Scattered and Mode-Converted Waves from the Halfmile Lake Massive Sulfide Orebody, New Brunswick. 72nd SEG International Exposition and Annual Meeting, Salt Lake City, Utah, October 6-11, 2002.

Drummond, B.J., Goleby, B.R., Owen, A.J., Yeates, A.N., Swager, C., Zhang, Y., Jackson, J.K. 2000. Seismic reflection imaging of mineral systems: Three case histories. Geophysics, Vol. 65, No. 6, pp. 1852-1861.

Eaton, D., Guest, S., Milkereit, B., Bleeker, W., Crick, D., Schmitt, D., Salisbury, M. 1996. Seismic Imaging of Massive Sulfide Deposits: Part III. Borehole Seismic Imaging of Near-Vertical Structures. Economic Geology, Vol. 91, pp. 835-840.

Eaton, D.W., Milkereit, B., Adam, E. 1997. 3-D Seismic Exploration. In "Proceedings of Exploration 97: Fourth Decennial International Conference on Mineral Exploration" edited by A.G. Gubins. pp. 65-78.

Eaton, D. 1999. Weak elastic-wave scattering from massive sulfide orebodies. Geophysics, Vol. 64, No. 1, pp. 1-11.

Gingerich, J.C., Matthews, L.W., Peshko, M.J. 2000. The Development of New Exploration Technologies at Noranda: Seeing More with Hyperspectral and Deeper with 3-D Seismic. Prospectors and Developers Association of Canada International Convention, March 5-10, 2000, Toronto.

Holliger, K. 1996. Upper-crustal seismic velocity heterogeneity as derived from a variety of P-wave sonic logs. Geophys. J. Int. Vol. 125, pp. 813-829.

Holliger, K., Robertsson, J.O.A. 1998. Effects of the shallow subsurface on upper crustal seismic reflection images. Tectonophysics Vol. 286. pp. 161-169.

Juhlin, C. 1997. Experiences from Shallow Reflection Seismics Over Granitic Rocks in Sweden. In "Proceedings of Exploration 97: Fourth Decennial International Conference on Mineral Exploration" edited by A.G. Gubins. pp. 455-460.

Kallweit, R.S., Wood, L.C. The limits of resolution of zero-phase wavelets. Geophysics, Vol. 47, No. 7 (July 1982), pp. 1035-1046.

Kelly, K.R., Ward, R.W., Treitel, S., Alford, R.M. 1976. Synthetic Seismograms: A Finite-Difference Approach. Geophysics, Vol. 41, No. 1, pp. 2-27.

Kirtland Grech, M.G., Lawton, D.C. Integrated prestack depth migration of VSP and surface seismic data. EAGE 63rd Conference and Technical Exhibition. Amsterdam, The Netherlands. 11-15 June, 2001.

Kocurko, T., Lines, L. 1998. Parallel Computation for Prestack Migration by Aplanatic Surfaces. In Proceedings of Advances in Scientific Computing and Modeling, ed. S.K. Dey, J.P. Ziebarth, J.M. Ferrandiz (Special Proceedings of IMACS '98), Alicante, Spain.

Li, Y., Calvert, A.J. 1997. Seismic Reflection Imaging of a Shallow, Fault-Controlled VMS deposit in the Matagami Mining Camp, Québec. In "Proceedings of Exploration 97: Fourth Decennial International Conference on Mineral Exploration" edited by A.G. Gubins. pp. 467-472.

Matthews, L. July 2003. Personal e-mail communication.

McMechan, G.A., Hu, L.-Z. 1986. Short Note On the effect of recording aperture in migration of vertical seismic profile data. Geophysics, Vol. 51, No. 10, pp. 2007-2010.

Milkereit, B., Eaton, D., Wu, J., Perron, G., Salisbury, M., Berrer, E.K., Morrison, G. 1996. Seismic Imaging of Massive Sulfide Deposits: Part II. Reflection Seismic Profiling. Economic Geology, Vol. 91, pp. 829-834.

Milkereit, B., Eaton, D. 1998. Imaging and interpreting the shallow crystalline crust. Tectonophysics, Vol. 286, pp. 5-18.

Milkereit, B., Berrer, E.K., King, A.R., Watts, A.H., Roberts, B., Adam, E., Eaton, D.W., Wu, J., Salisbury, M.H. 2000. Development of 3-D seismic exploration technology for deep nickel-copper deposits—A case history from the Sudbury basin, Canada. Geophysics, Vol. 65, No. 6, pp. 1890-1899.

Payne, M.A., Eriksen, E., Rape, T.D. 1994. Considerations for high-resolution VSP imaging. The Leading Edge, pp. 173-180.

Pflug, K.A., Mwenifumbo, C.J., Killeen, P.G. 1997. Full Waveform Acoustic Logging Applications in Mineral Exploration and Mining. Seismic Methods in Mineral Exploration Paper 61 In "Proceedings of Exploration 97: Fourth Decennial International Conference on Mineral Exploration" Edited by A.G. Gubins. pp. 477-480.

Roberts, B, Zaleski, E., Adam, E., Perron, G., Petrie, L., Darch, W., Salisbury, M.H., Eaton, D., Milkereit, B. 1997. Seismic Exploration of the Manitouwadge Greenstone Belt, Ontario. In "Proceedings of Exploration 97: Fourth Decennial International Conference on Mineral Exploration" edited by A.G. Gubins. pp. 451-454.

Salisbury, M.H., Milkereit, B., Bleeker, W. 1996. Seismic Imaging of Massive Sulfide Deposits: Part I. Rock Properties. Economic Geology. Vol. 91, No. 5, pp. 821-828.

Salisbury, M.H., Milkereit, B., Ascough, G., Adair, R., Matthews, L., Schmitt, D.R., Mwenifumbo, J., Eaton, D.W., Wu, J. 2000. Physical properties and seismic imaging of massive sulfides. Geophysics, Vol. 65, No. 6, pp. 1882-1889.

Sethian, J.A. 1996. *Level Set Methods: Evolving interfaces in geometry, fluid mechanics, computer vision, and materials science*: Cambridge, England, Cambridge University Press.

Sheriff, R.E. and Geldart, L.P. 1995. *Exploration Seismology*. 2nd ed. U.S.A., Cambridge University Press.

Spencer, C., Thurlow, G., Wright, J., White, D., Carroll, P., Milkereit, B., Reed, L. 1993. A vibroseis reflection seismic survey at the Buchans Mine in central Newfoundland. Geophysics, Vol. 58, No. 1, pp. 154-166.

Stevenson, F. and Durrheim, R.J. 1997. Reflection Seismic for Gold, Platinum and Base Metal Exploration and Mining in Southern Africa. In "Proceedings of Exploration 97: Fourth Decennial International Conference on Mineral Exploration" edited by A.G. Gubins. pp. 391-398.

Telford, W.M., Geldart, L.P., Sheriff, R.E. 1995. *Applied Geophysics*. 2nd ed. U.S.A., Cambridge University Press.

White, D., Boerner, D., Wu, J., Lucas, S., Berrer, E., Hannila, J., Somerville, R. 2000. Mineral exploration in the Thompson nickel belt, Manitoba, Canada, using seismic and controlled-source EM methods. Geophysics, Vol. 65, No. 6, pp. 1871-1881.

Wu, R., Aki, K. 1985. Scattering characteristics of elastic waves by an elastic heterogeneity. Geophysics, Vol. 50, No. 4, pp. 582-595.

Wu, R., and Toksoz, M.N. 1987. Diffraction tomography and multisource holography. Geophysics, Vol. 52, No. 1, pp. 11-25.

Appendix A: Past Applications of Seismics to Mineral Exploration

The following is a brief overview of the development and application of seismics for mineral exploration.

The Kidd Creek copper-zinc mine is located in the Sudbury, Ontario mining camp, in the Abitibi subprovince of the Superior province. At Kidd Creek, the mineralisation is associated with stratigraphic contacts in the North Rhyolite volcanic complex, which is a folded and steeply-dipping unit (Eaton *et al.*, 1996). The steep dips of the volcanic complex make surface seismic impractical because energy would be directed horizontally or downward, and none would return to the surface. To avoid this problem, Eaton *et al.* (1996) investigated the possibility of detecting the mineralisation using a VSP array. The downhole tool (sonde) contained 1 set of triaxial geophones and data was recorded from 150 m-1050 m measured depth, recording at 15 m intervals along the borehole. The source was located to the northwest of the borehole collar and was designed to illuminate the area of rock to the southwest of the borehole and above the bottom of the array. The data was processed by suppressing noise, rotating the data components into a shot-oriented frame of reference, coherency filtering to improve the quality of reflected arrivals, and using a VSP CDP (common depth point) transform method to place the reflectors at their point of origin. Data interpretation was carried out by comparing the processed VSP section to borehole sonic logs and core logging. This project was successful in delineating reflections correlating with stratigraphic contacts in the North Rhyolite volcanic complex (Eaton *et al.*, 1996).

Another survey in the Sudbury mining camp used a 2D array geometry integrated with 3D forward modelling to detect and delineate massive sulphide deposits hosted in a complex geological setting with moderate dips (<60°) (Milkereit *et al.*, 1996). The 3D forward modelling was developed using physical rock property studies, mine geology, and core logging and was used to adapt acquisition and processing strategies to the conditions in the Canadian Shield. They used small sensor separation to avoid spatial aliasing, equipment with large dynamic range and arrays with high stacking fold to accommodate the low S:N (signal-to-noise ratio) in crystalline environments. The project used an integrated approach to interpretation, using seismic data, synthetic seismic data obtained from models, mining and core logging data and successfully imaged a north-dipping contact between norite and the footwall complex that was truncated by a south-dipping shear zone. These results show that seismic reflection profiling can be adapted to image lithological contacts and geologic structures to identify and delineate large massive sulphide deposits, but it also indicates that geologic setting and survey geometry are as critical for detection as size, shape and depth of the orebody (Milkereit *et al.*, 1996). They also suggest that surveys over ground with steep target dips, or over fresh ground (no a priori knowledge of the geologic structures), should use large source and receiver offsets to record the reflected wavefield, or even to centre the array in the downplunge direction of the target so the reflected wavefield from dipping targets will be recorded (Milkereit *et al.*, 1996).

After completing extensive petrophysical studies and presite surveys, the Trill area of the Sudbury basin (Ontario) was chosen for the first 3D seismic survey for mineral exploration in North America, conducted in late October, 1995 (Milkereit *et al.*, 2000; also Eaton *et al.*,

1997). Through knowledge gained from previous 2D seismic, VSP seismic, petrophysical studies, and 3D seismic modelling (using the Born approximation of the elastic wave equation), the acquisition and processing parameters were adjusted to conditions in the Canadian Shield. As in previous surveys, this survey used an explosive source to provide an impulsive high-energy signal with high frequencies. The array was designed for 30 m receiver spacing and 50 m source spacing (adjustments were made onsite for poor ground conditions) and included a single triaxial geophone located in a borehole at 1070 m measured depth. Processing included static corrections, deconvolution, bandpass filtering, stacking velocity analysis, and 3D phase-shift migration (Milkereit *et al.*, 2000). 3D seismic data is superior to 2D because time slices of the data can be made to identify scattering bodies and the time at which they appear, whereas in 2D data, if the scattering body was out of the recording plane, the scattering would appear as if the body was in the plane, causing incorrect interpretations. The results of this project show that massive sulphides (as scattering bodies), important lithological contacts and geological structures can be directly detected by high-resolution seismic methods, and the most meaningful interpretations require an integrated knowledge of geological setting, physical rock properties, forward modelling, and high-resolution seismic data sets (Milkereit *et al.*, 2000).

The Matagami mining camp (PQ, Canada) is host to the Bell Allard VMS (volcanic massive sulphide) deposit (estimated at over 6 million tonnes), in which gabbro sills intrude much of the volcanic host rock (Li and Calvert, 1997). A 2D seismic profile was conducted over the Bell Allard deposit (across the southern end of the Matagami mining camp) in 1993 and processed data showed weak reflections from the volcanic stratigraphy and high

amplitude reflections from the gabbro sills. Also evident, in a seismic section processed specifically to preserve amplitude information, was a strong reflection from the top of the ore body but the reflector did not extend over the full width of the deposit (as defined by drilling) and no separate reflection from the base of the deposit was identifiable. Mineralisation was linked to an intersection of an apparent low-angle fault with the top of the Watson Lake Group; therefore faults appear to have controlled the formation of the Bell Allard deposit and can be used for further exploration (Li and Calvert, 1997). In addition to the 2D seismic profile, borehole geophysical logging, rock property measurements, a VSP and forward modelling were carried out to evaluate whether the reflectivity of the deposit and host rock was appropriate for seismic exploration (Adam *et al.*, 1997). The modelling indicated the deposit would have a complex diffraction response to seismic impulse and would be best imaged by a 3D seismic survey. In 1996, a 3D seismic reflection survey was designed and completed. The processed results show the ore body has a distinctive seismic response that depends upon seismic survey acquisition parameters, geometry and size of the deposit, ore zoning, and physical rock properties of the ore and host rock (Adam *et al.*, 1997). Seismic sections show reflections from the Lower Wabassee Group that are conformable with the Key Tuffite, which is an important exploration horizon (Eaton *et al.*, 1997). The results indicate that 3D seismic methods can be used to map deep volcanic stratigraphy and can provide direct detection of massive sulphide bodies (Adam *et al.*, 1997).

In 1993, Noranda, Inco and Falconbridge joined a collaborative programme headed by the GSC Downhole Seismic Imaging Group to conduct research into application of seismic methods for base metal mineral exploration. An independent seismic exploration

programme was later started by Noranda in 1995 (Gingerich *et al.*, 2000). The developed methodology used the following steps: 1) rock property measurements; 2) borehole logging and core rock property measurements; 3) forward stratigraphic and structural modelling; 4) 2D field parameter testing and templating; 5) 3D seismic survey acquisition and interpretation, then choosing drill locations for exploration and area sterilization (Gingerich *et al.*, 2000). As part of this research, the Halfmile Lake deposit in the Bathurst mining camp in New Brunswick, Canada was chosen to examine seismic response of volcanogenic massive sulphide deposits in low-grade metamorphic settings (Salisbury *et al.*, 2000). Halfmile Lake was chosen because it has been carefully mapped, extensively drilled providing abundant core samples to perform rock property tests on, and is the largest undeveloped deposit (there are no mine workings to create noise or large diffractions). The deposit was originally comprised of 2 zones of sulphide mineralisation, called the Upper and Lower zones. They occur on the faulted, overturned south limb of a large antiform, and extend 3 km along strike (Salisbury *et al.*, 2000). Rock property studies carried out at crack closure pressure (200 MPa) indicated that host rocks had an average compressional-wave velocity of 6.0 km/s and density of 2.75 g/cm^3, while ores ranged in velocity 5.1-7.3 km/s and density 2.95-3.4 g/ cm^3, indicating the mineralisation at Halfmile Lake should be a strong reflector in an almost transparent host rock. These laboratory findings were supported by impedance contrasts from borehole geophysical logging that was carried out through the deposit. A test VSP that was conducted to determine whether the deposit would be appropriate for seismic exploration successfully showed a prominent north-dipping reflector that corresponded to the deposit (Salisbury *et al.*, 2000). Following the VSP, a 2D surface seismic survey was conducted over and downdip of the Halfmile Lake

deposit. The resulting migrated seismic sections gave a clear image of the ore body that coincided with the known location of the deposit (Salisbury *et al.*, 2000). In 1998, Noranda conducted an 18 km^2 3D seismic survey over the Halfmile Lake deposit. Processed data from this survey showed two impedance contrasts that were selected as drill targets for subsequent drill testing in 1999. It was determined that the deeper target object was created by a large zone of deformation in a sequence of porphyry that produced significant velocity anisotropy, while the shallower target object (~1200 m) was created by 50 m of sub-economic massive sulphide mineralisation, making it the first reported direct detection of massive sulphide mineralisation for exploration purposes (Gingerich *et al.*, 2000). To establish whether there was a steeply-dipping zone of mineralisation connecting the previously-known mineralisation zones to the new, deeper zone, a multi-offset, multi-azimuth VSP was acquired at Halfmile Lake in 2001 (Bellefleur *et al.*, 2002). The irregular surface of the massive sulphide mineralisation sheet produced strong scattered and mode-converted waves (P-P, S-S, P-S, S-P) in all three components that had not previously been observed in VSP data (Bellefleur *et al.*, 2002). Separate migrations of vertical component data and radial component data show strong migrated energy coinciding with the Deep lens but there was no evidence of any connection between the zones (Bellefleur *et al.*, 2002).

In addition to extensive seismic testing and exploration surveys in the established mining camps mentioned above, smaller-scale projects have been carried out in other parts of Canada. In the Manitouwadge greenstone belt, Ontario, Canada, a high-resolution 2D seismic survey was acquired over copper-zinc deposits in 1995 (Roberts *et al.*, 1997). The survey was conducted after rock property studies and forward modelling had been

completed to indicate whether the geological structures would have adequate acoustic impedances to be detected in seismic data. In the migrated seismic data set, the structurally important contact between the Inner Volcanic Belt and overlying plutonic rocks is visible and therefore can be further defined with future seismic studies. The seismic data clearly imaged shallow levels of the target host structure (a synform) but deeper levels (where massive sulphides may be hosted) were not clearly defined, probably due to the complex geology and interference from off-line reflections (Roberts *et al.*, 1997).

The Thompson nickel belt of northern Manitoba is a highly strained, moderately- to steeply-dipping, medium- to high-grade Proterozoic collisional belt with lithological contacts and geological structures conducive to producing seismic reflections (White *et al.*, 2000). Borehole logs indicated that the mineralized Ospwagan Group should be a strong reflector in seismically transparent host rock of Archean basement gneisses. In 1991, a 2D seismic survey was conducted to map the subsurface extent of the Ni-ore-bearing Ospwagan Group using a vibroseis source (White *et al.*, 2000). The seismic data clearly imaged the folded Thompson Nappe, cored by the Ospwagan Group rocks, which are overlain by Archean basement gneisses. The main limitation of seismic exploration in the Thompson nickel belt is ground-truthing the data since data acquired around existing mine structures was poor quality due to subvertical structures in the area that would not preferentially return energy into the 2D surface array (White *et al.*, 2000).

The first major vibroseis seismic reflection survey at a mine site in North America was conducted in 1989 at the Buchans Mine in central Newfoundland, Canada (Spencer *et al.*, 1993). The Buchans deposit is a volcanogenic massive sulphide ore body bound above and

below by faults. 16 km of data was recorded over 3 lines using 10 m receiver groups, a source spacing of 20 m, 2 vibrators in nose-to-tail configuration (to suppress ground roll), and a 10 second sweep 40-125 Hz resulting in 60 fold subsurface coverage. Data processing steps were: muting, spectral balancing, crooked line binning, refraction static corrections, velocity analysis and correlation statics, poststack processing (e.g., coherency filtering), and migration. The migration was somewhat successful but contained artefacts (smiles) due to the discontinuity of reflections (Spencer *et al.*, 1993). The processed data were correlated with existing borehole information for meaningful interpretation and significantly influenced the geologic model of the ore body. The final seismic sections showed the thrust belt having antiformal stack structures that disrupt and repeat ore stratigraphy. The lower bounding fault was also visible so that good estimates of the volume of crust with ore-bearing potential could be made (Spencer *et al.*, 1993).

A seismic survey conducted over granitic rocks in Sweden found two predominant sources of seismic reflections: diabase sills and fracture zones (Julin, 1997). The seismic data successfully imaged diabase intrusions as laterally-continuous subhorizontal to gently dipping layers of high impedance in host rock, while fracture zones are less continuous subhorizontal to steeply-dipping layers of low impedance. Julin (1997) determined that the critical processing steps for these data included static corrections, spectral balancing, and velocity filtering.

Reflection seismology has been used in southern Africa since the early 1980s for gold, platinum and base metal exploration, and also for mine planning (Stevenson and Durrheim, 1997). A seismic section across Archean conglomerates in the northwest edge of the

Witwatersrand Basin, South Africa, shows the arrangement of the Archean and Early Proterozoic supracrustal rocks and the positions of the stratiform gold-bearing "reefs" as inferred by mapping marker horizons (Stevenson and Durrheim, 1997; Eaton *et al.*, 1997). Seismic surveys were conducted over Namibian base metal deposits that are associated with paleokarst structures hidden under younger cover rocks and successfully imaged a strong reflection at the interface between the Mulden Group (clastic sediments) and the Otavi Group (dolomitic sequence and paleokarsted host rock). The seismic sections also mapped faults that may have been conduits for hydrothermal fluid, which combined with the Otavi/Mulden contact affected exploration plans (Stevenson and Durrheim, 1997). Reflection seismic surveys have been conducted over the Bushveld Complex (an igneous intrusion in South Africa) to map out slump structures known as "potholes" that disrupt the main platinum ore body and cause mining problems related to the poor ground conditions associated with the slumps. The seismic data allowed successful detection of the PGE-bearing pyroxenite of the Bushveld Complex and mapping of different reef types and slump structures. This information was critical for planning mine operations and improved estimates of ore reserves (Stevenson and Durrheim, 1997). The Matchless Amphibolite Belt in central Namibia comprises mafic lavas and meta-intrusives with associated massive sulphide deposits, such as the Otjihase (Stevenson and Durrheim, 1997). The Otjihase's Main Shoot (the mined reserve) is subdivided into discrete ore bodies by major normal faulting that has delayed mining due to poor ground conditions. A reflection seismic survey was conducted in 1988 over the Main Shoot. This survey suffered from poor S:N but it did succeed in mapping the down-dip extension of the Main Shoot, and imaged the faults that cut the ore zone (Stevenson and Durrheim, 1997).

Many orebodies lie within or near major fault systems, which indicates that faults act as conduits for hydrothermal fluids. Large faults have deformation fabrics, which, when combined with metasomatic alteration, can make them strong seismic reflectors (Drummond *et al.*, 2000). Drummond *et al.* (2000) examined regional seismic data from Western Australia and observed that many highly-reflective large-scale faults that penetrate deep into the crust are spatially associated with major gold deposits (the deposits lie in the hanging-wall block of the fault). Similar observations were made from surveys in northeast Australia where two highly-reflective deeply-penetrating faults were located near copper and copper-gold deposits, and one fault was adjacent to the large Mt. Isa Ag-Pb-Zn deposit. Other large-scale, deeply-penetrating faults in the seismic section with no known associated mineralisation were not reflective and were identified only by the truncation of other reflections. The findings of Drummond *et al.* (2000) indicate that applying seismic methods early in an exploration programme may be useful to identify areas of possible mineralisation associated with large fault systems, especially when exploration is focussed on deeper targets (>500 m).

Appendix B: Aplanatic Pre-Stack Migration

This brief discussion of aplanatic pre-stack migration is based on the paper by Kocurko and Lines (1998).

Migration by aplanatic surfaces is calculated using four grids superimposed on the subsurface: 1) a velocity model of the subsurface; 2) first arrival times between shot locations and grid points in the subsurface; 3) first arrival times between grid points in the subsurface and recording positions; and 4) (initially filled with zeroes) holds the migrated depth image. First arrival times for energy travelling from source to receiver is calculated by adding the first arrival time of the energy from the shot to each node in the grid to the first arrival time of the energy from an imaginary source at the geophone to each node in the grid. Aplanatic surfaces, or isochrons, for each source-geophone pair can be drawn through the model of the subsurface that represent nodes that all have the same first arrival time (travel time) of energy from source to receiver, and include all points in space from which the energy could have been reflected (once) before reaching the geophone. The signal recorded at the time of each aplanatic surface is added to the grid nodes in the migration grid that correspond to the points on the aplanatic surface. Repeating this step for all aplanatic surfaces finishes the migration of a single trace and iterating the above procedure for all pairs of shots and geophones completes the migration of the full data set.

The aplanatic surface pre-stack migration algorithm used in this study calculated travel times by a "fast marching level set method", please see Kocurko and Lines (1998) and Sethian (1996) (chapters 1, 2, and 9).

Appendix C: Finite-Difference Modelling

This discussion is based mainly upon the paper by Kelly *et al.* (Geophysics, 1976).

Finite differences can be used to calculate synthetic seismograms of almost any subsurface geological model, while exact analytical solutions to the elastic wave equation do not exist for most subsurface geological models. This method gives reliable arrival times of seismic events and amplitudes that vary with the elastic impedance contrasts. The resulting seismograms can be used to identify and interpret as much of the recorded data as possible.

Finite difference modelling is a "time-marching" procedure that solves the appropriate elastic equations recursively to calculate motion in a perturbed elastic medium. Two different methods of finite differences exist: implicit and explicit. Implicit techniques use matrix inversion to simultaneously calculate the motion at all locations in the spatial grid at some future time from known values at previous times. Explicit techniques, which are computationally simpler and are discussed here, calculate the motion at a point in the spatial grid at some future time from the motion already calculated for previous times. There are two general formulations of explicit finite difference techniques: homogeneous and heterogeneous. For the homogeneous formulation, the elastic medium (subsurface geology) is approximated as a group of homogeneous lithologic regions, each with constant density and elastic parameter values. Motion in each region of the homogeneous case is calculated by an appropriate finite-difference approximation for that specific region. For this method, boundary conditions across each interface must be solved explicitly. Heterogeneous method can use different density and elastic parameter values with each grid point (excellent for

simulating complex structures) by using more general elastic equations that solve the boundary conditions implicitly.

Problems in finite difference modelling include placement of a point source in the model space, edge reflections, and grid dispersion. The source usually creates difficulties in calculations (because it is a point singularity) but can be avoided by subtracting the displacement created by the source from a rectangular region surrounding the source location (it actually inserts the source on the boundary of the rectangular region). The source contribution to motion is calculated analytically from the known solution for a source in an infinite region. Reflections from the sides and bottom of the numerical model space can interfere with resulting synthetic seismograms but can be minimised by requiring the boundaries to have viscous behaviour that will mathematically absorb the incident energy (attenuating the reflection strength). Grid dispersion is inherent to finite difference modelling and produces a delay between lower signal frequencies and higher ones as a wave propagates on a grid, which creates significant "tailing" of the signal. Grid dispersion can be minimised by ensuring the number of grid points per wavelength at the source's upper half-power frequency is at least 10.

Below is a brief description of the homogeneous elastic solution for a two-layer case in two dimensions (P- and SV-waves only). See Kelly *et al.* (Geophysics, 1976) for more detail. Note that the modelling for this paper was completed using the acoustic solution, which is a special case of the elastic solution that uses compressional energy (P-waves) only.

Variables:

x horizontal rectangular coordinates
z vertical rectangular coordinates (+ve down)
u horizontal displacement

w	vertical displacement
Δt	time step
ρ	density
λ, μ	Lamé's parameters
α	compressional (P-) wave velocity
β	shear (S-) wave velocity
h	grid interval in x and z directions
γ	$=\beta/\alpha$
m, n, l	integers (number of grid steps in x, z, and time, respectively)
F	$=(\alpha\Delta t)/h \leq (1+\beta^2/\alpha^2)^{-1/2}$
Subscript 1	upper layer in 2-layer model
Subscript 2	lower layer in 2-layer model (faster α,β)

The equations of motion are:

$$\rho\frac{\partial^2 u}{\partial t^2} = (\lambda+2\mu)(\frac{\partial^2 u}{\partial x^2}+\frac{\partial^2 w}{\partial x\partial z})+\mu(\frac{\partial^2 u}{\partial z^2}-\frac{\partial^2 w}{\partial x\partial z})$$

$$\rho\frac{\partial^2 w}{\partial t^2} = (\lambda+2\mu)(\frac{\partial^2 u}{\partial x\partial z}+\frac{\partial^2 w}{\partial z^2})+\mu(\frac{\partial^2 w}{\partial x^2}-\frac{\partial^2 u}{\partial x\partial z})$$

The above equations of motion have corresponding explicit, coupled finite-difference equations:

$$u(m,n,l+1) = 2u(m,n,l)-u(m,n,l-1)+F^2[u(m+1,n,l)-2u(m,n,l)+u(m-1,n,l)]$$
$$+F^2(1-\gamma^2)[w(m+1,n+1,l)-w(m+1,n-1,l)-w(m-1,n+1,l)+w(m-1,n-1,l)]/4$$
$$+F^2\gamma^2[u[m,n+1,l)-2u(m,n,l)+u(m,n-1,l)]$$

$$w(m,n,l+1) = 2w(m,n,l)-w(m,n,l-1)+F^2[w(m,n+1,l)-2w(m,n,l)+w(m,n-1,l)]$$
$$+F^2(1-\gamma^2)[u(m+1,n+1,l)-u(m+1,n-1,l)-u(m-1,n+1,l)+u(m-1,n-1,l)]/4$$
$$+F^2\gamma^2[w[m+1,n,l)-2w(m,n,l)+w(m-1,n,l)]$$

Boundary conditions at the free surface require the sum of stresses to be zero:

$$(\alpha^2-2\beta^2)\frac{\partial u}{\partial x}+\alpha^2\frac{\partial w}{\partial z}=0 \quad \text{(normal stress)} \qquad \frac{\partial u}{\partial z}+\frac{\partial w}{\partial x}=0 \quad \text{(tangential stress)}$$

One-sided differences are used to approximate normal derivatives and centred differences are used to approximate tangential derivatives, resulting in differenced boundary conditions for the free surface:

$$(\alpha_1^2 - 2\beta_1^2)\left[\frac{u_1(m+1,0,l) - u_1(m-1,0,l)}{2h}\right] + \alpha_1^2\left[\frac{w_1(m,0,l) - w_1(m,-1,l)}{h}\right] = 0$$

$$\frac{u_1(m,0,l) - u_1(m,-1,l)}{h} + \frac{w_1(m+1,0,l) - w_1(m-1,0,l)}{2h} = 0$$

But boundary conditions at a welded, horizontal interface at depth (interface is at layer n=N for the upper layer and n=1 for the lower) require continuous displacement and stress across the boundary:

$$\rho_1((\alpha_1^2 - 2\beta_1^{\,2})\frac{\partial u_1}{\partial x} + \alpha_1^{\,2}\frac{\partial w_1}{\partial z}) = \rho_2((\alpha_2^2 - 2\beta_2^{\,2})\frac{\partial u_2}{\partial x} + \alpha_2^{\,2}\frac{\partial w_2}{\partial z})$$

$$\rho_1\beta_1(\frac{\partial u_1}{\partial z} + \frac{\partial w_1}{\partial x}) = \rho_2\beta_2(\frac{\partial u_2}{\partial z} + \frac{\partial w_2}{\partial x})$$

The above two boundary conditions refer to the continuity of normal and tangential stresses.

$$w_1 = w_2$$

$$u_1 = u_2$$

The above two boundary conditions refer to normal and tangential displacement continuity. Using the same approach for approximating derivatives as for the free surface, four equations are developed for the boundary conditions:

$$\rho_1\left(\alpha_1^2\left[\frac{w_1(m,N+1,l) - w_1(m,N,l)}{h}\right] + (\alpha_1^2 - 2\beta_1^2)\left[\frac{u_1(m+1,N,l) - u_1(m-1,N,l)}{2h}\right]\right)$$
$$= \rho_2\left(\alpha_2^2\left[\frac{w_2(m,2,l) - w_2(m,1,l)}{h}\right] + (\alpha_2^2 - 2\beta_2^2)\left[\frac{u_2(m+1,1,l) - u_2(m-1,1,l)}{2h}\right]\right)$$

$$\rho_1\beta_1^2\left[\frac{u_1(m,N+1,l)-u_1(m,N,l)}{h}+\frac{w_1(m+1,N,l)-w_1(m-1,N,l)}{2h}\right]$$
$$=\rho_2\beta_2^2\left[\frac{u_2(m,2,l)-u_2(m,1,l)}{h}+\frac{w_2(m+1,2,l)-w_2(m-1,2,l)}{2h}\right]$$

$$u_1(m,N,l)=u_2(m,1,l)$$

$$w_1(m,N,l)=w_2(m,1,l)$$

These equations can be used to create an algorithm for finite-difference modelling.

Appendix D: Programs Used in this Study

The following is a list of Seismic Unix modules that were used for creation, processing and display of the data used in this study.

sumute—used for a front-end mute
sufilt—filters data
suximage—displays SU data on screen
supsimage—writes SU data to .eps file format for use in documents
sufdmod2—creates 2D acoustic synthetic seismograms
suvelandrho—creates velocity and density matrix for input to sufdmod2
suaddhead—adds headers to SU files
segyhdrs—writes SEG-Y headers
segywrite—writes SEG-Y file from SU format
segyread—reads SEG-Y file to SU format
sushw—adds header values to SU files
suvmapl—pre-stack aplanatic migration algorithm
suwind—strips off traces
suxmovie—used to view synthetic seismograms animated in time
farith—does calculations on two binary files (for combining scattering host velocity file with scattering or homogeneous target object)
sufft—creates a frequency spectrum with offset
suamp—creates an amplitude spectrum with offset
suspecfk—creates a frequency spectrum with wavenumber
a2b—used to convert ascii data (scattering velocity matrix) to binary format
suflip—used to transpose the scattering velocity matrix
sustack—used to stack synthetic seismograms
susort—used to sort traces in synthetic seismograms
suchw—used to change header word
sunmo—used to calculate normal-moveout correction
sumiggazdag—post-stack migration algorithm (Gazdag migration)
sumigfd—post-stack migration algorithm (finite difference migration)
sumigtk—post-stack migration algorithm (in T-K domain)
supswigb—writes .eps files of synthetic seismograms in wiggle format for use in documents

A sample of a file used as input to suvelandrho is as follows:

```
nx=400          # nodes in x-direction
nz=300          # nodes in z-direction
x0=0.0          origin of x-axis
xn=2000.0       length of x-axis
z0=0.0          origin of z-axis
```

zn=1500.0	depth of z-axis
defvel=5800.0	background velocity (m/s)
defrho=2.7	background density (g/cc)
xs=1140.0	x-coordinate of source location
zs=5.0	z-coordinate of source location
fmax=150.0	maximum frequency used
fpeak=85.0	peak frequency used
tmax=0.8	maximum time recorded (seconds)
hsz=0.0	depth of horizontal seismic array
vsx=1720	x-position of VSP array
5250.0 4.03 8	velocity (m/s), density (g/cc), #nodes of target object geometry
1080 700	x- and z-coordinates of target object geometry nodes
1200 700	
1320 820	
1320 940	
1200 1060	
1080 1060	
960 940	
960 820	

An example of an input file to supvmapl is as follows:

```
400 300 0.0 0.0 2000.0 0.0 0.0 1500.0 20
                {# nodes in x, # nodes in z, x-origin, y-origin, x-end, y-end, z-origin,
                z-end, # traces sent to each slave}
/net/srvr06/public/tina/velocity
                {downgoing velocity model}
--same—         {upgoing velocity model}
/net/srvr06/public/tina/velocity
                {input file with x,y,z coordinates of shot and receiver locations}
12              {# slaves}
/usr/local/bin/supvmapl srvr03.weland
/usr/local/bin/supvmapl srvr03.weland
```

```
/usr/local/bin/supvmapl srvr04.weland
/usr/local/bin/supvmapl srvr04.weland
/usr/local/bin/supvmapl srvr05.weland
/usr/local/bin/supvmapl srvr05.weland
/usr/local/bin/supvmapl srvr06.weland
/usr/local/bin/supvmapl srvr06.weland
/usr/local/bin/supvmapl srvr07.weland
/usr/local/bin/supvmapl srvr07.weland
/usr/local/bin/supvmapl srvr08.weland
/usr/local/bin/supvmapl srvr08.weland
/net/srvr06/public/tina/tina1_mig
                    {output file}
```